Eur. Phys. J. C (2025) 85:204
https://doi.org/10.1140/epjc/s10052-025-13783-0

THE EUROPEAN PHYSICAL JOURNAL C

Regular Article - Theoretical Physics

Weak decays of B_c involving vector mesons in self-consistent covariant light-front approach

Thejus Mary S.[1,a], **Avijit Hazra**[1,b], **Neelesh Sharma**[2,c], **Rohit Dhir**[1,d]

[1] Department of Physics and Nanotechnology, SRM Institute of Science and Technology, Kattankulathur 603203, India
[2] Paradigm of Science Cultivation and Ingenious, Kangra 176032, India

Received: 6 October 2024 / Accepted: 30 December 2024

Abstract We present a comprehensive analysis of weak transition form factors, semileptonic decays, and nonleptonic decays of B_c mesons involving pseudoscalar (P) and vector (V) mesons for bottom-conserving and bottom-changing decay modes. We employ the self-consistent covariant light-front quark model (CLFQM), termed type-II correspondence, to calculate the B_c to $P(V)$ transition form factors. The type-II correspondence in the CLF approach gives self-consistent results associated with the $B_j^{(i)}$ functions, which vanish numerically after the replacement $M'^{(\prime)} \to M_0'^{(\prime)}$ in traditional type-I correspondence, and the covariance of the matrix elements is also restored. We investigate these effects on bottom-conserving B_c to $P(V)$ form factors that have not yet been studied in CLFQM type-II correspondence. In addition, we quantify the implications of self-consistency propagating to weak decays involving both bottom-conserving and bottom-changing B_c transition form factors. We use two different parameterizations, the usual three-parameter function of q^2 and the model-independent z-series expansion, to establish a clear understanding of q^2 dependence. Using the numerical values of the form factors, we predict the branching ratios other physical observables, including forward-backward asymmetries, polarization fractions, etc. of the semileptonic B_c decays. Subsequently, we predict the branching ratios of two-body nonleptonic weak decays using the factorization hypothesis in self-consistent CLFQM. We also compare our results with those of other theoretical studies.

1 Introduction

The B_c meson is a quark–antiquark bound state composed of two heavy quarks (b and c) with distinct flavors that decay solely via weak interactions [1]. The study of B_c meson decays provides valuable insights into the fundamental aspects of the Standard Model (SM) and offers a unique platform to explore the underlying heavy flavor dynamics, which is of immense experimental and theoretical significance. A peculiarity of B_c decays, compared to B and B_s decays, is that both constituent quarks are involved in weak decays, i.e., b quark decays with c quark as spectator, and c quark transitions with spectator b quark, in addition to weak annihilation of constituent quarks. The weak annihilation processes decay to leptons or lighter mesons that are relatively suppressed and are, therefore, ignored in the current analysis. The phase space available for c quark decays is significantly smaller than for b quark decays, but the Cabibbo–Kobayashi–Maskawa (CKM) matrix elements strongly favor c quark decays [1,2]. The study of heavy flavor weak decays is a powerful tool for testing the SM and searching for new physics (NP) beyond the SM. The semileptonic decays are governed by tree-level processes in the SM, which provides a relatively simple theoretical description to capture the effects of the weak interaction in terms of Lorentz-invariant form factors. In addition, these decays are of immense importance for extracting the CKM matrix elements (and their phases) and for studying lepton flavor universality (LFU). On the other hand, the study of two-body weak decays of B_c mesons offers an excellent opportunity to explore quantum chromodynamics (QCD) in both perturbative and nonperturbative regimes to understand the interplay of strong and electroweak interactions. Additionally, these decays allow for testing QCD-motivated effective theories and models within and beyond the SM.

[a] e-mail: thejusmarys@gmail.com
[b] e-mail: hazra_avijit@outlook.com
[c] e-mail: nishu.vats@gmail.com
[d] e-mail: dhir.rohit@gmail.com (corresponding author)

Published online: 20 February 2025

Modern experimental collaborations such as Large Hadron Collider beauty (LHCb), Compact Muon Solenoid (CMS), ATLAS, and Collider Detector at Fermilab (CDF) have been exploring the B_c meson to provide valuable insights into heavy flavor physics in the SM and NP. The Large Hadron Collider (LHC) and Relativistic Heavy Ion Collider (RHIC) are expected to produce a sizable number of B_c meson events (about 10^6) via the proton-nucleus and nucleus-nucleus collision modes [3]. Therefore, in the near future, it will be possible to study the B_c meson properties by using collision modes other than the typically considered proton-proton collision mode. In the recent past, the LHCb has reported precise measurement of B_c meson mass and lifetime as $M_{B_c} = (6274.47 \pm 0.27 \pm 0.17)$ MeV and $\tau_{B_c} = (0.5134 \pm 0.011 \pm 0.0057)$ ps, respectively [4,5]. Although the spectroscopy and decays of B_c mesons are being probed extensively, their experimental observations and measurements are scarce [6–8]. So far, the LHCb has reported the observation of two-body nonleptonic $B_c^+ \to B_s^0\pi^+$ decay [9], and their experimental efforts have resulted in the observation of B_c decays involving two-charm mesons such as $B_c^+ \to D_{(s)}^{(*)+}\overline{D}^{(*)0}$ and $B_c^+ \to D_{(s)}^{(*)+}D^{(*)0}$ [10–12]. Recently, LHCb and ATLAS reported the ratios of branching fractions of two-body nonleptonic B_c decays involving a J/ψ meson in the final state, i.e., $\frac{\mathcal{B}(B_c^+\to J/\psi D_s^{(*)+})}{\mathcal{B}(B_c^+\to J/\psi\pi^+)}$, $\frac{\mathcal{B}(B_c^+\to J/\psi D_s^{*+})}{\mathcal{B}(B_c^+\to J/\psi D_s^+)}$, and $\frac{\mathcal{B}(B_c^+\to J/\psi K^+)}{\mathcal{B}(B_c^+\to J/\psi\pi^+)}$ [13–16]. Even though observations exist of a few semileptonic and nonleptonic decays of the B_c meson, further efforts are required for precise experimental measurements. Interestingly, the LHCb collaboration reported the LFU ratio for J/ψ in the final state as $\mathcal{R}_{J/\psi} = 0.71 \pm 0.18 \pm 0.17$ [17]. However, this ratio significantly exceeds the theoretical estimates, including the lattice QCD (LQCD) results [18]. Such discrepancies between theory and experiment garner significant attention for physics beyond the SM.

The aforementioned theoretical studies of the semileptonic and nonleptonic decays of heavy flavor b-mesons provide valuable insights into the weak interaction and allow us to measure fundamental parameters within the SM. Additionally, they offer information about quark mixing, CP violation, and heavy quark physics. Furthermore, investigations of semileptonic decays are essential for precise theoretical predictions and probing physics beyond the SM. Therefore, considering the imminent advancements in precision measurements of the B_c meson at hadron colliders and B-factories, several theoretical models have been used to study the semileptonic and nonleptonic B_c meson decays involving pseudoscalar (P) and vector (V) mesons, including the LQCD [19–21], QCD sum rules (QCDSR) [22–24], Bethe–Salpeter (BS) model [25,26], covariant light-front quark model (CLFQM) [27–31], relativistic quark model (RQM) [32–34], relativistic constituent quark model (RCQM) [35–37], relativistic independent quark model (RIQM) [38,39], perturbative QCD (pQCD) approach [40,41], and QCD factorization (QCDF) approach [42]. Current theoretical research has predominantly concentrated on the semileptonic weak decays of the B_c meson to ground state and orbitally excited charmonium states. It is noteworthy that studies examining bottom-conserving and bottom-changing semileptonic decays of B_c that result in B^*, B_s^*, D^*, or D_s^* mesons in the final state (excluding decays to charmonia) remain relatively limited in the literature. Moreover, among these studies, analyses based on the CLFQM are particularly scarce and require reinvestigation in light of recent issues pertaining to self-consistency and covariance in some of the involved form factors. Thus, in the present work, we focus on comprehensive investigations into the effects of self-consistency and covariance on bottom-conserving and bottom-changing semileptonic and nonleptonic decays within the CLFQM framework. Our main objectives are twofold: first, to examine the impact of self-consistency on weak semileptonic and nonleptonic decays using modified form factors within a CLFQM approach, and second, to establish self-consistency in bottom-conserving transition form factors, which have not yet been explored, and to quantify these effects on bottom-conserving weak decays. Additionally, we address the ambiguities related to the q^2 parameterization in our analysis to provide a more robust understanding of these decay processes.

The light-front quark model (LFQM) offers a comprehensive relativistic treatment of quark spins and center-of-mass motion. The Lorentz-invariant light-front wave function is defined in terms of momentum fraction variables. The accurate implementation of quark spins through the Melosh transformation [43,44] makes it particularly suitable for studying hadronic form factors. This is especially true at high recoil momenta where relativistic effects are significant [45,46]. Traditional nonrelativistic quark models face challenges in accurately representing these transitions. This is due to their inherent limitations in accounting for relativistic effects [47–51]. The CLFQM, in addition to providing a relativistic treatment of physical quantities such as decay constants and form factors, offers several advantages over the traditional LFQM. In contrast to the traditional LFQM, the CLFQM considers quark and antiquark states as off-shell, which enables more accurate calculations of matrix elements and form factors. This is important for more accurately capturing the dynamics of the meson decays. In the traditional LFQM, the Lorentz covariance of the matrix element is violated due to the spurious contributions, and it does not provide any systematic approach to determine the zero-mode contributions [47,51]. Jaus [52] proposed the CLFQM to provide resolution of these ambiguities by using the manifestly covariant BS approach [53,54]. The CLFQM ensures covariance of the

matrix elements by the inclusion of zero-mode contributions, which make the spurious contributions proportional to the light-like four-vector $\omega^\mu = (0, 2, 0_\perp)$ irrelevant [47,52,55]. Following this, CLFQM has been extensively used to investigate the semileptonic and nonleptonic decays of bottom mesons [28–30,44–46,56–65].

In this study, we employ the recent advancements in CLFQM, referred to as self-consistent CLFQM, to calculate the B_c to P and V meson transition form factors. The B_c meson decays involve c quark transitions $c \to s(d)$ and b quark transitions $b \to c(u)$. These quark-level transitions are categorized as bottom-conserving ($\Delta b = 0$) and bottom-changing ($\Delta b = -1$) CKM-favored and CKM-suppressed modes (their selection rules are defined in Sects. 2 and 3), respectively. It should be noted that the self-consistent CLFQM is referred to as type-II correspondence in CLFQM because of the challenges associated with type-I correspondence [44,45,52]. In the traditional type-I scheme, the CLF predictions for the P to V transition form factors suffer from the self-consistency problem; for example, the results obtained via the longitudinal ($\lambda = 0$) and transverse ($\lambda = \pm$) polarization states are different from each other due to the additional contributions characterized by the coefficients $B_1^{(2)}$ and $B_3^{(3)}$. These additional contributions affect $f(q^2)$ and $a_-(q^2)$ form factors only.[1] Moreover, the manifest covariance of the matrix element in CLFQM is also violated within the type-I scheme due to the residual ω-dependencies associated with $B_j^{(i)}$ functions that are independent of zero-mode contributions. Therefore, both these issues originate from the same source, which can be effectively resolved by incorporating type-II correspondence [62]. The CLFQM with type-II correspondence can, however, give self-consistent results, because integration over the terms associated with the coefficient $B_j^{(i)}$ vanish numerically after the replacement $M'^{(\prime)} \to M_0'^{(\prime)}$ and the covariance of the matrix elements is also restored. It should be noted that the type-II correspondence scheme has been employed to calculate the bottom-changing $B_c \to D_{(s)}^*(J/\psi)$ transition form factors [62]; however, the bottom-conserving $B_c \to B_{(s)}^*$ form factors have not yet been studied. Furthermore, the implications of self-consistency have not been investigated with respect to the decays involving both bottom-conserving and bottom-changing B_c transition form factors. It should be emphasized that the study of semileptonic and nonleptonic weak decays is necessary to quantitatively assess the effect of self-consistency on these decays. The self-consistency issues originating from form factors $A_0(q^2)$ and $A_1(q^2)$ affect the semileptonic decays of the B_c meson. On the other hand, $B_c \to PV$ decays explicitly involve the $A_0(q^2)$ (other than $F_1(q^2)$) form factor and provide an excellent scenario for quantitative analysis of self-consistency issues that are expected to be more serious in these decays. We further investigate the implication of q^2 dependence on the B_c to $P(V)$ transition form factors over the available momentum range. In order to establish a clear understanding of q^2 dependence, we utilize two different parameterizations, i.e., the usual three-parameter function of q^2 influenced by vector meson dominance (VMD), and model-independent z-series expansion. Furthermore, we plot these B_c to $P(V)$ transition form factors to analyze their behavior with respect to the available q^2 range. Using the numerical values of the form factors, we predict the physical observables, including branching ratios, forward-backward (FB) asymmetries, polarization fractions, etc., of the semileptonic B_c decays. In addition, we analyze the q^2 dependence of these physical observables by plotting them. Later, we extend our analysis to predict the branching ratios of two-body nonleptonic weak decays using the factorization hypothesis in self-consistent CLFQM. We also compare our results with existing results from other models.

Our paper is organized as follows. In Sect. 2, we present the methodology for the calculation of form factors and its q^2 dependence in self-consistent CLFQM. In addition, we provide the decay rate expressions for semileptonic B_c to $P(V)$ and nonleptonic B_c to PV decays. In Sect. 3, we give the numerical results and detailed discussion of the form factors as well as decay rates of semileptonic and nonleptonic B_c to PV decays. We summarize and conclude in Sect. 4. Appendices A and B contain details regarding the resolution of inconsistency in $B_c \to V$ transition form factors and the branching ratios of semileptonic $B_c \to P$ decays, respectively.

2 Methodology

2.1 Self-consistent covariant light-front approach

In this work, we focus on the self-consistent CLF approach [44,45,52,61–63] and summarize the theoretical framework for calculating the B_c to $P(V)$ form factors. In CLFQM, a meson transition, as shown in Fig. 1, is represented in terms of the four momenta of the parent and daughter mesons, i.e., $p' = k_1' + k_2$ and $p'' = k_1'' + k_2$, respectively. Here, $k_1'^{(\prime)}$ and k_2 represent the momenta of the quark and the antiquark of the incoming (outgoing) meson with masses $m_1'^{(\prime)}$ and m_2, respectively. These momenta can further be expressed using internal variables, namely, momentum fraction ($x_{1(2)}$) and transverse momentum ($\boldsymbol{k}'_\perp$) of the quark, as follows:

$$k'^{+}_{1(2)} = x_{1(2)} p'^{+}, \quad \boldsymbol{k}'_{1(2)\perp} = x_{1(2)} \boldsymbol{p}'_\perp \pm \boldsymbol{k}'_\perp, \tag{1}$$

[1] The form factors $f(q^2)$ and $a_-(q^2)$ can be related to the Bauer–Stech–Wirbel (BSW) form factors $A_1(q^2)$ and $A_0(q^2)$, and their transformation relations are given in Eq. (17).

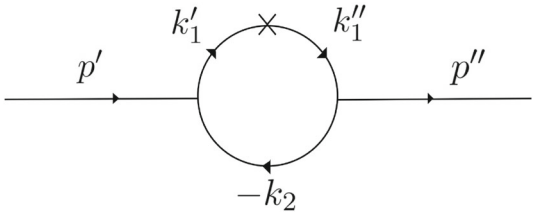

Fig. 1 Feynman diagram for meson transition amplitudes, where × denotes the vector or axial vector current vertex

where they must satisfy the relation $x_1 + x_2 = 1$. The meson momentum is defined as $p' = (p'^-, p'^+, \boldsymbol{p}'_\perp)$, with $p'^\pm = p'^0 \pm p'^3$, such that $(p')^2 = p'^+ p'^- - p'^2_\perp = M'^2$, where M' is the mass of the parent meson. The transverse momenta of the quark and meson are given by $\boldsymbol{k}'_\perp = (k'^x, k'^y)$ and $\boldsymbol{p}'_\perp = (p'^x, p'^y)$, respectively. The definition of the internal quantities for the outgoing meson can be obtained by replacing the prime notation with a double-prime.

Conventionally, a meson bound state $(q'_1, \bar{q}_2)$ can be represented as

$$\begin{aligned}|M(p,^{2S+1}L_J, J_z)\rangle &= \int \{\mathrm{d}^3\tilde{k}_1\}\{\mathrm{d}^3\tilde{k}_2\}\, 2(2\pi)^3\delta^3(\tilde{p} - \tilde{k}_1 - \tilde{k}_2) \\ &\times \sum_{h_1,h_2} \Psi^{JJ_z}_{LS}(\tilde{k}_1, \tilde{k}_2, h_1, h_2)|q'_1(k'_1, h_1)\bar{q}_2(k_2, h_2)\rangle,\end{aligned} \tag{2}$$

where L and J are orbital angular and total spin quantum numbers, respectively [44]. Further, $\tilde{p} = (p'^+, \boldsymbol{p}'_\perp)$ and $\tilde{k}_{1,2} = (k'^+_{1,2}, \boldsymbol{k}'_{1,2\perp})$ represent the on-mass-shell light-front momenta, and $\{\mathrm{d}^3\tilde{k}\} \equiv \frac{1}{2(2\pi)^3}\mathrm{d}k'^+\mathrm{d}^2\boldsymbol{k}'_\perp$. The wave function $\Psi^{JJ_z}_{LS}(\tilde{k}_1, \tilde{k}_2, h_1, h_2)$, which describes the distribution of momentum in space for the $^{2S+1}L_J$ meson, satisfies the normalization condition

$$\sum_{h_1,h_2}\int \frac{\mathrm{d}x_1\mathrm{d}^2\boldsymbol{k}'_\perp}{2(2\pi)^3}|\Psi^{JJ_z}_{LS}(x_1, \boldsymbol{k}'_\perp, h_1, h_2)|^2 = 1, \tag{3}$$

and can be written as

$$\Psi^{JJ_z}_{LS}(x_1, \boldsymbol{k}'_\perp, h_1, h_2) = R^{SS_z}_{h_1h_2}(x_1, \boldsymbol{k}'_\perp)\, \psi_{LL_z}(x_1, \boldsymbol{k}'_\perp). \tag{4}$$

The radial wave function $\psi_{LL_z}(x_1, \boldsymbol{k}'_\perp)$ characterizes how the momenta of the constituent quarks are distributed in a bound state that possesses orbital angular momentum L [44]. The spin-orbital light-front wave function $(R^{SS_Z}_{h_1h_2})$ represents the definite spin state (S, S_Z) corresponding to the light-front helicity (h_1, h_2) eigenstates. Additional details for the treatment of spin, polarization, and complete normalization procedures are discussed in Refs. [44,48,51]. A suitable choice for the radial wave function is the phenomenological Gaussian-type wave function, i.e.,

$$\psi(x_1, \boldsymbol{k}'_\perp) = 4\frac{\pi^{\frac{3}{4}}}{\beta^{\frac{3}{2}}}\sqrt{\frac{\partial k'_z}{\partial x_1}}\exp\Big[-\frac{k'^2_z + k'^2_\perp}{2\beta^2}\Big], \tag{5}$$

for s-wave mesons [48]. The shape parameter (also called Gaussian parameter), β, in Eq. (5) describes the momentum distribution and is expected to be of the order Λ_{QCD} [46]. At Λ_{QCD} scale, nonperturbative phenomena govern the strong interaction dynamics, rendering perturbative QCD methods inadequate [66,67]. However, the hadronic wave function serves as a fundamental link between the hadronic phenomena at this scale. These wave functions are significant for determining the hadronic matrix elements which fundamentally capture the low-energy manifestations, i.e., nonperturbative contributions [68–70]. Furthermore, the specific form of the light-front wave function given by Eq. (5) ensures compliance with the covariant requirement and is manifestly Lorentz-invariant, as expressed in terms of the momentum fraction variables with the plus component [47]. It is remarkable to note that the phenomenological light-front wave functions used to describe the hadronic structure incorporate well-known properties of QCD, such as the expected decline at high relative transverse momentum and endpoint behavior, into a proper functional form [71]. The relative momentum k'_z (in the z-direction) is given by

$$k'_z = \Big(x_1 - \frac{1}{2}\Big)M'_0 + \frac{m'^2_2 - m'^2_1}{2M'_0}, \tag{6}$$

which yields [45]

$$\frac{\partial k'_z}{\partial x_1} = \frac{M'_0}{4x_1(1-x_1)}\Big\{1 - \Big[\frac{m'^2_1 - m'^2_2}{M'^2_0}\Big]^2\Big\}, \tag{7}$$

where

$$M'_0 = \sqrt{\frac{m'^2_1 + k'^2_\perp}{x_1} + \frac{m'^2_2 + k'^2_\perp}{x_2}} \tag{8}$$

is the kinetic invariant mass of the incoming meson. In addition, the kinetic invariant mass of the outgoing meson is denoted as

$$M''_0 = \sqrt{\frac{m''^2_1 + k''^2_\perp}{x_1} + \frac{m'^2_2 + k''^2_\perp}{x_2}}, \tag{9}$$

with $\boldsymbol{k}''_\perp = \boldsymbol{k}'_\perp - x_2\boldsymbol{q}_\perp$. The detailed formalism for the CLFQM is described in Refs. [44,45,52,56,61–63].

In general, the transition form factors $B_c \to M''$ (where $M'' = P,\ V$) corresponding to the Feynman diagram of Fig. 1 are obtained from explicit expressions for matrix elements of currents between meson states [48]

$$\mathcal{B} \equiv \langle M''(p'')|V_\mu - A_\mu|B_c(p')\rangle, \tag{10}$$

where V_μ and A_μ are the vector and axial vector (A) currents, respectively. The form factors for B_c meson to P and V transitions are defined by the following matrix elements [44]:

$$\langle P(p'')|V_\mu|B_c(p')\rangle = p_\mu f_+(q^2) + q_\mu f_-(q^2), \tag{11}$$

$$\langle V(p'',\varepsilon'')|V_\mu|B_c(p')\rangle = \epsilon_{\mu\nu\alpha\beta}\varepsilon''^{*\nu}p^\alpha q^\beta g(q^2) \tag{12}$$

$$\langle V(p'',\varepsilon'')|A_\mu|B_c(p')\rangle = -i\{\varepsilon''^*_\mu f(q^2) + \varepsilon''^* \cdot \boldsymbol{p}[p_\mu a_+(q^2) + q_\mu a_-(q^2)]\}, \tag{13}$$

where $p_\mu = p' + p''$ and $q_\mu = p' - p''$. The polarization of the outgoing vector meson is denoted by ε_μ, and the convention $\epsilon_{0123} = 1$ is adopted. The matrix element expressions Eqs. (11)–(13) are conventionally represented in terms of the BSW [72] form factors as

$$\langle P(p'')|V_\mu|B_c(p')\rangle = \left(p_\mu - \frac{M^2_{B_c} - M^2_P}{q^2}q_\mu\right)F_1^{B_cP}(q^2) + \frac{M^2_{B_c} - M^2_P}{q^2}q_\mu F_0^{B_cP}(q^2), \tag{14}$$

$$\langle V(p'',\varepsilon'')|V_\mu|B_c(p')\rangle = -\frac{1}{M_{B_c} + M_V}\epsilon_{\mu\nu\alpha\beta}\varepsilon''^{*\nu}p^\alpha q^\beta V^{B_cV}(q^2), \tag{15}$$

$$\langle V(p'',\varepsilon'')|A_\mu|B_c(p')\rangle = i\{(M_{B_c} + M_V)\varepsilon''^*_\mu A_1^{B_cV}(q^2) - \frac{\varepsilon''^* \cdot \boldsymbol{p}}{M_{B_c} + M_V}p_\mu A_2^{B_cV}(q^2) - 2M_V\frac{\varepsilon''^* \cdot \boldsymbol{p}}{q^2}q_\mu[A_3^{B_cV}(q^2) - A_0^{B_cV}(q^2)]\}, \tag{16}$$

where the meson masses are denoted by M_{B_c} and $M_{P(V)}$. The BSW-type form factors can be related to the CLFQM form factors as [44]

$$\begin{aligned}
&F_1^{B_cP}(q^2) = f_+(q^2),\ F_0^{B_cP}(q^2) = f_+(q^2) + \frac{q^2}{q\cdot p}f_-(q^2),\\
&V^{B_cV}(q^2) = -(M_{B_c} + M_V)g(q^2),\\
&A_1^{B_cV}(q^2) = -\frac{f(q^2)}{M_{B_c} + M_V},\\
&A_2^{B_cV}(q^2) = (M_{B_c} + M_V)a_+(q^2),\\
&A_3^{B_cV}(q^2) - A_0^{B_cV}(q^2) = \frac{q^2}{2M_V}a_-(q^2),
\end{aligned} \tag{17}$$

with

$$\begin{aligned}
&F_1^{B_cP}(0) = F_0^{B_cP}(0),\\
&A_3^{B_cV}(0) = A_0^{B_cV}(0), \quad \text{and}\\
&A_3^{B_cV}(q^2) = \frac{M_{B_c} + M_V}{2M_V}A_1^{B_cV}(q^2) - \frac{M_{B_c} - M_V}{2M_V}A_2^{B_cV}(q^2).
\end{aligned} \tag{18}$$

In contrast to the LFQM, the quark and antiquark within a meson system are off-shell in CLFQM. As mentioned before, the CLFQM provides a systematic way to handle zero-mode contributions. The light-front matrix element obtained in CLFQM receives additional spurious contributions proportional to the light-like vector $\omega^\mu = (0, 2, 0_\perp)$ which violate the covariance [52]. However, these spurious contributions are canceled out by the addition of zero-mode contributions, restoring the covariance of current matrix elements in CLFQM, thus allowing the calculation of physical quantities in terms of manifestly covariant Feynman momentum loop-integrals. Customarily, for the $B_c(p') \to M''(p'')$ transition, it is convenient to use the Drell–Yan–West frame, $q^+ = 0$, which implies that the form factors are known only for space-like momentum transfer, $q^2 = -q^2_\perp \le 0$, and for the time-like region ($q^2 = -q^2_\perp \ge 0$), an additional q^2 extrapolation is needed. Furthermore, we consider a Lorentz frame in which $\boldsymbol{p}'_\perp = 0$ and $\boldsymbol{p}''_\perp = -\boldsymbol{q}_\perp$ leads to $\boldsymbol{k}''_\perp = \boldsymbol{k}'_\perp - x_2\boldsymbol{q}_\perp$ [64]. Note that $q^2 = q^2_{\rm max} = (M_{B_c} - M_{P(V)})^2$ corresponds to zero-recoil of the final meson in the initial meson rest frame, and $q^2 = 0$ indicates the maximum recoil of the final meson [65]. Following the CLF approach [52,61,62], the form factors in Eqs. (11), (12), and (13) can be extracted from one-loop approximation as a momentum integral given by

$$\mathcal{B} = N_c\int\frac{{\rm d}^4k'_1}{(2\pi)^4}\frac{H_{M'}H_{M''}}{N'_1\,N''_1\,N_2}iS_{\mathcal{B}}, \tag{19}$$

where N_c denotes the number of colors, ${\rm d}^4k'_1 = \frac{1}{2}{\rm d}k'^-_1{\rm d}k'^+_1{\rm d}^2\boldsymbol{k}'_\perp$, and $H_{M'^{(\prime)}}$ is the bound-state vertex functions. The terms $N'^{(\prime)}_1 = k'^{(\prime)2}_1 - m'^{(\prime)2}_1 + i\varepsilon$ and $N_2 = k_2^2 - m_2^2 + i\varepsilon$ arise from the quark propagators, and the trace $S_{\mathcal{B}}$ can be directly obtained by using the Lorentz contraction

$$S_{\mathcal{B}} = {\rm Tr}[\Gamma(\not{k}'_1 + m'_1)(i\Gamma_{M'})(-\not{k}_2 + m_2)(i\gamma^0\Gamma^\dagger_{M''}\gamma^0) \times(\not{k}''_1 + m''_1)], \tag{20}$$

where the vertex operator $\Gamma_{M'^{(\prime)}}$ corresponds to the relevant meson, and has the forms

$$i\Gamma_P = -i\gamma_5 \quad \text{and} \quad i\Gamma_V = i\left[\gamma^\mu - \frac{(k_1 - k_2)^\mu}{D_{V,con}}\right] \tag{21}$$

for P and V mesons, respectively [62].

The method proposed by Jaus [52] would be most effective if vertex functions could be determined by solving the QCD bound-state equation. However, in practice, phenomenological vertex functions similar to those in the conventional light-front model are often employed. The covariant approach represents hadronic matrix elements of one-body currents as one-loop diagrams, evaluable using standard space-time formalism. This yields a covariant matrix element expressed as a Feynman momentum loop integral. Alternatively, light-front matrix elements can be obtained through light-front decomposition of the loop momentum and integration over the minus component (k'^-_1) using contour methods [52]. This integration technique requires vertex functions free of singu-

larities, with only quark propagator singularities contributing within the contour. A class of covariant meson vertex functions exhibits this property, characterized by asymmetry in the constituent quark–antiquark pair variables. The integration over the negative component of loop momentum defines the corresponding light-front vertex functions. This approach eliminates the spurious contributions that are proportional to the vector $\omega^\mu = (0, 2, 0_\perp)$. Consequently, transforming the covariant BS approach to the standard LFQM necessitates a light-front decomposition of the loop momentum and integration over its minus component. This transformation entails the following replacements:

$$N_1^{\prime(\prime\prime)} \to \hat{N}_1^{\prime(\prime\prime)} = x_1(M^{\prime(\prime\prime)2} - M_0^{\prime(\prime\prime)2}), \tag{22}$$

and

$$\chi_{M^{\prime(\prime\prime)}} = \frac{H_M^{\prime(\prime\prime)}}{N_1^{\prime(\prime\prime)}} \to \frac{h_M^{\prime(\prime\prime)}}{\hat{N}_1^{\prime(\prime\prime)}}, \quad D_{V,con}^{\prime(\prime\prime)} \to D_{V,LF}^{\prime(\prime\prime)}, \quad \text{(Type-I)} \tag{23}$$

where the D factor $D_{V,con}^{\prime(\prime\prime)} = M^{\prime(\prime\prime)} + m_1^{\prime(\prime\prime)} + m_2$ present in the vertex operator is substituted with $D_{V,LF}^{\prime(\prime\prime)} = M_0^{\prime(\prime\prime)} + m_1^{\prime(\prime\prime)} + m_2$ [45,63]. The light-front forms of vertex functions $h_{M'}$ for P and V mesons are given by

$$\frac{h_P}{\hat{N}_1^{\prime(\prime\prime)}} = \frac{h_V}{\hat{N}_1^{\prime(\prime\prime)}} = \frac{1}{\sqrt{2N_c}}\sqrt{\frac{x_2}{x_1}}\frac{\psi(x_1, \boldsymbol{k}_\perp^{\prime(\prime\prime)})}{\hat{M}_0^{\prime(\prime\prime)}}, \tag{24}$$

where $\hat{M}_0^{\prime(\prime\prime)} \equiv \sqrt{M_0^{\prime(\prime\prime)} - (m_1^{\prime(\prime\prime)} - m_2)^2}$. It should be noted that there is some debate regarding the self-consistency of the CLFQM [44,45,63]. The explicit validity of replacing $D_{V,con}^{\prime(\prime\prime)}$ with $D_{V,LF}^{\prime(\prime\prime)}$ leads to inconsistency issues in type-I correspondence. Chang et al. [62] found that the resulting $P \to V$ form factors extracted with the longitudinal ($\lambda = 0$) and transverse ($\lambda = \pm$) polarization states were not consistent with each other. This is because the $P \to V$ form factors obtained from the longitudinal polarization state receive an additional contribution characterized by the coefficients $B_1^{(2)}$ and $B_3^{(3)}$, which is noticeable in the B_c to V form factor expressions of $f(q^2)$ and $a_-(q^2)$. Furthermore, the manifest covariance of the matrix element in CLFQM is also violated in the type-I correspondence scheme because of the residual ω-dependencies associated with $B_j^{(i)}$ functions, which are independent of zero-mode contributions. Therefore, a proposed solution to address these inconsistencies observed in the type-I CLF form factors is to modify the relationship between the manifestly covariant BS approach and the standard LFQM [44,45,52]. In regard to this, Choi and Ji [45] suggested the replacement of $M^{\prime(\prime\prime)}$ with kinetic invariant mass $M_0^{\prime(\prime\prime)}$ in every term that contains $M^{\prime(\prime\prime)}$ within the integrand, in addition to the D factor. As a result, the correspondence given by Eq. (23) can be generalized to

$$\chi_{M^{\prime(\prime\prime)}} = \frac{H_M^{\prime(\prime\prime)}}{N_1^{\prime(\prime\prime)}} \to \frac{h_M^{\prime(\prime\prime)}}{\hat{N}_1^{\prime(\prime\prime)}}, \quad M^{\prime(\prime\prime)} \to M_0^{\prime(\prime\prime)}. \quad \text{(Type-II)} \tag{25}$$

Thus, by employing type-II correspondence from Eq. (25), the matrix element $\mathcal{B}$ in Eq. (19) will reduce to the light-front form,

$$\hat{\mathcal{B}} = N_c \int \frac{\mathrm{d}x_1 \mathrm{d}^2\boldsymbol{k}_\perp'}{2(2\pi)^3} \frac{h_{M'} h_{M''}}{x_2 \hat{N}_1' \hat{N}_1''} \hat{S}_{\mathcal{B}}. \tag{26}$$

Essentially, by embracing the type-II correspondence described by Eq. (25), the manifest covariance of the CLFQM can be restored, which in turn should yield numerically equal form factors for $\lambda = 0$ and $\lambda = \pm$ polarization states. Therefore, it can be inferred that type-II correspondence offers a potentially self-consistent framework that resolves the issues connected to the covariance of the matrix elements and the inconsistencies.

The determination of transition form factors for the B_c to ground-state s-wave meson for $q^2 = -q_\perp^2 \le 0$ is a straightforward process, since the calculation of the zero-mode contribution is obtained in a frame where the momentum transfer q^+ becomes zero. As a result, the form factors are only known for space-like momentum transfer $q^2 = (p' - p'')^2 = -q_\perp^2 \le 0$ [52]. Nevertheless, the transition form factors in the time-like region can be obtained through extrapolation, which will be discussed in the following subsection.

Furthermore, the B_c to $P(V)$ transition form factors are explicitly expressed as [62]

$$F(q^2) = N_c \int \frac{\mathrm{d}x_1 \mathrm{d}^2\boldsymbol{k}_\perp'}{(2\pi)^3} \frac{\chi'_{B_c} \chi''_{P(V)}}{2x_2} \widetilde{F}(x_1, \boldsymbol{k}_\perp', q^2), \tag{27}$$

where

$$\chi'_{B_c} = \frac{1}{\sqrt{2N_c}}\sqrt{\frac{x_2}{x_1}}\frac{\psi(x_1, \boldsymbol{k}_\perp')}{\hat{M}_0'},$$
$$\text{and } \chi''_{P(V)} = \frac{1}{\sqrt{2N_c}}\sqrt{\frac{x_2}{x_1}}\frac{\psi(x_1, \boldsymbol{k}_\perp'')}{\hat{M}_0''}. \tag{28}$$

It should be noted that the integration is carried out within the limits of [0, 1] and [0, ∞] for x_1 and $\boldsymbol{k}_\perp'$, respectively, in Eq. (27). The form factor functions $\widetilde{F}(x_1, \boldsymbol{k}_\perp', q^2) \equiv \{\widetilde{f}_\pm(x_1, \boldsymbol{k}_\perp', q^2), \ \widetilde{g}(x_1, \boldsymbol{k}_\perp', q^2), \ \widetilde{f}(x_1, \boldsymbol{k}_\perp', q^2), \ \widetilde{a}_\pm(x_1, \boldsymbol{k}_\perp', q^2)\}$ corresponding to B_c to $P(V)$ transitions are defined as follows:

(i) B_c to P form factors [44,63],

$$\widetilde{f}_+(x_1, \boldsymbol{k}_\perp', q^2) = x_1 M_0'^2 + x_1 M_0'' + x_2 q^2 - x_1(m_1' - m_2)^2 - x_1(m_1'' - m_2)^2 - x_2(m_1' - m_1'')^2, \tag{29}$$
$$\widetilde{f}_-(x_1, \boldsymbol{k}_\perp', q^2) = -2x_1 x_2 M'^2 - 2k_\perp'^2 - 2m_1' m_2$$

$$
\begin{aligned}
&+2(m_1''-m_2)(x_2m_1'+x_1m_2)\\
&-2\frac{\boldsymbol{k}'_\perp\cdot\boldsymbol{q}_\perp}{q^2}\Big[(x_1-x_2)M'^2+M''^2\\
&+x_2(q^2+q\cdot p)+2x_1M_0'^2\\
&-2(m_1'+m_1'')(m_1'-m_2)\Big]\\
&+4\frac{p\cdot q}{q^2}\Big[k_\perp'^2+\frac{2(\boldsymbol{k}'_\perp\cdot\boldsymbol{q}_\perp)^2}{q^2}\Big]\\
&+4\frac{(\boldsymbol{k}'_\perp\cdot\boldsymbol{q}_\perp)^2}{q^2}. \qquad (30)
\end{aligned}
$$

(ii) B_c to V form factors [44,62],

$$
\begin{aligned}
\widetilde{g}(x_1,\boldsymbol{k}'_\perp,q^2)&=-2\Big\{x_2m_1'+x_1m_2+(m_1'-m_1'')\frac{\boldsymbol{k}'_\perp\cdot\boldsymbol{q}_\perp}{q^2}\\
&+\frac{2}{D''_{V,con}}\Big[k_\perp'^2+\frac{(\boldsymbol{k}'_\perp\cdot\boldsymbol{q}_\perp)^2}{q^2}\Big]\Big\}, \qquad (31)\\
\widetilde{f}(x_1,\boldsymbol{k}'_\perp,q^2)&=-2\Big\{-(m_1'+m_1'')^2(m_1'-m_2)+(x_1m_2\\
&-x_2m_1')M'^2+(x_1m_2+x_2m_1')M''^2\\
&-x_1(m_2-m_1')(M_0'^2+M_0''^2)+2x_1m_1''M_0'^2\\
&-4(m_1'-m_2)\Big(k_\perp'^2+\frac{(\boldsymbol{k}'_\perp\cdot\boldsymbol{q}_\perp)^2}{q^2}\Big)\\
&-m_2q^2-(m_1'+m_1'')(q^2+q\cdot p)\frac{\boldsymbol{k}'_\perp\cdot\boldsymbol{q}_\perp}{q^2}\\
&+4(m_1'-m_2)B_1^{(2)}+\frac{2}{D''_{V,con}}\Big[\Big(k_\perp'^2\\
&+\frac{(\boldsymbol{k}'_\perp\cdot\boldsymbol{q}_\perp)^2}{q^2}\Big)\Big((x_1-x_2)M'^2+M''^2\\
&-2(m_1'-m_1'')(m_1'-m_2)+2x_1M_0'^2\\
&-q^2-2(q^2+q\cdot p)\frac{\boldsymbol{k}'_\perp\cdot\boldsymbol{q}_\perp}{q^2}\Big)\\
&-\Big(M'^2+M''^2-q^2+2(m_1'-m_2)(m_1''\\
&+m_2)\Big)B_1^{(2)}+2B_3^{(3)}\Big]\Big\}, \qquad (32)\\
\widetilde{a}_+(x_1,\boldsymbol{k}'_\perp,q^2)&=2\Big\{(m_1''-2x_1m_1'+m_1'+2x_1m_2)\frac{\boldsymbol{k}'_\perp\cdot\boldsymbol{q}_\perp}{q_\perp^2}\\
&+(x_1-x_2)(x_2m_1'+x_1m_2)+\frac{2}{D'_{V,con}}\\
&\times\frac{\boldsymbol{k}''_\perp\cdot\boldsymbol{q}_\perp}{x_2q_\perp^2}\Big[\boldsymbol{k}'_\perp\cdot\boldsymbol{k}''_\perp+(x_1m_2-x_2m_1'')\\
&\times(x_1m_2+x_2m_1')\Big]\Big\}, \qquad (33)\\
\widetilde{a}_-(x_1,\boldsymbol{k}'_\perp,q^2)&=-2\Big\{(3-2x_1)(x_2m_1'+x_1m_2)-\Big[(6x_1\\
&-7)m_1'+(4-6x_1)m_2+m_1''\Big]\frac{\boldsymbol{k}'_\perp\cdot\boldsymbol{q}_\perp}{q^2}\\
&+4(m_1'-m_2)\Big[2\Big(\frac{\boldsymbol{k}'_\perp\cdot\boldsymbol{q}_\perp}{q^2}\Big)^2+\frac{k_\perp'^2}{q^2}\Big]\\
&-4\frac{(m_1'-m_2)}{q^2}B_1^{(2)}+\frac{1}{D''_{V,con}}\Big[-2\big(M'^2\\
&+M''^2-q^2+2(m_1'-m_2)(m_1''+m_2)\big)\\
&\big(A_3^{(2)}+A_4^{(2)}-A_2^{(1)}\big)+\Big(2M'^2-q^2\\
&-x_1(M'^2-M_0'^2)+x_1(M''^2-M_0''^2)\\
&-2(m_1'-m_2)^2+(m_1'+m_1'')^2\Big)\big(A_1^{(1)}\\
&+A_2^{(1)}-1\big)+2Z_2\big(2A_4^{(2)}-3A_2^{(1)}+1\big)\\
&+2\frac{q\cdot p}{q^2}\big(4A_2^{(1)}A_1^{(2)}-3A_1^{(2)}\big)\\
&+\frac{2}{q^2}\Big(\big(M'^2+M''^2-q^2+2(m_1''-m_2)\\
&(m_1'+m_2)\big)B_1^{(2)}-2B_3^{(3)}\Big)\Big]\Big\}. \qquad (34)
\end{aligned}
$$

The coefficients $A_j^{(i)}$ and $B_j^{(i)}$ are given as [44,62]

$$
\begin{aligned}
&A_1^{(1)}=\frac{x_1}{2},\qquad A_1^{(2)}=-k_\perp'^2-\frac{(\boldsymbol{k}'_\perp\cdot\boldsymbol{q}_\perp)^2}{q^2},\\
&A_2^{(1)}=A_1^{(1)}-\frac{\boldsymbol{k}'_\perp\cdot\boldsymbol{q}_\perp}{q^2},\\
&A_3^{(2)}=A_1^{(1)}A_2^{(1)},\qquad A_4^{(2)}=(A_2^{(1)})^2-\frac{1}{q^2}A_1^{(2)},\\
&B_1^{(2)}=A_1^{(1)}Z_2-A_2^{(1)},\\
&B_3^{(3)}=B_1^{(2)}Z_2+\Big(p^2-\frac{(q\cdot p)^2}{q^2}\Big)A_1^{(1)}A_1^{(2)},\ \text{and} \qquad (35)\\
&Z_2=x_1(M'^2-M_0'^2)+m_1'^2-m_2^2+(1-2x_1)M'^2\\
&\quad+(q^2+q\cdot p)\frac{\boldsymbol{k}'_\perp\cdot\boldsymbol{q}_\perp}{q^2}. \qquad (36)
\end{aligned}
$$

It should be noted that the above given expressions for the form factors correspond to the traditional type-I scheme, for which type-II correspondence can be obtained by an additional replacement of $M'^{(\prime)}$ to $M_0'^{(\prime)}$ [62]. Moreover, the above form factor expressions are for the case of $\lambda=0$ (i.e., longitudinal polarization state), and the results for the case of $\lambda=\pm$ (i.e., transverse polarization states) can be obtained from these expressions by omitting the terms associated with $B_j^{(i)}$ functions.

It is well established that the light-front formalism, coupled with time-ordered perturbation theory, provides a systematic framework for calculating higher-order QCD corrections [71,73]. Nonetheless, significant challenges persist, including nonperturbative regimes, higher-order corrections, higher Fock states, and infrared divergences. Improving the precision and applicability of the light-front approach requires the incorporation of a more appropriate choice of wave functions and vertex functions [52]. Despite the computational challenges, however, incorporating higher-order QCD corrections is essential for the precise determination of

hadronic quantities such as form factors. Although scale-breaking effects are generally small, higher-order contributions through strong coupling constant and higher-twist effects are expected to modify QCD predictions [74,75]. Moreover, while zero-mode contributions partially account for higher Fock states, their direct inclusion presents substantial computational challenges. Furthermore, comprehending the nonperturbative aspects of QCD within the light-front approach requires the extension of renormalization techniques beyond perturbative methods [76,77].

2.2 q^2 dependence of the form factors

The numerical evaluation of B_c to $P(V)$ transition form factors requires an understanding of the momentum dependence of these form factors over the entire q^2 region in the CLFQM. Conventionally, the meson transition in the Drell–Yan–West frame with $q^+ = 0$ restricts the evaluation of the form factors for the momentum transfer $q^2 = -q_\perp^2 \leq 0$, i.e., space-like region [48,52,56,78]. However, only the form factors in the time-like region ($q^2 = -q_\perp^2 \geq 0$) are relevant for physical decay processes [44,52]. Therefore, to evaluate the total decay rate of B_c decays, the momentum dependence of the form factors should be reproduced in the space-like region and extrapolated to the time-like region using simplified parameterizations.

Jaus [48] proposed estimating the invariant form factors as functions of q^2, extending them analytically from space-like ($q^2 \leq 0$) to time-like regions ($q^2 \geq 0$) [29,44,62,65,78]. This reformulation relies on the assumption that the form factors are continuously differentiable with respect to q^2, emphasizing the importance of understanding their behavior near $q^2 = 0$ [48]. Therefore, understanding wave function overlaps between the initial- and final-state mesons near $q^2 = 0$ is significant. Furthermore, it has been argued that the form factors obtained directly in the time-like region ($q^+ > 0$) are equivalent to those from analytic continuation from the space-like region [59]. A more refined approach to computing form factors at $q^2 > 0$ involves calculations in a frame where the momentum transfer is purely longitudinal ($\boldsymbol{q}_\perp = 0$), covering the entire range of momentum transfer, as shown in Refs. [44,59], and more recently in Ref. [79]. However, it introduces additional complexity: beyond the conventional valence-quark contribution, one must also consider nonvalence configurations. These include phenomena such as the Z-graph, which arises from quark-pair creation from the vacuum. Consequently, uncertainties arise in transition form factors calculated for $q^2 \geq 0$ (with $\boldsymbol{q}_\perp = 0$) due to nonvalence configurations [79,80]. However, the estimations of these Z-graph contributions are still lacking within the CLFQM formalism. Recent efforts [81] show that the Z-graph contributions to form factors become more significant in the time-like regime ($q^2 > 0$). In the annihilation process of the emitted quark–antiquark system into a W-boson, intermediate vector-meson states dominate. This allows for approximation of the Z-graph contributions using a VMD-like decay mechanism [81]. Parameterizing form factors as meromorphic functions of q^2, with analytic continuation from $q^2 < 0$ to $q^2 > 0$ is proposed to reasonably describe form factors at time-like momentum transfers. However, considering a frame with purely transverse momentum transfer ($q^+ = 0$) is suggested to reduce nonvalence contributions [44]. In addition, zero-mode contributions affecting these transition form factors are addressed by the type-II self-consistent CLF approach.

In continuation of the previous section, it is well-established that the theoretical expressions formulated within the $q^+ = 0$ frame are specifically applicable for calculating form factors exclusively in the space-like domain. However, to extend our understanding to the time-like region, we require parameterization as explicit functions of q^2 to describe the form factors [78]. These descriptions of form factors in both space-like and time-like regions complement each other, providing valuable insights into the complete decay dynamics across the entire q^2 range. The literature suggests numerous functions of q^2 dependence influenced by the VMD approach, which has been used to parameterize and reproduce the transition form factors in space-like region and then extrapolate to physical form factors for $q^2 \geq 0$ [82–85]. The conventional form factor dependence on q^2 is often expressed as a BSW-type monopole approximation [72], $F(q^2) = F(0)/(1 - \frac{q^2}{M_{\rm pole}^2})$, based on VMD. However, this approach is not sufficient to explain the experimental observations. Moreover, higher resonance contributions are likely necessary beyond the monopole form. The nearest pole dominance assumption may not always apply because multiple resonances can be significant. Furthermore, given the complexity of nonperturbative physics governing q^2 dependence, no single parameterization is universally accurate. A more general approach involves using a simple pole and summing effective poles, though this requires multiple parameters to be determined experimentally [86,87].

In our analysis, the q^2 dependence of form factors in the space-like region can be effectively parameterized and reproduced using a three-parameter form [85] as follows:

$$F(q^2) = \frac{F(0)}{\left(1 - \frac{q^2}{M_{\rm pole}^2}\right)\left(1 - a\frac{q^2}{M_{\rm pole}^2} + b\frac{q^4}{M_{\rm pole}^4}\right)}, \quad \text{(referred to as T2A)} \tag{37}$$

where $M_{\rm pole}$ is the transition pole mass. The parameters a, b, and $F(0)$ are determined by fitting Eq. (37) in the space-like region and the extrapolation to the physical region $q^2 \geq 0$. In the type-II correspondence scheme, the numerical results obtained using the parameterization Eq. (37) are referred to

Table 1 Transition pole masses for $B_c \to P$ and V form factors (in GeV)

Quark transition	$F_1(q^2), V(q^2)$ $J^P = 1^-$	$F_0(q^2)$ 0^+	$A_0(q^2)$ 0^-	$A_1(q^2), A_2(q^2)$ 1^+
Bottom-conserving transitions				
$c \to d$	2.010	2.308	1.870	2.422
$c \to s$	2.112	2.318	1.968	2.460
Bottom-changing transitions				
$b \to u$	5.325	5.670	5.279	5.726
$b \to s$	5.415	5.762	5.367	5.829
$b \to c$	6.473	6.836	6.274	6.866

as "T2A" throughout the manuscript. Typically, the parameterization presented in Eq. (37) is characterized as a four-parameter fit, wherein the parameters $F(0)$, a, b, and $M_{\rm pole}$ are ideally determined from the available experimental data. In order to maintain the validity of our calculations and select appropriate quark-model parameters due to the lack of experimental data, we utilize the mass of the nearest pole (listed in Table 1) as the pole mass ($M_{\rm pole}$) to describe it as a three-parameter fit [85,88]. The parameterization (Eq. (37)) incorporates slope parameters a and b to account for effective poles. These poles deviate from the single resonance typically observed in the $q_1' \to q_1''$ transition. In simpler terms, slope parameters represent additional poles beyond the pole mass ($M_{\rm pole}$), reflecting the influence of higher-order resonances [13]. The phenomenological accuracy and reliability of q^2 dependence, given in Eq. (37), have been extensively discussed in Refs. [85–88].

It is worth mentioning that the available q^2 range for the bottom-conserving $B_c \to P(V)$ transitions is $0 \le q^2 \lesssim 1$ GeV^2. However, for bottom-changing transitions, the q^2 range is considerably larger, i.e., $0 \le q^2 \lesssim 20$ GeV^2. Since the $M^2_{\rm pole}$ is greater than the available q^2 in heavy-to-heavy meson transitions, the contributing poles lie farther from the kinematic region. Therefore, it is important to accurately determine the q^2 dependence in decay amplitudes across the entire kinematic range [88]. The implementation of the aforementioned parameterization is particularly relevant in bottom-changing decays due to the extensive q^2 range, wherein contributions from bottom, bottom-strange, and bottom-charmed resonances may be substantial. This can be explained through the confining interaction, for example, between b and $\bar{u}$ to produce B meson resonances that fluctuate into W-boson. In transitions involving significant momentum transfer ($q^2_{\rm max} \simeq 20$ GeV^2), the incorporation of higher-order contributions becomes imperative for accurate modeling of physical decay processes. Form factors spanning such extensive q^2 ranges cannot be adequately described by considering only a limited number of initial physical poles [89]. Consequently, the poles associated with these form factors are situated at $q^2 = M^2_{\rm pole}$ (as detailed in Table 1), typically at unphysical values of time-like momentum transfer, distinct from $q^2_{\rm max}$. The parameterization outlined in Eq. (37) offers a viable solution for such scenarios. This parameterization (Eq. (37)) is also applicable to $B_c \to B^{(*)}_{(s)}$ transitions. Note that the production threshold for mesons (e.g., $D_{(s)}$ resonances being lightest) from the $c \to d(s)$ current occurs at q^2 values where the poles are significantly far from the physical region of $q^2_{\rm max} \simeq 1$ GeV^2. This integration enables a comprehensive exploration of the entire physical momentum transfer range, potentially leading to a significant enhancement in the accuracy of our predictions.

Furthermore, the q^2 dependence of the form factors defined by Eq. (37) involves contributions from said resonances of particular spin in the available q^2 range; for example, the form factors $F_1(q^2)$ and $V(q^2)$ exhibit a pole at $q^2 = M^2_{1^-}$, while $A_0(q^2)$ contains a pole at $q^2 = M^2_{0^-}$. It is important to note that the remaining form factors, namely, $F_0(q^2)$, $A_1(q^2)$, and $A_2(q^2)$, do not receive contributions from the lowest-lying negative parity states [90]. The form factor $F_0(q^2)$ includes the pole mass corresponding to the 0^+ state, whereas $A_1(q^2)$ and $A_2(q^2)$ incorporate the 1^+ state; interestingly, both have significantly higher masses [85–87], as shown in Table 1. As a result, these form factors are expected to show less variation in the decay region for the available q^2.

It should also be noted that for the calculation of transition form factors, several other theoretical studies have employed the following q^2 dependence [44,62]:

$$F(q^2) = \frac{F(0)}{1 - a\frac{q^2}{M^2_{B_c}} + b\frac{q^4}{M^4_{B_c}}}, \quad \text{(referred to as T1)} \qquad (38)$$

where the mass of the parent meson $M_{B_c} = 6274.47$ MeV [12] is taken as the pole mass. We use this parameterization in the type-I correspondence, denoted as "T1" in the numerical results, for the sake of comparison. It is expected that the parameterization presented in Eq. (38) is also valid for the physical decay region [88].

Alternatively, many experimental and lattice observations are made using a model-independent parameterization fol-

lowing the general QCD constraints, which is known as z-series (expansion) parameterization. The utilization of forms such as Eqs. (37) and (38) for data fitting, while mathematically feasible, presents interpretative challenges due to the absence of clear physical significance for the resulting fit parameters. This ambiguity raises concerns that different experimental (small q^2) or lattice (large q^2) determinations may not converge to a single value. Therefore, discrepancies arising from fitting different datasets to models like single-pole or modified pole models become ambiguous [91,92]. This issue becomes especially challenging when comparing lattice and experimental data due to differing emphasized ranges of the parameter q^2 (usually represented as t). To navigate these challenges, it is advisable to use a general parameterization like z-series parameterization, which ensures the inclusion of the true form factor. This approach facilitates more robust comparisons of physical quantities, ensuring that the analysis remains grounded in observable phenomena rather than potentially arbitrary fitting parameters [87].

In order to establish a clear understanding of q^2 dependence and comparison among different q^2 formulations, we also incorporate z-series expansion form. Furthermore, the z-series parameterization is given in terms of a complex parameter z, which is the analytic continuation of q^2 into the complex plane [13]. This parameterization of the form factor is based on the power series expansion around the value $q^2 = t_0$. Thus, the form factor is expressed as [93],

$$F(q^2) = \frac{1}{1-\frac{q^2}{M_{\rm pole}^2}} \sum_{k=0}^{K} a_k' \big[z(q^2) - z(0)\big]^k, \quad \text{(referred to as T2B)} \tag{39}$$

where a_k are real coefficients and $z(q^2) \equiv z(q^2, t_0)$ is the function

$$z(q^2) = \frac{\sqrt{t_+ - q^2} - \sqrt{t_+ - t_0}}{\sqrt{t_+ - q^2} + \sqrt{t_+ - t_0}}, \tag{40}$$

which maps the q^2-plane cut for $q^2 \geq t_+$ onto the disk $|z(q^2, t_0)| < 1$ in the z-complex plane, such that $|z(t_+, t_0)| = -1$ and $|z(\infty, t_0)| = 1$. The arbitrary parameter $t_0 < t_+$ determines the point q^2 mapped onto the origin in the z-plane, i.e., $|z(t_0, t_0)| = 0$ corresponding to $q^2 = t_0$, and the physical region extends in either direction up to $\pm|z|_{\rm max}$ [94]. The parameters t_+ and t_0 are $(M_{B_c} + M_{P(V)})^2$ and $(M_{B_c} + M_{P(V)})(\sqrt{M_{B_c}} - \sqrt{M_{P(V)}})^2$, respectively [93,94]. In comparison to other phenomenological approaches, the fitted coefficients a_k' have no physical interpretation [13]. Since the higher-order terms in the z-series parameterization given in Eq. (39) have trivial contributions, we restrict ourselves to the power $K = 2$, which contains the free parameters a_0' ($\approx F(0)$), a_1', and a_2'. Unlike Eq. (37), the numerical results corresponding to parameterization by Eq. (39) in the type-II correspondence are designated as "T2B".

2.3 Semileptonic decay widths and other physical observables

The differential decay width of B_c to $P(V)$ semileptonic decays is expressed in terms of the helicity components as [32,95]

$$\frac{{\rm d}\Gamma(B_c^+ \to P(V) l^+ \nu_l)}{{\rm d}q^2} = \frac{G_F^2}{(2\pi)^3} |V_{q_1q_2}|^2 \frac{q^2\sqrt{\lambda}}{24 M_{B_c}^3} \left(1 - \frac{m_l^2}{q^2}\right)^2 \mathcal{H}_{\rm total}, \tag{41}$$

where G_F is the Fermi constant and $V_{q_1q_2}$ is the relevant CKM matrix element for $q_1 \to q_2$ transition. The term $\lambda \equiv \lambda(M_{B_c}^2, M_{P(V)}^2, q^2) = (M_{B_c}^2 + M_{P(V)}^2 + q^2)^2 - 4M_{B_c}^2 M_{P(V)}^2$ is the Källén function, and m_l is the lepton mass ($l = e,\ \mu,\ \tau$). The total helicity structure, $\mathcal{H}_{\rm total}$, is given by

$$\mathcal{H}_{\rm total} = (\mathcal{H}_U + \mathcal{H}_L)\left(1 + \frac{m_l^2}{2q^2}\right) + \frac{3m_l^2}{2q^2}\mathcal{H}_S, \tag{42}$$

where $\frac{m_l^2}{2q^2}$ is referred to as the helicity flip factor, and the helicity components $\mathcal{H}_U$, $\mathcal{H}_L$, and $\mathcal{H}_S$ can be defined as

$$\mathcal{H}_U = |H_+|^2 + |H_-|^2, \quad \mathcal{H}_L = |H_0|^2, \quad \text{and} \quad \mathcal{H}_S = |H_t|^2, \tag{43}$$

where $H_\pm$, H_0, and H_t are the helicity amplitudes. These helicity amplitudes are related to the corresponding invariant form factors by the following relations:

(i) For B_c to P meson transitions,

$$H_\pm(q^2) = 0, \quad H_0(q^2) = \frac{\sqrt{\lambda}}{\sqrt{q^2}} F_1(q^2), \quad \text{and} \quad H_t(q^2) = \frac{1}{\sqrt{q^2}}(M_{B_c}^2 - M_P^2) F_0(q^2). \tag{44}$$

(ii) For B_c to V meson transitions,

$$H_\pm(q^2) = (M_{B_c} + M_V) A_1(q^2) \mp \frac{\sqrt{\lambda}}{M_{B_c} + M_V} V(q^2), \tag{45}$$

$$H_0(q^2) = \frac{1}{2M_V\sqrt{q^2}}(M_{B_c} + M_V)(M_{B_c}^2 - M_V^2 - q^2) \times A_1(q^2) - \frac{\lambda}{M_{B_c} + M_V} A_2(q^2), \tag{46}$$

$$H_t(q^2) = \frac{\sqrt{\lambda}}{\sqrt{q^2}} A_0(q^2). \tag{47}$$

Following Eq. (41), the longitudinal and transverse differential decay widths are given by

$$\frac{d\Gamma_L(B_c^+ \to Vl^+\nu_l)}{dq^2} = \frac{G_F^2}{(2\pi)^3}|V_{q_1q_2}|^2 \frac{q^2\sqrt{\lambda}}{24M_{B_c}^3}\left(1-\frac{m_l^2}{q^2}\right)^2 \times\left[\mathcal{H}_L\left(1+\frac{m_l^2}{2q^2}\right)+\frac{3m_l^2}{2q^2}\mathcal{H}_S\right], \quad \text{and} \tag{48}$$

$$\frac{d\Gamma_T(B_c^+ \to Vl^+\nu_l)}{dq^2} = \frac{G_F^2}{(2\pi)^3}|V_{q_1q_2}|^2 \frac{q^2\sqrt{\lambda}}{24M_{B_c}^3}\left(1-\frac{m_l^2}{q^2}\right)^2\left[\mathcal{H}_U\left(1+\frac{m_l^2}{2q^2}\right)\right], \tag{49}$$

respectively.

In order to gain a deeper understanding of semileptonic decays beyond just the branching ratios, it is helpful to investigate the influence of the lepton mass. Moreover, by defining additional physical observables that are experimentally measurable, we can obtain a more comprehensive and intricate depiction of the underlying physics in these decays. Some of these physical observables are FB asymmetry ($A_{\rm FB}(q^2)$), leptonic convexity parameter ($C_F^l(q^2)$), longitudinal (transverse) ($P_{L(T)}^l(q^2)$) polarization of the charged lepton, and asymmetry parameter ($\alpha^*(q^2)$). These observables can be expressed by the above helicity structure functions as [32,96]

$$A_{FB}(q^2) = \frac{3}{4}\frac{\mathcal{H}_P - 2\frac{m_l^2}{q^2}\mathcal{H}_{SL}}{\mathcal{H}_{\rm total}}, \tag{50}$$

$$C_F^l(q^2) = \frac{3}{4}\left(1-\frac{m_l^2}{q^2}\right)\frac{\mathcal{H}_U - 2\mathcal{H}_L}{\mathcal{H}_{\rm total}}, \tag{51}$$

$$P_L^l(q^2) = \frac{(\mathcal{H}_U+\mathcal{H}_L)\left(1-\frac{m_l^2}{2q^2}\right)-\frac{3m_l^2}{2q^2}\mathcal{H}_S}{\mathcal{H}_{\rm total}}, \tag{52}$$

$$P_T^l(q^2) = -\frac{3\pi m_l}{8\sqrt{q^2}}\frac{\mathcal{H}_P+2\mathcal{H}_{SL}}{\mathcal{H}_{\rm total}}, \quad \text{and} \tag{53}$$

$$\alpha^*(q^2) = \frac{\mathcal{H}_U+\widetilde{\mathcal{H}}_U-2(\mathcal{H}_L+\widetilde{\mathcal{H}}_L+3\widetilde{\mathcal{H}}_S)}{\mathcal{H}_U+\widetilde{\mathcal{H}}_U+2(\mathcal{H}_L+\widetilde{\mathcal{H}}_L+3\widetilde{\mathcal{H}}_S)}, \tag{54}$$

where $\widetilde{\mathcal{H}}_i = \frac{m_l^2}{2q^2}\mathcal{H}_i$ for ($i = U, L, S$). The A_{FB} quantifies the difference between the number of leptons (l^+/l^-) emitted in the (forward) direction of B_c momentum and those emitted in the opposite (backward) direction in the rest frame of the lepton pair ($l\nu_l$) [97,98]. The helicity components $\mathcal{H}_P$ and $\mathcal{H}_{SL}$ are defined by $\mathcal{H}_P = |H_+|^2 - |H_-|^2$ and $\mathcal{H}_{SL} = \mathcal{R}(H_0H_t^\dagger)$. Similarly, the remaining observables defined in terms of helicity amplitudes are expected to be crucial for probing potential NP beyond the SM. Modern experimental facilities are expected to provide precise measurements of the angular distributions of semileptonic decay. These observables can serve as powerful probes for detecting NP in low-energy semileptonic decay processes, with the advantage of minimal sensitivity to hadronic uncertainties [99]. For $B_c^- \to Vl^-\bar{\nu}_l$ decays, the physical observables like FB asymmetry, longitudinal polarization and transverse polarization of the charged lepton are altered due to the opposite sign in the leptonic tensor [32]. However, there is no change in the expression for other observables. In this study, we calculate the mean values of all the abovementioned physical observables by separately integrating the numerator and denominator over q^2, with the inclusion of a kinematic factor $q^2\sqrt{\lambda}(1-\frac{m_l^2}{q^2})^2$, where $(1-\frac{m_l^2}{q^2})$ represents the velocity-type parameter.

2.4 Nonleptonic decay widths

The QCD-modified weak Hamiltonian generating the B_c^+ decay involving $b \to c(u)$ transitions is expressed as follows [100]:

$$H_w^{(\Delta b=-1)} = \frac{G_F}{\sqrt{2}}\sum_{Q(q)=u,c}\sum_{q'=d,s} V_{Qb}^*V_{qq'} \times\left(a_1(\mu)O_1^{qq'}(\mu)+a_2(\mu)O_2^{qq'}(\mu)\right)+\text{h.c.}, \tag{55}$$

where a_1 and a_2 are the standard perturbative QCD coefficients, evaluated at renormalization scale $\mu \approx m_b^2$. Local tree-level operators $O_{1,2}$ involving $b \to q$ transition can be expressed as products of color-singlet currents, as given below:

$$\begin{aligned} O_1^{qd} &= (\bar{b}_\alpha q_\alpha)_{V-A}\cdot(\bar{q}_\beta d_\beta)_{V-A},\\ O_2^{qd} &= (\bar{b}_\alpha q_\beta)_{V-A}\cdot(\bar{q}_\beta d_\alpha)_{V-A},\\ O_1^{qs} &= (\bar{b}_\alpha q_\alpha)_{V-A}\cdot(\bar{q}_\beta s_\beta)_{V-A},\\ O_2^{qs} &= (\bar{b}_\alpha q_\beta)_{V-A}\cdot(\bar{q}_\beta s_\alpha)_{V-A}, \end{aligned} \tag{56}$$

where $(\bar{q}q')_{V-A} \equiv \bar{q}\gamma_\mu(1-\gamma_5)q'$, α and β are $SU(3)$ color indices. Selection rules for various decay modes corresponding to the Hamiltonian, Eq. (55), are as follows:

(i) CKM-enhanced modes $\Delta b = -1, \Delta C = -1, \Delta S = 0$; $\Delta b = -1, \Delta C = 0, \Delta S = 1$;
(ii) CKM-suppressed modes $\Delta b = -1, \Delta C = -1, \Delta S = 1$; $\Delta b = -1, \Delta C = 0, \Delta S = 0$;
(ii) CKM-doubly-suppressed modes $\Delta b = -1, \Delta C = 1, \Delta S = 1$; $\Delta b = -1, \Delta C = 1, \Delta S = 0$.

In addition to the bottom-changing decays, the B_c^+ meson can exhibit bottom-conserving decay modes for the c quark

Table 2 Decay constants for P and V mesons (in MeV)

Decay constants			
f_π	130.56 [12]	f_ρ	210 [111]
f_K	155.7 [12]	f_{K^*}	204 [111]
f_η	(181.14) [113]	f_ϕ	(228.5) [114]
f_D	203.8 [12]	f_{D^*}	(223.5) [115]
f_{D_s}	250.1 [12]	$f_{D_s{}^*}$	213 [112]
f_{η_c}	335 [12]	$f_{J/\psi}$	416 [12]

Available experimental values are listed. The numerical values in the parentheses are from LQCD. Note that we only listed the central values (uncertainties are ignored)

decaying to an s or d quark. The weak Hamiltonian generating the c quark decays, $H_w^{(\Delta C=-1)}$, is expressed by replacing b with c, $Q(q) = d, s$, and $q' = u$ in Eq. (55). The selection rules for various bottom-conserving decay channels are given as

(i) CKM-enhanced mode $\Delta b = 0, \Delta C = -1, \Delta S = -1$;
(ii) CKM-suppressed mode $\Delta b = 0, \Delta C = -1, \Delta S = 0$;
(ii) CKM-doubly-suppressed mode $\Delta b = 0, \Delta C = -1, \Delta S = 1$.

The factorization scheme expresses the decay amplitudes as a product of the matrix elements of weak currents, i.e.,

$$\mathcal{A}(B_c \to PV) \simeq \langle P|J^\mu|0\rangle\langle V|J_\mu|B_c\rangle + \langle V|J^\mu|0\rangle\langle P|J_\mu|B_c\rangle, \tag{57}$$

where J^μ stands for $V - A$ current. The matrix element of the J^μ between vacuum and final meson (P or V) is parameterized by the decay constants $f_{P(V)}$ as

$$\begin{aligned}\langle 0|J_\mu|P(p')\rangle &= \langle 0|A_\mu|P(p')\rangle = if_P p'_\mu,\\ \langle 0|J_\mu|V(p',\varepsilon')\rangle &= \langle 0|V_\mu|V(p',\varepsilon')\rangle = M'_V f_V \varepsilon'_\mu.\end{aligned} \tag{58}$$

The values of the decay constants used in our calculations are given in Table 2.

The nonleptonic B_c decays can be categorized based on the color-favored and color-suppressed contribution into three classes, as follows [101–103]:

(i) Class I: Decays primarily governed by color-favored diagrams, which can be generated from the color singlet current, and their decay amplitudes are proportional to a_1, given by $a_1(\mu) = c_1(\mu) + \frac{1}{N_c}c_2(\mu)$, where N_c represents the number of colors, and $c_1(\mu)$ and $c_2(\mu)$ are the QCD coefficients.
(ii) Class II: Decays primarily influenced by color-suppressed diagrams, which can be generated from the neutral current, and their decay amplitudes are proportional to a_2, defined as $a_2(\mu) = c_2(\mu) + \frac{1}{N_c}c_1(\mu)$.
(iii) Class III: Decays resulting from a combination of both color-favored and color-suppressed diagrams, which can be generated from the interference of color singlet and color neutral currents, i.e., the a_1 and a_2 amplitudes interfere.

In general, the color-favored decay amplitude can be expressed as [104]

$$\begin{aligned}\mathcal{A}(B_c \to PV) = \frac{G_F}{\sqrt{2}} \times \text{CKM factors} \times 2M_V a_1 \\ \times (\text{CG Coeff.} f_V F_1^{B_c P}(M_V^2) \\ + \text{CG Coeff.} f_P A_0^{B_c V}(M_P^2)).\end{aligned} \tag{59}$$

For the color-suppressed modes, the QCD factor a_1 is replaced by a_2. It is important to note that a_1 and a_2 are undetermined coefficients assigned to the effective charged current and effective neutral current, respectively [105]. For the sake of consistency with the large N_c limit (i.e., $N_c = \infty$), we adopt the convention of setting the QCD coefficients $a_1 \approx c_1$ and $a_2 \approx c_2$, as suggested in Refs. [101,102]. The numerical values we employ are as follows:

$$\begin{aligned}&\text{For } c \text{ decays } (i.e., \mu \approx m_c^2):\\ &\quad c_1(\mu) = 1.26;\ c_2(\mu) = -0.51,\\ &\text{For } b \text{ decays } (i.e., \mu \approx m_b^2):\\ &\quad c_1(\mu) = 1.12;\ c_2(\mu) = -0.26.\end{aligned} \tag{60}$$

The relatively small magnitudes of a_2 imply that, unlike in the charm sector, one anticipates a more pronounced pattern of color suppression in B_c meson decays [101]. Since B_c decays primarily occur through tree diagrams or are tree-dominated, we neglect the anticipated small nonfactorizable and penguin contributions within our formalism. It may be noted that N_c may be treated as a phenomenological parameter in weak meson decays, which account for nonfactorizable contributions [106,107]. Therefore, we also use $N_c = 3$ to obtain the effective coefficients $a_1(\mu) = c_1(\mu) + \frac{1}{3}c_2(\mu)$ and $a_2(\mu) = c_2(\mu) + \frac{1}{3}c_1(\mu)$,

$$\begin{aligned}&\text{for } c \text{ decays (at } N_c = 3):\ a_1(\mu) = 1.09;\ a_2(\mu) = -0.09,\\ &\text{for } b \text{ decays (at } N_c = 3):\ a_1(\mu) = 1.03;\ a_2(\mu) = 0.11.\end{aligned} \tag{61}$$

We have calculated nonleptonic branching ratios of $B_c \to PV$ decays at both $N_c = \infty$ and $N_c = 3$. It is worth noting that for bottom-conserving decays, experimental charm decay studies have provided a parameterization for a_1 and a_2. These results suggest that considering the large N_c limit is

Table 3 Constituent quark masses and the Gaussian parameters β for P and V mesons

Constituent quark masses (in GeV)					
$m_u = m_d = 0.26 \pm 0.04$;		$m_s = 0.45 \pm 0.05$;		$m_c = 1.45 \pm 0.20$;	$m_b = 4.64 \pm 0.20$
Gaussian parameters β (in GeV)					
$^{2S+1}L_J$	$^1S_0$	$^3S_1$	$^{2S+1}L_J$	$^1S_0$	$^3S_1$
$\beta_{c\bar{q}}$	$0.4656^{+0.0217}_{-0.0212}$	0.4255 ± 0.0426	$\beta_{b\bar{q}}$	$0.5547^{+0.0260}_{-0.0261}$	0.5183 ± 0.0518
$\beta_{c\bar{s}}$	$0.5358^{+0.0137}_{-0.0135}$	0.4484 ± 0.0448	$\beta_{b\bar{s}}$	$0.6103^{+0.0330}_{-0.0331}$	0.5589 ± 0.0559
$\beta_{c\bar{c}}$	0.7690 ± 0.0049	0.6492 ± 0.0069	$\beta_{b\bar{c}}$	0.9207 ± 0.0921	–

Note that here, q denotes either u or d quark

appropriate for c quark decays [108]. On the other hand, for bottom-changing decays, phenomenological analyses [109] indicate variations in the magnitudes of the Wilson coefficients a_1 and a_2, as well as sub-leading contributions from the $1/N_c$ term. This can be accounted for by allowing a certain range of values for these coefficients, as shown in Eq. (61). We would like to emphasize that the decay amplitudes can be expressed as factorizable contributions multiplied by their respective a_i values, which are independent of the (renormalization) scale and process.

Using the decay amplitude defined in Eq. (59), the decay rate for the B_c to PV decay is given by

$$\Gamma(B_c \to PV) = \frac{\mathbf{k}^3}{8\pi M_V^2} |\mathcal{A}(B_c \to PV)|^2, \tag{62}$$

where $\mathbf{k}$ is the three-momentum of the final-state particle in the rest frame of the B_c meson and is expressed as

$$\mathbf{k} = \frac{1}{2M_{B_c}} \sqrt{[M_{B_c}^2 - (M_P + M_V)^2][M_{B_c}^2 - (M_P - M_V)^2]}. \tag{63}$$

The numerical results for semileptonic and nonleptonic weak decays of the B_c meson are discussed in the following section.

3 Numerical results and discussion

In the present work, we calculate the transition form factors for B_c to P and V using the type-II self-consistent CLFQM across the available range of momentum transfer. Furthermore, we provide a comprehensive investigation into their dependence on q^2 and compare our results with other formalisms. We compute the transition form factors for B_c to P and V mesons using the constituent quark masses and β values provided in Table 3. The variation in quark masses introduces uncertainties in form factor calculations. Therefore, we incorporate a range of values based on established literature as the default input [27–29,31,46,62,63]. It may be noted that the Gaussian parameter β, which characterizes the momentum distribution, is commonly determined by fitting the meson decay constant. In our work, we use the β values from Ref. [46] for the majority of s-wave mesons (corresponding to the input quark masses), which typically match with the latest decay constants provided in the Particle Data Group (PDG) [12], and other analysis based on experimental results[2] [111–115], as shown in Table 2. Furthermore, the values used for β parameters are reasonably close to the latest results obtained in the self-consistent CLFQM approach [61–63], although the theoretical uncertainties used in our work correspond to a wider range. On the other hand, for the B_c meson, the scenario is different due to the lack of experimental data and a wide range of decay constant estimates available in the literature [28,63,116–119]. Thus, we have used $\beta_{b\bar{c}} = (0.9207 \pm 0.0921)$ GeV, where the central value (as obtained in Ref. [62]) reproduces the LQCD estimates for decay constants.[3] In addition, we have allowed larger uncertainties typically to address the wide domain of decay constant predictions that range from $f_{B_c} = (371-489)$ MeV, for various theoretical models [28,63,116–119]. In this work, we have investigated the variation in the form factors and their slope parameters for q^2 dependence concerning changes in constituent quark masses and β values. We contrast our results in type-I and type-II correspondence schemes for form factors as well as branching ratios for semileptonic and nonleptonic decays. As mentioned earlier, we use three different q^2 formulations, namely, T2A, T2B, and T1, following Eqs. (37), (39), and (38), respectively. The transition pole masses given in Table 1 are used to calculate the form factors for both T2A and T2B, while we fix the mass of the parent meson as the pole for T1. The form factors obtained for bottom-conserving and bottom-changing transitions are tabulated in Tables 4 and 5, respectively. We plot their q^2 dependence for the available range $0 \le q^2 \le q^2_{\rm max} =$

[2] The experimental averages for b-meson decay constants are not available in PDG; however, recent LQCD predictions yield $f_B = (190.0 \pm 1.3)$ MeV [110], $f_{B_s} = (230.3 \pm 1.3)$ MeV [110].

[3] The LQCD predicts the decay constant for B_c as $f_{B_c} = (434 \pm 15)$ MeV [119], for which the values of $\beta_{b\bar{c}}$ can be obtained.

$(M_{B_c} - M_{P(V)})^2$, as shown in Figs. 2, 3, 4, and 5. We also plot corresponding wave function overlap (Eq. (5)) and overlap integrand (Eq. (27)) at $q^2 = 0$, as shown in Figs. 6, 7, 8, and 9. Using the numerical values of the form factors, we predict the branching ratios for semileptonic decays of the B_c meson,[4] as shown in Tables 6 and 7. In our calculations, we use the following values for the lepton mass: $m_e = 0.511$ MeV, $m_\mu = 105.66$ MeV, and $m_\tau = 1776.86$ MeV; CKM matrix elements: $|V_{ub}| = (3.82 \pm 0.20) \times 10^{-3}$, $|V_{cd}| = 0.221 \pm 0.004$, $|V_{cs}| = 0.975 \pm 0.006$, and $|V_{cb}| = (40.8 \pm 1.4) \times 10^{-3}$, and lifetime of B_c meson: $\tau_{B_c} = 0.51$ ps [12]. It should be noted that the uncertainties in the masses of mesons (leptons) and other parameters have been neglected due to their considerably smaller magnitude in comparison to the uncertainties in both quark masses and β parameters. Also, we compare our results of semileptonic branching ratios with the existing literature, as shown in Table 7. Besides determining the branching ratios, we also calculate the numerical values of various physical observables, such as $A_{\rm FB}(q^2)$, $C_F^l(q^2)$, $P_{L(T)}^l(q^2)$, and $\alpha^*(q^2)$, as listed in Table 6. Additionally, we plot the differential decay rates and FB asymmetries for $B_c^+ \to V l^+ \nu_l$ decays in Figs. 10 and 11, respectively. Finally, we utilize the obtained form factors and the decay constants listed in Table 2 to predict the branching ratios of nonleptonic B_c to PV decays[5]. The obtained results are presented in Tables 8, 9, 10, and 11. We also compare our predictions for nonleptonic branching ratios with other theoretical works, as shown in Tables 12, 13, and 14. We discuss our numerical results as follows.

3.1 Form factors

In this subsection, we discuss the results for the self-consistent B_c to V transition form factors along with B_c to P for bottom-conserving CKM-enhanced ($\Delta b = 0, \Delta C = -1, \Delta S = -1$) and suppressed ($\Delta b = 0, \Delta C = -1, \Delta S = 0$) modes, as well as bottom-changing CKM-enhanced ($\Delta b = -1, \Delta C = -1, \Delta S = 0$; $\Delta b = -1, \Delta C = 0, \Delta S = 1$) and suppressed ($\Delta b = -1, \Delta C = 0, \Delta S = 0$) modes. We also contrast the form factors in type-I and type-II schemes corresponding to different q^2 dependence formulations, as presented in Tables 4 and 5. The form factors are presented at $q^2 = 0$ and at the maximum q^2. The first and second uncertainties on the form factors and slope parameters (a, b, a_1', and a_2') are from the constituent quark masses and the β values, respectively. As noted earlier, to observe the variation in both T2A and T2B form factors with respect to q^2, we plot these transition form factors, as shown in Figs. 2, 3, 4, and 5. In order to numerically show the resolution of self-consistency, we analyzed the affected $f(q^2)$ and $a_-(q^2)$ form factors for $\lambda = 0$ and $\lambda = \pm$ polarization states. As was mentioned, these form factors are affected by inconsistency issues arising from the additional contributions characterized by the coefficients $B_1^{(2)}$ and $B_3^{(3)}$. We present the numerical results for these form factors for respective $\lambda = 0$ and $\lambda = \pm$ polarization states in both type-I and type-II correspondence schemes. These results are shown in Tables 15 and 16 of Appendix A. We list our observations as follows.

3.1.1 *Bottom-conserving transition form factors*

(i) The bottom-conserving $B_c \to B_{(s)}$ transitions are governed by c quark decays, for which the observed q^2 range is limited to a narrow interval of $0 \le q^2 \le (M_{B_c} - M_{B_{(s)}})^2 \simeq 1\ \text{GeV}^2$. As a result, we expect these form factors to show minimal variations corresponding to the available q^2 range, as shown in Fig. 2. The T2B form factors, corresponding to z-series parameterization, show more deviation than T2A form factors. This is because different q^2 formulations (Eqs. (37) and (39)) are used in the analyses. It must be noted that $B_c \to P$ form factors are free from self-consistency issues, by replacement of $M'^{(\prime\prime)} \to M_0'^{(\prime\prime)}$ in type-II correspondence, which results in modified numerical values. In addition, the choice of q^2 dependence between the two schemes, i.e., Eqs. (37) and (39) in type-II and Eq. (38) in type-I correspondence, will also lead to changes in the numerical values of form factors and parameters (a, b, a_1', and a_2'). It is important to note that for the type-I correspondence scheme, the numerical values are computed using the parent pole mass in Eq. (38), as recommended in previous studies [44,63]. This approach contrasts with the type-II correspondence, where we employ transition pole masses in Eqs. (37) and (39). We observe that $B_c \to B_{(s)}$ form factors in the type-I scheme show marginal change in $F(0)$ values as compared to the type-II scheme. However, the slope parameters differ significantly between the two.[6] In type-II correspondence, the slope parameters a and b in T2A are characterized by values less than unity. Conversely, for the z-series parameterization (T2B), the coefficients a_1' and a_2' exhibit substantially larger magnitudes; unfortunately, there cannot be any physical interpretation asso-

[4] The branching ratio is calculated from the decay rate expression given in Eq. (41) by multiplying by $\frac{\tau_{B_c}}{\hbar}$.

[5] Note that for η and η' pseudoscalar states, we use $\eta = \frac{1}{\sqrt{2}}(u\bar{u} + d\bar{d})\sin\phi_P - (s\bar{s})\cos\phi_P$, $\eta' = \frac{1}{\sqrt{2}}(u\bar{u} + d\bar{d})\cos\phi_P + (s\bar{s})\sin\phi_P$, with $\phi_P = \theta_{ideal} - \theta_{physical}$, where $\theta_{physical} = -15.4°$; for ω and ϕ vector states, we consider ideal mixing, i.e., $\omega = \frac{1}{\sqrt{2}}(u\bar{u} + d\bar{d})$ and $\phi = \frac{1}{\sqrt{2}}(s\bar{s})$ [12].

[6] Note that the sign and magnitude of the slope parameters signify how sharply the form factor varies with respect to allowed q^2.

Table 4 Form factors of bottom-conserving transitions. Note that T2A (T2B) results represent the transition form factors calculated using q^2 dependence given in Eq. (37) (Eq. (39)) with transition pole masses as listed in Table 1. T1 results represent the transition form factors calculated using q^2 dependence given in Eq. (38) with parent pole mass (M_{B_c})

Form factor	Type-II scheme				Type-I scheme			
	T2A (T2B)				T1			
	$F(0)$ (a_0')	$F(q^2_{\max})$	a (a_1')	b (a_2')	$F(0)$	$F(q^2_{\max})$	a	b
$B_c \to P$ transitions								
$F_0^{B_c B}$	$0.60^{+0.05+0.01}_{-0.05-0.03}$	$0.79^{+0.10+0.03}_{-0.09-0.08}$	$0.39^{+0.21+0.04}_{-0.16-0.20}$	$0.74^{+0.08+0.61}_{-0.07-0.31}$	$0.53^{+0.04+0.03}_{-0.04-0.05}$	$0.48^{+0.02+0.09}_{-0.02-0.12}$	$-2.77^{+0.81+4.16}_{-0.84-8.05}$	$193.24^{+23.70+90.89}_{-20.63-54.55}$
	$(0.62^{+0.05+0.01}_{-0.05-0.02})$	$(0.86^{+0.09+0.00}_{-0.09-0.01})$	$(-41.53^{+10.69+6.16}_{-12.72-6.95})$	$(816.36^{+539.60+299.35}_{-418.37-227.35})$				
$F_1^{B_c B}$	$0.60^{+0.05+0.02}_{-0.05-0.04}$	$0.82^{+0.08+0.07}_{-0.08-0.15}$	$0.31^{+0.11+0.09}_{-0.08-0.39}$	$0.79^{+0.06+0.68}_{-0.05-0.34}$	$0.53^{+0.04+0.05}_{-0.04-0.08}$	$0.36^{+0.02+0.14}_{-0.02-0.14}$	$-9.40^{+0.64+9.63}_{-0.46-18.11}$	$336.00^{+28.16+179.78}_{-25.74-114.81}$
	$(0.62^{+0.05+0.01}_{-0.05-0.02})$	$(0.97^{+0.09+0.00}_{-0.09-0.01})$	$(-57.32^{+9.42+8.68}_{-10.46-8.32})$	$(1570.88^{+443.22+425.90}_{-373.30-402.62})$				
$F_0^{B_c B_s}$	$0.71^{+0.04+0.01}_{-0.05-0.02}$	$0.90^{+0.08+0.02}_{-0.08-0.05}$	$0.42^{+0.22+0.00}_{-0.16-0.10}$	$0.57^{+0.07+0.46}_{-0.06-0.23}$	$0.65^{+0.04+0.02}_{-0.04-0.04}$	$0.66^{+0.02+0.08}_{-0.03-0.12}$	$1.06^{+0.27+2.68}_{-0.37-5.76}$	$145.33^{+19.18+72.71}_{-15.73-41.72}$
	$(0.72^{+0.04+0.01}_{-0.05-0.02})$	$(0.95^{+0.07+0.00}_{-0.08-0.01})$	$(-44.78^{+12.00+7.16}_{-14.15-8.46})$	$(819.02^{+618.20+346.16}_{-487.84-249.38})$				
$F_1^{B_c B_s}$	$0.71^{+0.04+0.02}_{-0.05-0.04}$	$0.92^{+0.08+0.04}_{-0.07-0.10}$	$0.44^{+0.12+0.01}_{-0.09-0.23}$	$0.70^{+0.04+0.62}_{-0.04-0.30}$	$0.65^{+0.03+0.04}_{-0.04-0.07}$	$0.56^{+0.03+0.14}_{-0.03-0.18}$	$-2.33^{+0.13+6.33}_{-0.00-13.18}$	$246.92^{+20.73+146.43}_{-19.08-87.66}$
	$(0.72^{+0.04+0.01}_{-0.05-0.02})$	$(1.00^{+0.07+0.00}_{-0.08-0.01})$	$(-62.2^{+9.28+10.56}_{-10.23-10.53})$	$(1632.53^{+444.96+516.17}_{-378.08-469.00})$				
$B_c \to V$ transitions								
$V^{B_c B^*}$	$2.92^{+0.57+0.19}_{-0.49-0.42}$	$3.77^{+0.83+0.52}_{-0.68-1.24}$	$0.24^{+0.11+0.17}_{-0.08-0.95}$	$1.01^{+0.07+1.33}_{-0.07-0.54}$	$2.50^{+0.46+0.38}_{-0.40-0.69}$	$1.61^{+0.26+0.95}_{-0.23-0.87}$	$-15.12^{+0.89+14.94}_{-0.59-32.31}$	$401.10^{+30.03+295.09}_{-28.38-171.43}$
	$(3.05^{+0.60+0.11}_{-0.52-0.18})$	$(4.63^{+0.99+0.01}_{-0.84-0.11})$	$(-310.53^{+72.96+57.52}_{-93.01-50.27})$	$(9099.36^{+3556.99+2872.49}_{-2634.10-2800.86})$				
$A_0^{B_c B^*}$	$0.57^{+0.01+0.06}_{-0.02-0.09}$	$0.79^{+0.04+0.12}_{-0.05-0.24}$	$0.27^{+0.14+0.05}_{-0.10-0.56}$	$0.56^{+0.03+0.79}_{-0.03-0.30}$	$0.05^{+0.00+0.03}_{-0.00-0.03}$	$0.01^{+0.00+0.01}_{-0.00-0.01}$	$-135.91^{+5.83+11.16}_{-4.07-9.17}$	$1146.17^{+20.76+51.33}_{-30.30-71.22}$
	$(0.59^{+0.01+0.05}_{-0.02-0.06})$	$(0.92^{+0.03+0.04}_{-0.05-0.06})$	$(-53.55^{+7.75+10.17}_{-8.11-8.25})$	$(1450.99^{+418.80+515.74}_{-362.52-524.15})$				
$A_1^{B_c B^*}$	$0.56^{+0.02+0.05}_{-0.03-0.08}$	$0.69^{+0.03+0.07}_{-0.04-0.16}$	$0.49^{+0.08+0.00}_{-0.07-0.46}$	$1.00^{+0.03+1.56}_{-0.05-0.56}$	$0.43^{+0.01+0.04}_{-0.02-0.07}$	$0.39^{+0.01+0.10}_{-0.02-0.16}$	$0.22^{+0.57+4.17}_{-0.47-14.67}$	$156.17^{+3.56+178.42}_{-6.51-77.85}$
	$(0.57^{+0.02+0.05}_{-0.03-0.06})$	$(0.76^{+0.03+0.04}_{-0.04-0.05})$	$(-42.68^{+3.36+10.37}_{-2.87-8.74})$	$(987.30^{+118.88+490.91}_{-121.78-472.79})$				
$A_2^{B_c B^*}$	$0.33^{+0.08+0.05}_{-0.06-0.07}$	$0.37^{+0.09+0.07}_{-0.07-0.09}$	$-0.31^{+0.03+0.07}_{-0.00-0.40}$	$0.95^{+0.05+0.96}_{-0.04-0.39}$	$0.31^{+0.07+0.06}_{-0.06-0.07}$	$0.27^{+0.06+0.09}_{-0.05-0.10}$	$-4.52^{+0.45+4.00}_{-0.33-10.51}$	$130.55^{+8.70+114.52}_{-6.33-54.28}$
	$(0.33^{+0.08+0.05}_{-0.06-0.06})$	$(0.39^{+0.10+0.04}_{-0.07-0.06})$	$(-2.84^{+0.40+6.75}_{-1.70-5.64})$	$(-599.95^{+129.24+334.33}_{-114.68-310.04})$				
$V^{B_c B_s^*}$	$3.24^{+0.55+0.12}_{-0.48-0.31}$	$4.04^{+0.78+0.27}_{-0.65-0.88}$	$0.40^{+0.12+0.08}_{-0.09-0.69}$	$0.96^{+0.06+1.27}_{-0.06-0.51}$	$2.89^{+0.47+0.28}_{-0.42-0.60}$	$2.30^{+0.35+0.85}_{-0.31-1.04}$	$-7.77^{+0.41+10.71}_{-0.13-25.51}$	$316.65^{+24.33+253.27}_{-22.74-136.51}$
	$(3.33^{+0.57+0.06}_{-0.50-0.13})$	$(4.54^{+0.83+0.00}_{-0.72-0.05})$	$(-325.09^{+70.36+65.50}_{-88.67-63.62})$	$(9358.97^{+3415.09+3360.58}_{-2561.76-3029.92})$				
$A_0^{B_c B_s^*}$	$0.69^{+0.00+0.05}_{-0.01-0.08}$	$0.89^{+0.03+0.08}_{-0.03-0.19}$	$0.37^{+0.14+0.00}_{-0.10-0.40}$	$0.56^{+0.03+0.77}_{-0.03-0.30}$	$0.22^{+0.00+0.08}_{-0.01-0.09}$	$0.08^{+0.00+0.05}_{-0.00-0.04}$	$-87.46^{+9.41+23.14}_{-8.76-26.24}$	$901.96^{+62.69+179.05}_{-69.01-177.30}$
	$(0.70^{+0.00+0.04}_{-0.01-0.05})$	$(0.97^{+0.01+0.03}_{-0.03-0.04})$	$(-61.95^{+7.55+12.56}_{-7.67-11.45})$	$(1659.03^{+420.38+650.22}_{-375.56-610.42})$				
$A_1^{B_c B_s^*}$	$0.68^{+0.01+0.05}_{-0.02-0.07}$	$0.83^{+0.02+0.05}_{-0.03-0.12}$	$0.60^{+0.09+0.00}_{-0.08-0.25}$	$0.84^{+0.02+1.31}_{-0.04-0.47}$	$0.53^{+0.00+0.03}_{-0.01-0.06}$	$0.53^{+0.01+0.08}_{-0.02-0.16}$	$2.67^{+0.62+2.81}_{-0.50-11.04}$	$129.44^{+2.02+148.11}_{-4.14-64.15}$
	$(0.69^{+0.01+0.04}_{-0.02-0.05})$	$(0.87^{+0.02+0.02}_{-0.03-0.04})$	$(-51.25^{+3.61+13.01}_{-3.25-12.23})$	$(1203.10^{+158.75+628.56}_{-153.39-559.18})$				
$A_2^{B_c B_s^*}$	$0.55^{+0.13+0.05}_{-0.10-0.07}$	$0.63^{+0.15+0.06}_{-0.11-0.11}$	$0.15^{+0.09+0.00}_{-0.05-0.34}$	$0.96^{+0.06+1.17}_{-0.05-0.45}$	$0.52^{+0.12+0.06}_{-0.09-0.09}$	$0.49^{+0.11+0.11}_{-0.08-0.16}$	$-1.00^{+0.10+3.77}_{-0.00-11.18}$	$140.50^{+11.29+133.79}_{-8.72-62.02}$
	$(0.56^{+0.13+0.04}_{-0.10-0.05})$	$(0.68^{+0.17+0.03}_{-0.13-0.04})$	$(-28.58^{+7.13+10.55}_{-11.23-9.81})$	$(262.57^{+288.06+517.66}_{-143.74-457.48})$				

Table 5 Form factors of bottom-changing transitions. For the definitions of T2A, T2B, and T1, refer to the caption of Table 4

Form factor	Type-II scheme				Type-I scheme			
	T2A (T2B)				T1			
	$F(0)$ (a_0')	$F(q^2_{\max})$	a (a_1')	b (a_2')	$F(0)$	$F(q^2_{\max})$	a	b
$B_c \to P$ transitions								
$F_0^{B_c D}$	$0.17^{+0.04+0.03}_{-0.03-0.03}$	$0.67^{+0.22+0.08}_{-0.19-0.15}$	$1.09^{+0.09+0.27}_{-0.10-0.23}$	$0.79^{+0.33+0.58}_{-0.29-0.32}$	$0.17^{+0.04+0.03}_{-0.03-0.03}$	$0.22^{+0.14+0.12}_{-0.08-0.10}$	$2.36^{+0.08+0.21}_{-0.11-0.22}$	$3.82^{+1.13+1.97}_{-1.01-1.22}$
	$(0.17^{+0.04+0.03}_{-0.03-0.03})$	$(0.85^{+0.13+0.01}_{-0.12-0.02})$	$(-1.56^{+0.18+0.15}_{-0.14-0.09})$	$(4.45^{+0.15+1.81}_{-0.23-1.77})$				
$F_1^{B_c D}$	$0.17^{+0.04+0.03}_{-0.03-0.03}$	$0.74^{+0.42+0.30}_{-0.27-0.31}$	$1.51^{+0.05+0.19}_{-0.07-0.20}$	$1.59^{+0.48+0.93}_{-0.43-0.55}$	$0.17^{+0.04+0.03}_{-0.03-0.03}$	$0.10^{+0.06+0.07}_{-0.04-0.05}$	$3.01^{+0.03+0.00}_{-0.07-0.11}$	$9.02^{+1.92+3.90}_{-1.78-2.49}$
	$(0.17^{+0.04+0.03}_{-0.03-0.03})$	$(1.50^{+0.25+0.05}_{-0.22-0.08})$	$(-2.45^{+0.35+0.06}_{-0.34-0.00})$	$(12.11^{+1.11+1.25}_{-1.33-1.64})$				
$F_0^{B_c D_s}$	$0.25^{+0.04+0.02}_{-0.04-0.02}$	$0.85^{+0.17+0.02}_{-0.16-0.06}$	$0.88^{+0.08-0.18}_{-0.08+0.16}$	$0.51^{+0.22+0.29}_{-0.20-0.18}$	$0.25^{+0.04+0.02}_{-0.04-0.02}$	$0.44^{+0.17+0.10}_{-0.13-0.12}$	$2.10^{+0.09+0.16}_{-0.11-0.16}$	$2.51^{+0.72+0.96}_{-0.65-0.66}$
	$(0.25^{+0.04+0.02}_{-0.04-0.02})$	$(0.95^{+0.11+0.02}_{-0.11-0.02})$	$(-1.85^{+0.12+0.23}_{-0.08-0.20})$	$(3.57^{+0.13+1.85}_{-0.04-1.57})$				
$F_1^{B_c D_s}$	$0.25^{+0.04+0.02}_{-0.04-0.02}$	$1.15^{+0.39+0.16}_{-0.31-0.25}$	$1.35^{+0.06+0.17}_{-0.07-0.16}$	$1.09^{+0.32+0.49}_{-0.29-0.32}$	$0.25^{+0.04+0.02}_{-0.04-0.02}$	$0.24^{+0.13+0.10}_{-0.08-0.08}$	$2.85^{+0.00+0.09}_{-0.01-0.12}$	$6.29^{+1.23+2.02}_{-1.16-1.42}$
	$(0.25^{+0.04+0.02}_{-0.04-0.02})$	$(1.61^{+0.18+0.01}_{-0.19-0.02})$	$(-3.17^{+0.32+0.17}_{-0.28-0.11})$	$(13.91^{+0.78+2.21}_{-0.97-2.27})$				
$F_0^{B_c \eta_c}$	$0.62^{+0.01+0.01}_{-0.01-0.02}$	$0.94^{+0.00+0.01}_{-0.00-0.02}$	$0.68^{+0.08+0.06}_{-0.08-0.06}$	$0.30^{+0.13+0.14}_{-0.12-0.11}$	$0.62^{+0.01+0.01}_{-0.01-0.02}$	$0.92^{+0.01+0.01}_{-0.01-0.03}$	$1.39^{+0.08+0.05}_{-0.08-0.05}$	$0.79^{+0.22+0.18}_{-0.21-0.15}$
	$(0.62^{+0.01+0.01}_{-0.01-0.02})$	$(0.95^{+0.00+0.00}_{-0.00-0.02})$	$(-3.14^{+0.34+0.24}_{-0.34-0.21})$	$(1.57^{+0.55+0.32}_{-0.00-0.27})$				
$F_1^{B_c \eta_c}$	$0.62^{+0.01+0.01}_{-0.01-0.02}$	$1.18^{+0.03+0.00}_{-0.03-0.01}$	$1.31^{+0.03+0.12}_{-0.02-0.12}$	$0.74^{+0.18+0.22}_{-0.18-0.17}$	$0.62^{+0.01+0.01}_{-0.01-0.02}$	$1.05^{+0.06+0.02}_{-0.05-0.05}$	$2.10^{+0.01+0.09}_{-0.00-0.09}$	$2.25^{+0.29+0.44}_{-0.29-0.36}$
	$(0.62^{+0.01+0.01}_{-0.01-0.02})$	$(1.18^{+0.01+0.00}_{-0.01-0.01})$	$(-6.65^{+0.08+0.49}_{-0.09-0.41})$	$(26.69^{+0.74+3.82}_{-0.27-3.99})$				
$B_c \to V$ transitions								
$V^{B_c D^*}$	$0.22^{+0.07+0.07}_{-0.06-0.07}$	$0.74^{+0.55+0.58}_{-0.32-0.46}$	$1.65^{+0.04+0.22}_{-0.07-0.27}$	$2.12^{+0.65+2.02}_{-0.58-0.95}$	$0.22^{+0.07+0.07}_{-0.06-0.07}$	$0.11^{+0.09+0.14}_{-0.05-0.07}$	$3.04^{+0.08+0.00}_{-0.14-0.29}$	$11.31^{+2.55+8.08}_{-2.35-4.15}$
	$(0.22^{+0.07+0.07}_{-0.06-0.07})$	$(1.73^{+0.43+0.21}_{-0.39-0.31})$	$(-3.65^{+0.75+0.55}_{-0.83-0.24})$	$(20.36^{+3.55+0.00}_{-3.53-2.14})$				
$A_0^{B_c D^*}$	$0.20^{+0.02+0.07}_{-0.02-0.07}$	$0.84^{+0.31+0.51}_{-0.25-0.51}$	$1.44^{+0.07+0.29}_{-0.08-0.29}$	$1.44^{+0.53+1.50}_{-0.46-0.68}$	$0.14^{+0.00+0.05}_{-0.02-0.05}$	$0.01^{+0.00+0.01}_{-0.00-0.00}$	$-6.38^{+3.92+3.30}_{-16.28-6.01}$	$70.78^{+67.77+33.42}_{-17.98-20.16}$
	$(0.20^{+0.02+0.07}_{-0.02-0.07})$	$(1.46^{+0.03+0.22}_{-0.08-0.30})$	$(-2.89^{+0.10+0.46}_{-0.00-0.22})$	$(14.42^{+0.20+0.27}_{-0.88-2.00})$				
$A_1^{B_c D^*}$	$0.15^{+0.03+0.00}_{-0.03-0.10}$	$0.52^{+0.11+0.00}_{-0.13-0.52}$	$1.25^{+0.18+0.43}_{-0.22-47.77}$	$1.15^{+0.55+160.81}_{-0.44-0.00}$	$0.14^{+0.03+0.05}_{-0.03-0.04}$	$0.17^{+0.10+0.15}_{-0.07-0.11}$	$2.42^{+0.11+0.29}_{-0.18-0.36}$	$4.48^{+1.57+4.11}_{-1.37-1.96}$
	$(0.15^{+0.03+0.05}_{-0.03-0.05})$	$(0.70^{+0.04+0.00}_{-0.07-0.88})$	$(-1.68^{+0.06+1.6}_{-0.00-0.00})$	$(5.86^{+0.81+1.94}_{-1.50-53.93})$				
$A_2^{B_c D^*}$	$0.11^{+0.04+0.03}_{-0.03-0.03}$	$0.32^{+0.19+0.18}_{-0.13-0.19}$	$1.65^{+0.09+0.32}_{-0.13-0.34}$	$2.25^{+0.74+2.26}_{-0.64-1.02}$	$0.11^{+0.04+0.03}_{-0.03-0.03}$	$0.07^{+0.06+0.08}_{-0.03-0.05}$	$2.74^{+0.00+0.00}_{-0.03-0.21}$	$8.40^{+2.11+6.47}_{-1.90-3.23}$
	$(0.11^{+0.04+0.03}_{-0.03-0.03})$	$(0.64^{+0.16+0.04}_{-0.14-0.09})$	$(-1.65^{+0.33+0.19}_{-0.34-0.01})$	$(7.94^{+0.84+0.77}_{-1.13-1.85})$				

Table 5 continued

Form factor	Type-II scheme				Type-I scheme			
	T2A (T2B)				T1			
	$F(0)$ (a_0')	$F(q^2_{\max})$	a (a_1')	b (a_2')	$F(0)$	$F(q^2_{\max})$	a	b
$V^{B_c D_s^*}$	$0.27^{+0.08+0.07}_{-0.06-0.08}$	$0.93^{+0.57+0.53}_{-0.36-0.53}$	$1.64^{+0.05+0.26}_{-0.07-0.28}$	$1.95^{+0.59+1.82}_{-0.53-0.87}$	$0.27^{+0.08+0.07}_{-0.06-0.08}$	$0.17^{+0.13+0.19}_{-0.07-0.11}$	$3.02^{+0.05+0.00}_{-0.09-0.14}$	$9.82^{+2.15+6.85}_{-1.99-3.55}$
	$(0.27^{+0.08+0.07}_{-0.06-0.08})$	$(1.73^{+0.38+0.15}_{-0.33-0.26})$	$(-4.45^{+0.79+0.47}_{-0.84-0.12})$	$(24.49^{+3.49+1.24}_{-3.57-3.41})$				
$A_0^{B_c D_s^*}$	$0.24^{+0.01+0.08}_{-0.02-0.08}$	$0.99^{+0.25+0.44}_{-0.24-0.53}$	$1.43^{+0.07+0.31}_{-0.09-0.29}$	$1.34^{+0.48+1.37}_{-0.43-0.63}$	$0.18^{+0.02+0.06}_{-0.03-0.06}$	$0.02^{+0.00+0.02}_{-0.01-0.01}$	$-1.21^{+1.46+1.56}_{-4.91-3.15}$	$43.38^{+22.88+21.37}_{-7.41-12.40}$
	$(0.25^{+0.01+0.08}_{-0.02-0.08})$	$(1.47^{+0.00+0.19}_{-0.04-0.26})$	$(-3.53^{+0.15+0.42}_{-0.00-0.14})$	$(17.40^{+0.82+1.26}_{-1.50-2.95})$				
$A_1^{B_c D_s^*}$	$0.20^{+0.03+0.06}_{-0.03-0.06}$	$0.64^{+0.09+0.13}_{-0.13-0.25}$	$1.27^{+0.18+0.44}_{-0.21-0.37}$	$1.06^{+0.52+1.28}_{-0.41-0.54}$	$0.18^{+0.03+0.05}_{-0.03-0.05}$	$0.25^{+0.12+0.17}_{-0.09-0.15}$	$2.39^{+0.12+0.33}_{-0.17-0.36}$	$3.96^{+1.36+3.57}_{-1.19-1.73}$
	$(0.20^{+0.03+0.06}_{-0.03-0.06})$	$(0.79^{+0.02+0.06}_{-0.05-0.10})$	$(-2.14^{+0.13+0.19}_{-0.00-0.00})$	$(7.58^{+1.20+2.83}_{-1.86-3.60})$				
$A_2^{B_c D_S^*}$	$0.15^{+0.05+0.04}_{-0.04-0.04}$	$0.44^{+0.22+0.18}_{-0.16-0.23}$	$1.71^{+0.09+0.35}_{-0.13-0.35}$	$2.16^{+0.73+2.12}_{-0.61-0.98}$	$0.15^{+0.05+0.04}_{-0.04-0.04}$	$0.12^{+0.09+0.11}_{-0.05-0.07}$	$2.76^{+0.00+0.04}_{-0.04-0.23}$	$7.58^{+1.89+5.65}_{-1.67-2.87}$
	$(0.15^{+0.05+0.04}_{-0.04-0.04})$	$(0.73^{+0.17+0.05}_{-0.15-0.09})$	$(-2.20^{+0.39+0.16}_{-0.39-0.00})$	$(10.91^{+1.04+1.47}_{-1.36-2.53})$				
$V^{B_c J/\psi}$	$0.81^{+0.07+0.01}_{-0.06-0.02}$	$1.57^{+0.16+0.00}_{-0.14-0.03}$	$1.63^{+0.03+0.18}_{-0.03-0.17}$	$1.27^{+0.30+0.46}_{-0.30-0.33}$	$0.81^{+0.07+0.01}_{-0.06-0.02}$	$1.31^{+0.19+0.03}_{-0.16-0.08}$	$2.35^{+0.00+0.13}_{-0.00-0.13}$	$3.32^{+0.47+0.84}_{-0.47-0.63}$
	$(0.81^{+0.07+0.01}_{-0.06-0.02})$	$(1.58^{+0.12+0.03}_{-0.10-0.04})$	$(-11.01^{+0.50+1.06}_{-0.55-0.99})$	$(55.79^{+3.70+10.67}_{-2.72-10.06})$				
$A_0^{B_c J/\psi}$	$0.66^{+0.06+0.02}_{-0.06-0.03}$	$1.25^{+0.11+0.00}_{-0.11-0.02}$	$1.34^{+0.04+0.17}_{-0.04-0.17}$	$0.85^{+0.24+0.34}_{-0.23-0.24}$	$0.57^{+0.02+0.01}_{-0.02-0.02}$	$0.70^{+0.05+0.08}_{-0.10-0.11}$	$2.54^{+0.00+0.03}_{-0.03-0.07}$	$7.15^{+1.39+1.90}_{-0.52-1.41}$
	$(0.66^{+0.06+0.02}_{-0.06-0.03})$	$(1.26^{+0.13+0.00}_{-0.13-0.01})$	$(-7.90^{+1.08+0.74}_{-1.14-0.64})$	$(35.06^{+4.93+7.19}_{-4.05-7.14})$				
$A_1^{B_c J/\psi}$	$0.60^{+0.03+0.02}_{-0.03-0.03}$	$0.96^{+0.07+0.00}_{-0.08-0.01}$	$1.08^{+0.15+0.20}_{-0.17-0.18}$	$0.55^{+0.28+0.27}_{-0.24-0.17}$	$0.55^{+0.01+0.02}_{-0.02-0.02}$	$0.84^{+0.02+0.00}_{-0.04-0.02}$	$1.67^{+0.09+0.15}_{-0.11-0.14}$	$1.27^{+0.38+0.43}_{-0.36-0.31}$
	$(0.60^{+0.03+0.02}_{-0.03-0.03})$	$(0.97^{+0.08+0.00}_{-0.08-0.01})$	$(-4.87^{+0.99+0.66}_{-0.99-0.59})$	$(13.23^{+4.74+5.02}_{-4.11-4.71})$				
$A_2^{B_c J/\psi}$	$0.48^{+0.03+0.03}_{-0.03-0.03}$	$0.87^{+0.05+0.02}_{-0.06-0.04}$	$1.67^{+0.09+0.17}_{-0.11-0.16}$	$1.35^{+0.38+0.46}_{-0.36-0.34}$	$0.48^{+0.03+0.03}_{-0.03-0.03}$	$0.77^{+0.07+0.05}_{-0.07-0.07}$	$2.14^{+0.05+0.11}_{-0.07-0.11}$	$2.67^{+0.49+0.63}_{-0.48-0.49}$
	$(0.48^{+0.03+0.03}_{-0.03-0.03})$	$(0.88^{+0.04+0.02}_{-0.04-0.03})$	$(-5.99^{+0.04+0.29}_{-0.00-0.17})$	$(27.50^{+0.62+3.25}_{-1.00-3.57})$				

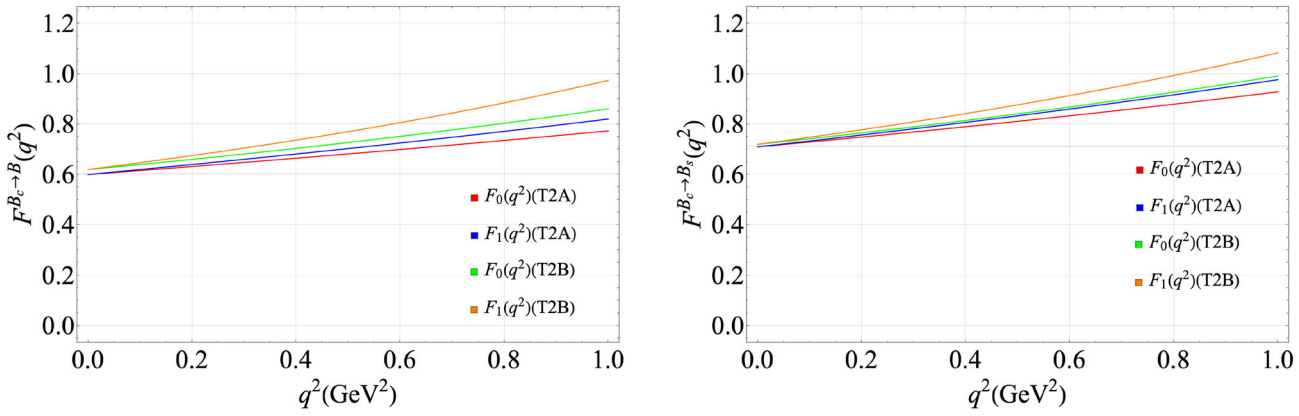

(a) $B_c \to B$ transition (b) $B_c \to B_s$ transition

Fig. 2 q^2 dependence of bottom-conserving $B_c \to P$ form factors in T2A (T2B) CLFQM using Eq. (37) (Eq. (39))

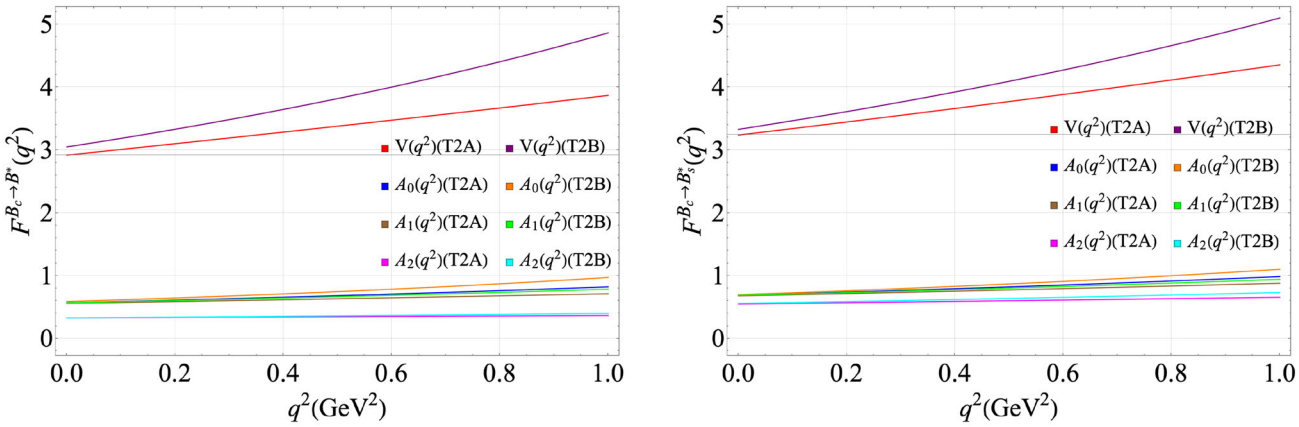

(a) $B_c \to B^*$ transition (b) $B_c \to B_s^*$ transition

Fig. 3 q^2 dependence of bottom-conserving $B_c \to V$ form factors in T2A (T2B) CLFQM using Eq. (37) (Eq. (39))

ciated with these coefficients [13]. It is important to note that the numerical values of the form factors in type-I correspondence show a decreasing trend with respect to q^2 variation, in contrast to type-II correspondence. This observed trend is the opposite of what has been expected based on LQCD predictions [20]. As discussed in Sect. 2.2, the parameters a, b, and $F(0)$ are determined by fitting Eq. (38) in the space-like region and then extrapolation to the physical region. The form factors within the type-I scheme take negative values for the slope parameter a and substantially larger positive values for slope parameter b, which decreases on account of transition pole masses, as reported in our previous work [64]. This discrepancy is primarily attributed to the specific q^2 dependence formulation employed.[7]

(ii) As stated earlier, we analyze the effect of the variation in quark masses and β parameters on these form factors, and we observe that the form factors are less sensitive to the variation in constituent quark masses and β values, which produce a collective uncertainty up to $\sim$ 10% (for both T2A and T2B). In contrast, the corresponding slope parameters a and b demonstrate substantially higher uncertainties. Notably, the uncertainties for T2A and T2B show broadly similar patterns in response to quark mass and β parameter variations, with a few exceptions. For the sake of comparison, we

[7] It is worth mentioning that the q^2 dependence given by Eq. (38) exhibits a decreasing trend even for type-II correspondence. Similar trends can be observed in the numerical values of the form factors reported in other analyses within the type-I scheme [27,118]

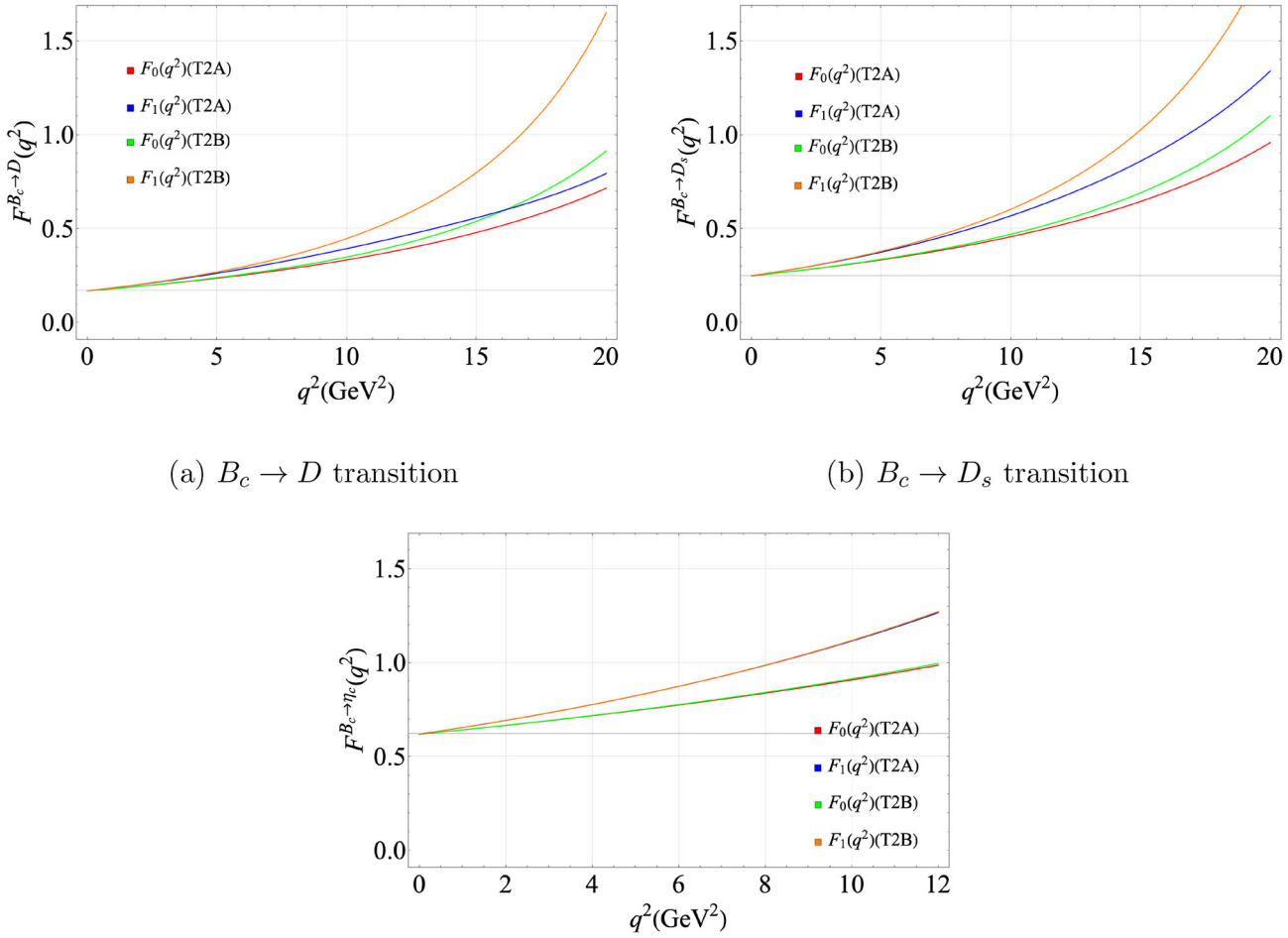

Fig. 4 q^2 dependence of bottom-changing $B_c \to P$ form factors in T2A (T2B) CLFQM using Eq. (37) (Eq. (39))

list numerical results for $P \to P$ form factors in Table 4. We observe that the numerical values of the form factors in type-II correspondence are larger than those of the type-I scheme. Among the T2A and T2B results, we observe that form factors are marginally different, but uniformly larger numerical values are found for T2B form factors, as shown in Table 4. Furthermore, we wish to emphasize that the T2A (T2B) numerical results for the form factors $F_0^{B_c B_{(s)}}(q^2)$ and $F_1^{B_c B_{(s)}}(q^2)$ are in very good agreement with the LQCD observations [20], both at $q^2 = 0$ and at $q^2_{\rm max}$. The LQCD form factor results at both $q^2 = 0$ and $q^2_{\rm max}$ are as follows [20]: $F_{0[1]}^{B_c B}(0) = 0.555 \pm 0.016$ [0.555 ± 0.016], $F_{0[1]}^{B_c B}(q^2_{\rm max}) = 0.756 \pm 0.016$ [0.910 ± 0.028]; $F_{0[1]}^{B_c B_s}(0) = 0.621 \pm 0.010$ [0.621 ± 0.010], $F_{0[1]}^{B_c B_s}(q^2_{\rm max}) = 0.817 \pm 0.011$ [0.911 ± 0.018]. For T2A and T2B, the numerical values of $B_c \to B_{(s)}$ form factors differ by $\sim 8\%(14\%)$ and $\sim 12\%(16\%)$ at $q^2 = 0$, respectively, when compared to the LQCD results. However, the consistency improves at $q^2_{\rm max}$, particularly for $F_0^{B_c B}(q^2_{\rm max})$ in the T2A formulation, where the difference with LQCD results reduces to $\sim 3\%$. Furthermore, the LQCD results also show an increasing trend with respect to the q^2 variation as observed in the T2A and T2B results. The characteristic feature of bottom-conserving transitions, which was reported in our previous work [64], is that these form factors in the small available q^2 range show nearly flat behavior.

(iii) Similar to $B_c \to P$ transitions, we calculate the form factors for bottom-conserving $B_c \to V$ transitions for both type-I and type-II correspondences, as shown in Table 4. It should be noted that in $B_c \to V$ transitions, $V(q^2)$ and $A_2(q^2)$ form factors remain unaffected by the spurious contributions associated with

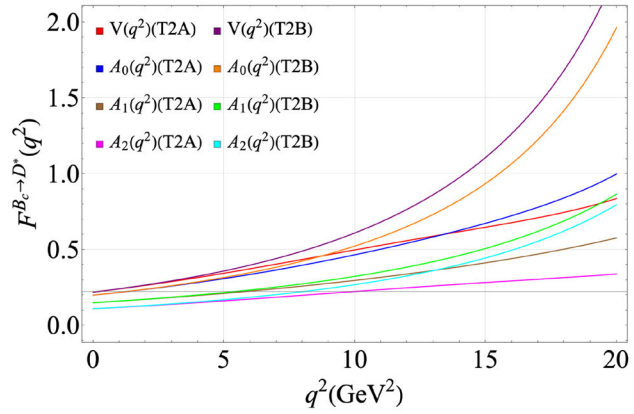

(a) $B_c \to D^*$ transition

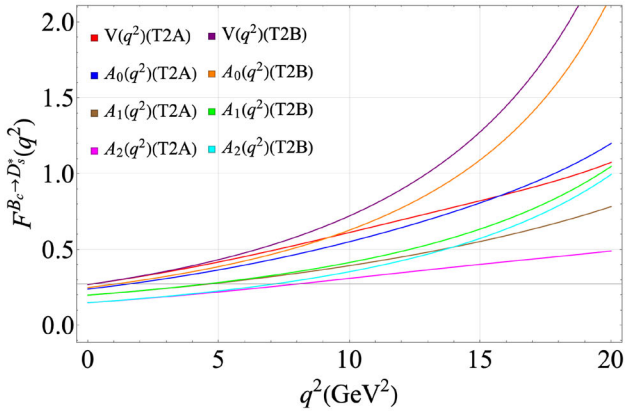

(b) $B_c \to D_s^*$ transition

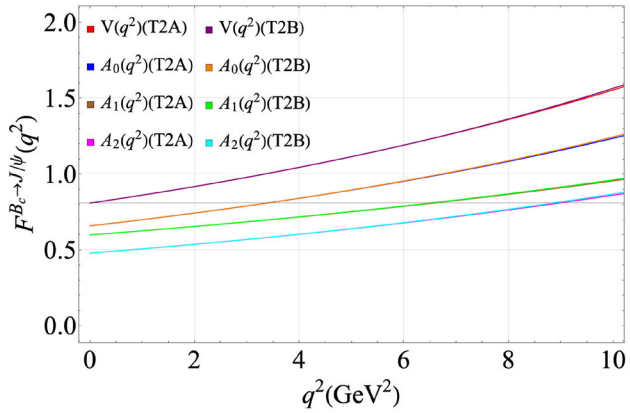

(c) $B_c \to J/\psi$ transition

Fig. 5 q^2 dependence of bottom-changing $B_c \to V$ form factors in T2A (T2B) CLFQM using Eq. (37) (Eq. (39))

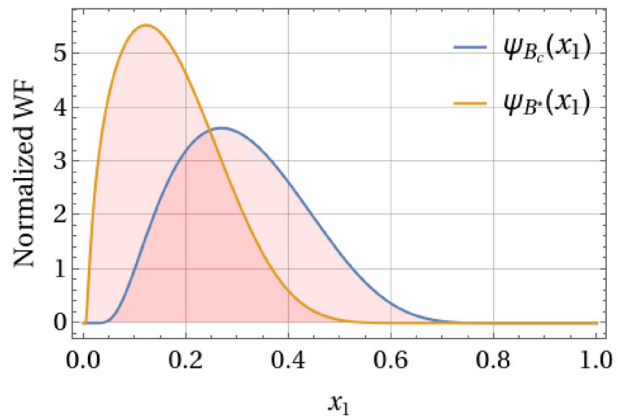

(a) B_c and B^* (Overlap area = 0.723)

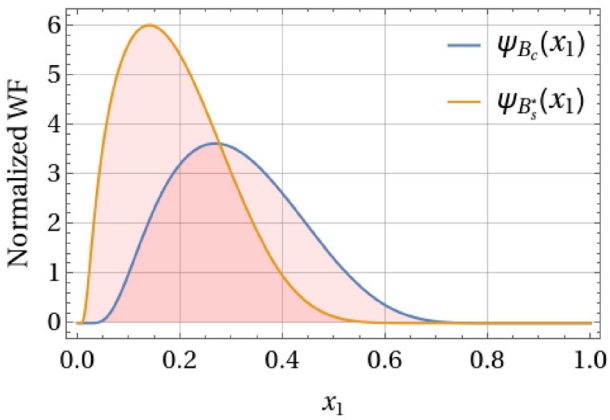

(b) B_c and B_s^* (Overlap area = 0.831)

Fig. 6 Overlap plots of B_c and B^*, B_s^* light-front wave function using Eq. (5), in T2A CLFQM. Note that overlap plots of B_c and B, B_s wave function are similar to B^*, B_s^*, with roughly 10% increase in overlap area

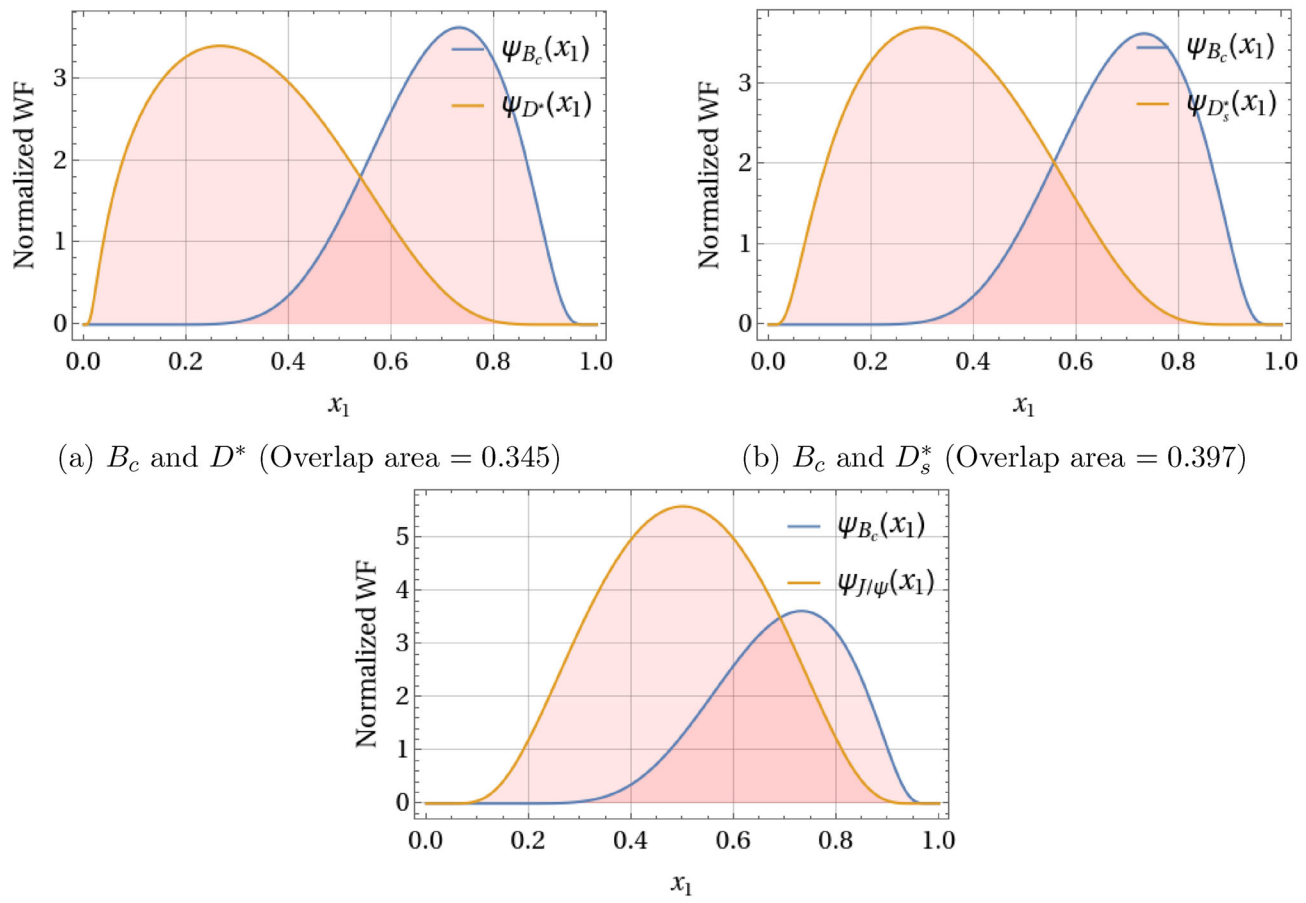

(a) B_c and D^* (Overlap area = 0.345)

(b) B_c and D_s^* (Overlap area = 0.397)

(c) B_c and J/ψ (Overlap area = 0.874)

Fig. 7 Overlap plots of B_c and D^*, D_s^*, J/ψ light-front wave function using Eq. (5), in T2A CLFQM. Note that overlap plots of B_c and D, D_s, η_c wave function will be similar; however, we observe approximately 15% and 26% change between B_c and D, η_c, and between B_c and D_s, respectively

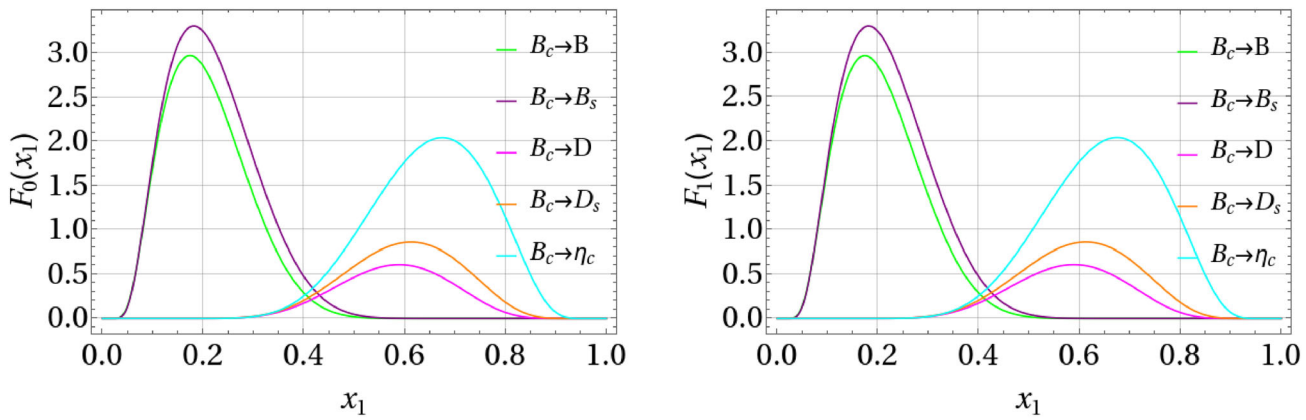

(a) $F_0(x_1)$ versus x_1

(b) $F_1(x_1)$ versus x_1

Fig. 8 Dependence of form factor $F(x_1)$ on x_1 for $B_c \to P$ transition at $q^2 \approx 0$ GeV^2, in T2A CLFQM using Eq. (27)

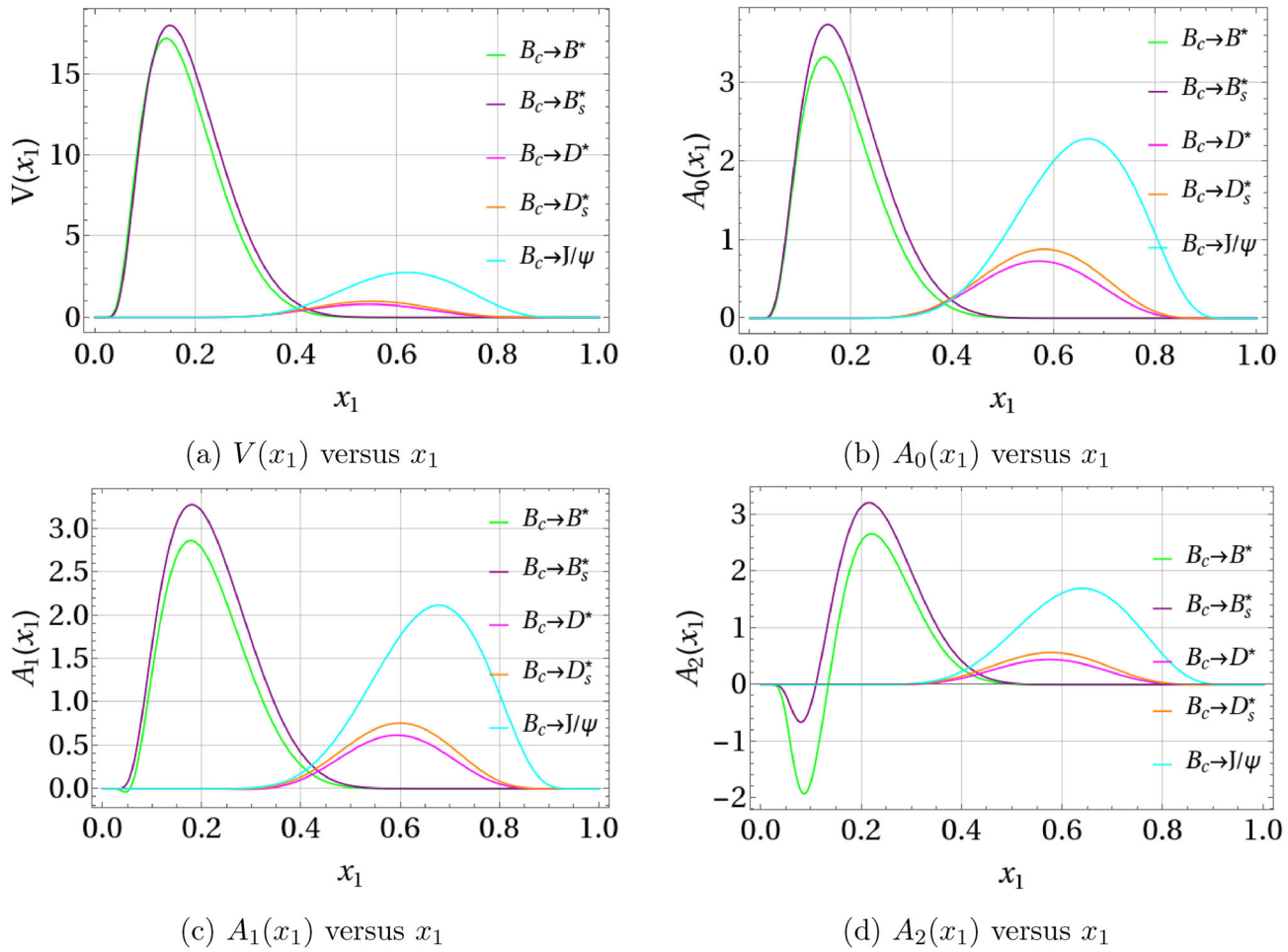

(a) $V(x_1)$ versus x_1 (b) $A_0(x_1)$ versus x_1

(c) $A_1(x_1)$ versus x_1 (d) $A_2(x_1)$ versus x_1

Fig. 9 Dependence of form factor $F(x_1)$ on x_1 for $B_c \to V$ transition at $q^2 \approx 0$ GeV^2, in T2A CLFQM using Eq. (27)

the $B_j^{(i)}$ functions. Consequently, the results obtained with the CLF approach for $\lambda = 0$ and $\lambda = \pm$ polarization states of vector mesons are in agreement with each other, regardless of whether type-I or type-II correspondence schemes are employed. However, in the type-I scheme, these zero-mode contributions lead to inconsistency in $A_0(q^2)$ and $A_1(q^2)$ form factors for $B_c \to V$ transitions. As described in the methodology in Sect. 2, the type-II scheme effectively resolves the issues corresponding to self-consistency and covariance of the matrix elements [62]. We observe that in the type-II scheme, zero-mode contributions associated with the $B_1^{(2)}$ and $B_3^{(3)}$ functions vanish numerically in the form factors $f(q^2)$ and $a_-(q^2)$, as shown in Tables 15 and 16, in Appendix A. The obtained numerical results for $\lambda = 0$ and $\lambda = \pm$ polarization states of $f(q^2)$ and $a_-(q^2)$ form factors show substantial disagreement in the type-I scheme, whereas they are numerically equal in the type-II correspondence. In addition, $A_0(q^2)$ and $A_1(q^2)$ are related to the form factors $f(q^2)$ and $a_-(q^2)$ by the transformation relations given in Eq. (17). Thus, the form factors $A_0(q^2)$ and $A_1(q^2)$ corresponding to the longitudinal ($\lambda = 0$) and transverse ($\lambda = \pm$) polarization states are numerically equal. Hence, the numerical results demonstrate that the type-II correspondence effectively addresses these inconsistencies by substituting $M'^{(\prime\prime)} \to M_0'^{(\prime\prime)}$. Furthermore, we plot all the bottom-conserving $B_c \to B_{(s)}^*$ transition form factors to observe their variation with respect to q^2, as shown in Fig. 3. The form factors $A_0(q^2)$, $A_1(q^2)$, and $A_2(q^2)$ display a nearly flat behavior with respect to q^2 like the $B_c \to P$ form factors. In addition, the form factor $V(q^2)$ shows a reasonable variation in magnitude corresponding to the available q^2. However, while the variations in $V(q^2)$ form factors seem to be significant in Fig. 3 (due to their higher numerical values), they are only roughly 20% larger than $q^2 = 0$ for the T2A form factors. In contrast, $V(q^2_{\rm max})$ is $\sim 30\%$ larger than $V(0)$ for T2B. It should be noted that $B_c \to B_{(s)}^*$ form factors are more sensitive to the uncertainties in constituent

Table 6 Branching ratios, relative decay widths and physical observables of $B_c^+ \to V l^+ \nu_l$ decays in T2A CLFQM

Quark transition	Decay	$\mathcal{B}$	$\frac{\Gamma_L}{\Gamma}$	$\frac{\Gamma_T}{\Gamma}$	$\frac{\Gamma_L}{\Gamma_T}$	$\langle A_{FB}\rangle$	$\langle C_F^l\rangle$	$\langle P_L^l\rangle$	$\langle P_T^l\rangle$	α^*
$c \to d$	$B_c^+ \to B^{*0} e^+ \nu_e$	$(2.09^{+0.20+0.38}_{-0.25-0.69}) \times 10^{-3}$	0.53	0.47	1.13	$-0.17^{+0.02+0.01}_{-0.03-0.00}$	$-0.44^{+0.02+0.00}_{-0.02-0.03}$	1.00	-1.03×10^{-3}	$-0.39^{+0.02+0.00}_{-0.01-0.02}$
	$B_c^+ \to B^{*0} \mu^+ \nu_\mu$	$(1.98^{+0.19+0.37}_{-0.23-0.66}) \times 10^{-3}$	0.52	0.48	1.11	$-0.20^{+0.02+0.01}_{-0.03-0.00}$	$-0.35^{+0.02+0.00}_{-0.01-0.02}$	0.91	-0.13	$-0.38^{+0.02+0.00}_{-0.01-0.02}$
$c \to s$	$B_c^+ \to B_s^{*0} e^+ \nu_e$	$(3.53^{+0.15+0.49}_{-0.24-0.81}) \times 10^{-2}$	0.53	0.47	1.14	$-0.14^{+0.02+0.01}_{-0.02-0.00}$	$-0.45^{+0.02+0.00}_{-0.01-0.01}$	1.00	-1.20×10^{-3}	$-0.39^{+0.02+0.00}_{-0.01-0.01}$
	$B_c^+ \to B_s^{*0} \mu^+ \nu_\mu$	$(3.30^{+0.14+0.46}_{-0.22-0.77}) \times 10^{-2}$	0.53	0.47	1.11	$-0.18^{+0.02+0.01}_{-0.02-0.00}$	$-0.35^{+0.02+0.00}_{-0.01-0.01}$	0.90	-0.15	$-0.38^{+0.01+0.00}_{-0.01-0.01}$
$b \to u$	$B_c^+ \to D^{*0} e^+ \nu_e$	$(1.04^{+0.38+0.00}_{-0.39-0.81}) \times 10^{-4}$	0.50	0.50	1.00	$-0.25^{+0.05+0.24}_{-0.07-0.00}$	$-0.37^{+0.10+0.47}_{-0.08-0.06}$	1.00	-1.49×10^{-4}	$-0.33^{+0.09+0.43}_{-0.06-0.05}$
	$B_c^+ \to D^{*0} \mu^+ \nu_\mu$	$(1.04^{+0.38+0.00}_{-0.39-0.80}) \times 10^{-4}$	0.50	0.50	1.00	$-0.26^{+0.05+0.24}_{-0.07-0.00}$	$-0.37^{+0.10+0.47}_{-0.08-0.06}$	0.99	-2.84×10^{-2}	$-0.33^{+0.09+0.41}_{-0.06-0.05}$
	$B_c^+ \to D^{*0} \tau^+ \nu_\tau$	$(5.82^{+2.28+0.00}_{-2.23-3.94}) \times 10^{-5}$	0.49	0.51	0.97	$-0.32^{+0.03+0.45}_{-0.05-0.00}$	$-0.13^{+0.05+0.26}_{-0.03-0.04}$	0.61	-0.14	$-0.32^{+0.07+0.00}_{-0.06-0.13}$
$b \to c$	$B_c^+ \to J/\psi e^+ \nu_e$	$(2.35^{+0.36+0.04}_{-0.33-0.12}) \times 10^{-2}$	0.52	0.48	1.10	$-0.19^{+0.03+0.00}_{-0.03-0.00}$	$-0.43^{+0.04+0.01}_{-0.03-0.00}$	1.00	-2.90×10^{-4}	$-0.38^{+0.03+0.00}_{-0.03-0.00}$
	$B_c^+ \to J/\psi \mu^+ \nu_\mu$	$(2.34^{+0.36+0.04}_{-0.33-0.12}) \times 10^{-2}$	0.52	0.48	1.10	$-0.19^{+0.03+0.00}_{-0.03-0.00}$	$-0.42^{+0.04+0.00}_{-0.03-0.00}$	0.99	-5.25×10^{-2}	$-0.38^{+0.03+0.00}_{-0.03-0.00}$
	$B_c^+ \to J/\psi \tau^+ \nu_\tau$	$(5.77^{+0.88+0.03}_{-0.82-0.23}) \times 10^{-3}$	0.46	0.54	0.84	$-0.27^{+0.02+0.00}_{-0.02-0.00}$	$-0.06^{+0.01+0.00}_{-0.01-0.00}$	0.51	-0.13	$-0.25^{+0.02+0.00}_{-0.02-0.00}$

quark masses and β values, leading to larger collective uncertainties on the order of $\sim$ 30% and $\sim$ 40% for $V(0)$ and $A_2(0)$ form factors, respectively, in T2A predictions. For T2B, the maximum uncertainties are about 23% and 40% for $V(0)$ and $A_2(0)$ form factors, respectively. Such significant uncertainties were anticipated, given the incorporation of a broad range of β parameter values alongside variations in quark masses. Furthermore, the degree of sensitivity to quark mass and β uncertainties varies among different form factors. On the other hand, the uncertainties are substantially large specifically for $A_0(0)$, i.e., up to $\sim$ 60%, in the type-I scheme. At the same time, the slope parameters also show larger uncertainties.

(iv) In general, the transition form factors essentially involve the overlap integral of the initial- and final-state meson wave functions, which depend upon the internal degrees of freedom, mainly transverse momentum distributions and constituent quark masses. Furthermore, in CLFQM, the actual magnitude of these transitions has contributions originating from vertex functions and current operators. Therefore, we first plot the overlap[8] of the initial and final wave functions at $q^2 \approx 0$, where we have integrated out $k_\perp^2$ using Eq. (5), as shown in Fig. 6 with the corresponding overlap factor. The larger wave function overlap can be explained by the internal momentum distribution peaks at $x_1 \sim 0$ for $\psi_{B_{(s)}^{(*)}}(x_1)$ and $x_1 \sim 0.25$ for $\psi_{B_c}(x_1)$, as per Eq. (5). The location and width of the peak are governed by constituent quark masses, where heavier quarks take a larger fraction of momentum [120–122]. This results in a large overlap between the initial and final states. The overlap factor inside the total integrand, therefore, leads to a decisive change in the magnitude of the total form factor. For further analysis, we also plot the total integrand defined by Eq. (27) with respect to the momentum fraction x_1 for the B_c meson to $P(V)$ transition form factors at $q^2 \approx 0$, as shown in Figs. 8 and 9. To obtain these plots, we included the mass factors (given by Eq. (17)) in Eq. (27) and integrated out $\boldsymbol{k}_\perp$. It should be noted that the total integrand of transition form factors, e.g., $B_c \to B_{(s)}^{(*)}$, follows exactly the same overlap region which is governed by the initial and final wave functions. The bottom-conserving transition form factors have larger amplitudes than the bottom-changing form factors (as seen in Figs. 8 and 9). The area under the curves gives the magnitude of the form factor for the respective transitions, and we observe constructive interference for the transition form factors except for

[8] The normalization of Gaussian-type radial wave function of a meson is described as $\int_0^1 dx \int \frac{d^2\boldsymbol{k}'_\perp}{2(2\pi)^3} |\psi(x_1, \boldsymbol{k}'_\perp)|^2 = 1$ [65,120].

Table 7 Branching ratios of $B_c^+ \to V l^+ \nu_l$ decays. For the definitions of T2A, T2B, and T1, refer to the caption of Table 4

Decay	Ours		[27]	[32]	[29]	[35]
	T2A (T2B)	T1				
$B_c^+ \to B^{*0} e^+ \nu_e$	$(2.09^{+0.20+0.38}_{-0.25-0.69}) \times 10^{-3}$ $((2.32^{+0.19+0.31}_{-0.26-0.37}) \times 10^{-3})$	$(9.42^{+0.63+3.28}_{-0.95-4.57}) \times 10^{-4}$	7.77×10^{-4}	1.79×10^{-3}	1.41×10^{-3}	6.30×10^{-3}
$B_c^+ \to B^{*0} \mu^+ \nu_\mu$	$(1.98^{+0.19+0.37}_{-0.23-0.66}) \times 10^{-3}$ $((2.20^{+0.18+0.29}_{-0.24-0.35}) \times 10^{-3})$	$(8.57^{+0.59+9.89}_{-0.87-4.25}) \times 10^{-4}$	7.36×10^{-4}	1.72×10^{-3}	1.34×10^{-3}	-
$B_c^+ \to B_s^{*0} e^+ \nu_e$	$(3.53^{+0.15+0.49}_{-0.24-0.81}) \times 10^{-2}$ $((3.76^{+0.13+0.32}_{-0.23-0.41}) \times 10^{-2})$	$(1.80^{+0.02+0.35}_{-0.08-0.65}) \times 10^{-2}$	1.42×10^{-2}	2.30×10^{-2}	1.96×10^{-2}	2.37×10^{-2}
$B_c^+ \to B_s^{*0} \mu^+ \nu_\mu$	$(3.30^{+0.14+0.46}_{-0.22-0.77}) \times 10^{-2}$ $((3.52^{+0.12+0.29}_{-0.22-0.38}) \times 10^{-2})$	$(1.62^{+0.02+0.33}_{-0.07-0.61}) \times 10^{-2}$	1.32×10^{-2}	2.20×10^{-2}	1.83×10^{-2}	-
$B_c^+ \to D^{*0} e^+ \nu_e$	$(1.04^{+0.38+0.00}_{-0.39-0.81}) \times 10^{-4}$ $((1.37^{+0.28+0.00}_{-0.33-0.84}) \times 10^{-4})$	$(4.44^{+2.82+5.08}_{-2.05-2.85}) \times 10^{-5}$	1.26×10^{-4}	8.40×10^{-5}	4.50×10^{-5}	3.80×10^{-5}
$B_c^+ \to D^{*0} \mu^+ \nu_\mu$	$(1.04^{+0.38+0.00}_{-0.39-0.80}) \times 10^{-4}$ $((1.37^{+0.28+0.00}_{-0.33-0.84}) \times 10^{-4})$	$(4.42^{+2.81+5.06}_{-2.05-2.84}) \times 10^{-5}$	1.25×10^{-4}	8.40×10^{-5}	4.50×10^{-5}	-
$B_c^+ \to D^{*0} \tau^+ \nu_\tau$	$(5.82^{+2.28+0.00}_{-2.23-3.94}) \times 10^{-5}$ $((8.18^{+1.52+0.00}_{-1.82-5.33}) \times 10^{-5})$	$(1.79^{+1.43+2.39}_{-0.92-1.28}) \times 10^{-5}$	6.01×10^{-5}	5.50×10^{-5}	2.70×10^{-5}	2.20×10^{-5}
$B_c^+ \to J/\psi e^+ \nu_e$	$(2.35^{+0.36+0.04}_{-0.33-0.12}) \times 10^{-2}$ $((2.36^{+0.38+0.04}_{-0.34-0.12}) \times 10^{-2})$	$(1.88^{+0.11+0.06}_{-0.18-0.08}) \times 10^{-2}$	2.13×10^{-2}	1.31×10^{-2}	1.49×10^{-2}	2.07×10^{-2}
$B_c^+ \to J/\psi \mu^+ \nu_\mu$	$(2.34^{+0.36+0.04}_{-0.33-0.12}) \times 10^{-2}$ $((2.35^{+0.37+0.04}_{-0.34-0.12}) \times 10^{-2})$	$(1.87^{+0.11+0.06}_{-0.18-0.08}) \times 10^{-2}$	2.12×10^{-2}	1.30×10^{-2}	1.49×10^{-2}	-
$B_c^+ \to J/\psi \tau^+ \nu_\tau$	$(5.77^{+0.88+0.03}_{-0.82-0.23}) \times 10^{-3}$ $((5.82^{+0.96+0.03}_{-0.86-0.21}) \times 10^{-3})$	$(4.46^{+0.22+0.14}_{-0.41-0.21}) \times 10^{-3}$	4.89×10^{-3}	3.70×10^{-3}	3.70×10^{-3}	4.90×10^{-3}

$A_2^{B_c B^*}$. We observe that the overlap integrand of $A_2^{B_c B^*}$ traverses both positive and negative regions with respect to changes in x_1. The positive and negative peaks are due to the constructive and destructive interference of their corresponding wave functions, and therefore should be added with their respective signs to give the total magnitude of the overlap integrand. It is worth noting that among the $B_c \to B^*$ transition form factors, the area under the peak corresponding to the $V(x_1)$ integrand is larger, which leads to the larger magnitude of the form factor $V^{B_c B^*}(0)$, as listed in Table 4. Similar conclusions can be drawn for other transition form factors. Thus, the overlap integrand plots represent the true behavior of form factors at $q^2 = 0$. Furthermore, the magnitude of the overlap is expected to increase with respect to q^2 to reach a maximum at $q^2_{\max}$. Since the available q^2 range is small, the overlap at $q^2_{\max}$ is expected to be roughly the same as that at $q^2 = 0$. Therefore, a flat behavior of the form factor is expected, as seen in Figs. 2 and 3.

(v) As noted previously, the choice of the $q^+ = 0$ frame of reference restricts the calculation of the form factors only in the space-like region for momentum transfer $q^2 \leq 0$. To understand the physical decay process, we need to know the form factors in the time-like region, i.e., $q^2 > 0$. This can be achieved by extrapolating the form factors as appropriate functions of q^2 (given by Eqs. (37) and (39)), for which the knowledge of form factors at $q^2 = 0$ (see Figs. 8 and 9) is crucial. While the two methods provide independent descriptions of the form factors in space-like and time-like regions, they are nonetheless complementary in nature [78] and therefore provide a complete description of the decay dynamics of the transition process for the full q^2 range. In our work, to determine the form factors over the entire range, we utilize parameterization in Eq. (37) that accommodates the contributions of meson resonances of relevant spin and parity for the entire q^2-channel. Similarly, the parameterization in Eq. (39) isolates meson resonances below the transition threshold for the corresponding meson poles given in Table 1. In the case of B_c to $B_{(s)}^{(*)}$, we use resonances $D_{(s)}^{**}$ as pole masses to analyze q^2 behavior throughout the available range. This can be explained through the confining interaction between c and $\bar{d}(\bar{s})$ to produce $D_{(s)}$ meson resonances that fluctuate into W-boson. In the physical region, the form factors at $q^2 = 0$ are larger than

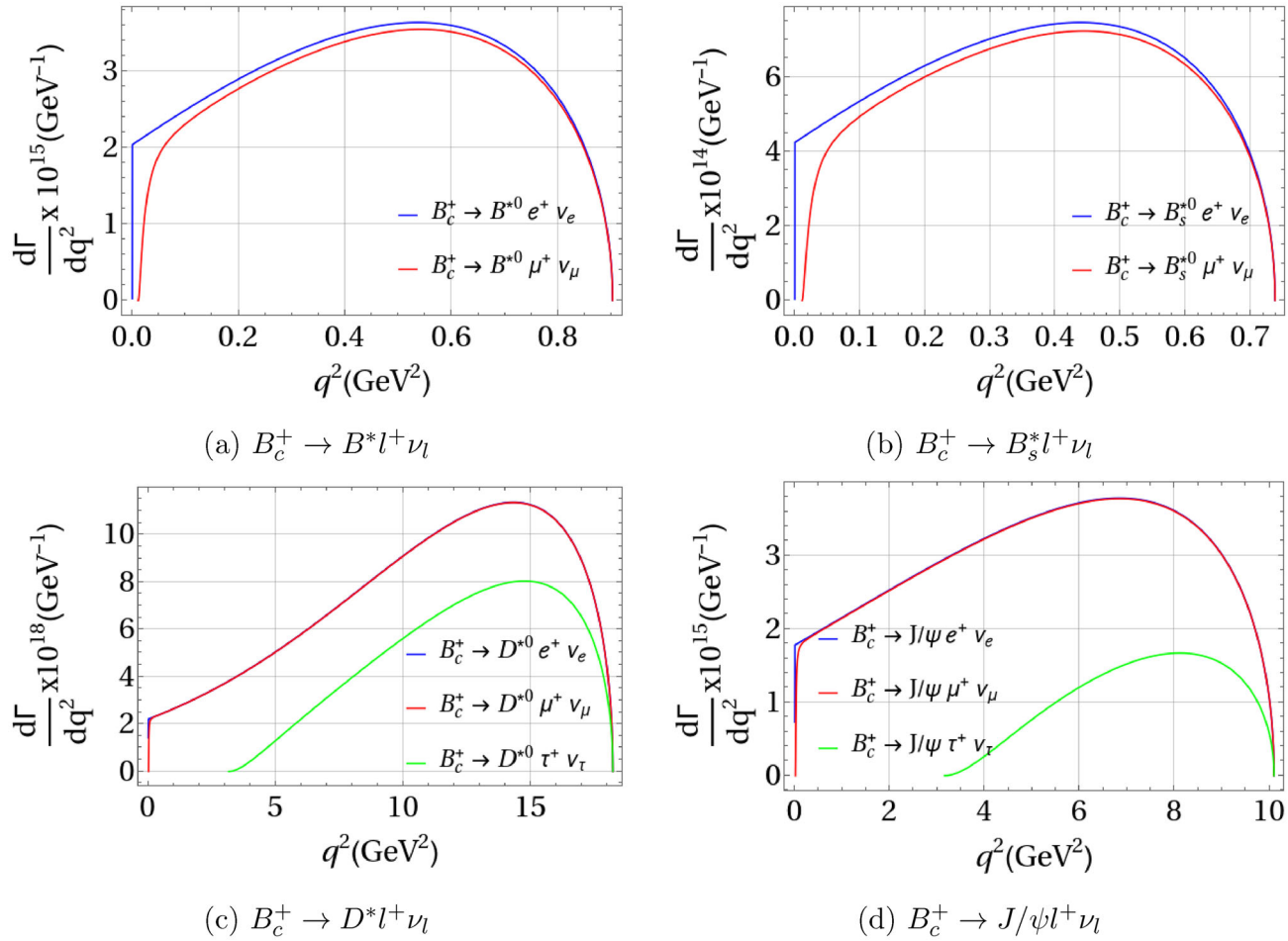

Fig. 10 q^2 variation in differential decay rates of $B_c^+ \to V l^+ \nu_l$ decays in T2A CLFQM using Eq. (41)

the values for bottom-changing transitions. This can be understood as follows: For $B_c \to B_{(s)}^{(*)}$ transition, the energy released to the final state is much smaller than m_b (because $m_c \ll m_b$, and $M_0' \sim m_b$); therefore, the b quark remains almost unaffected. This is reflected in the larger amplitude of the overlap integrand between the initial and final states. The pole at $M^2_{D_{(s)}^{**}}$ lies far from the $q^2_{\rm max}$ ($\lesssim 1$ GeV^2), which is less than $\sim 25\%$ as compared to $M^2_{D_{(s)}^{**}}$ (square of the pole mass). Therefore, the effect of the pole contribution to the q^2 variation in bottom-conserving $B_c \to B_{(s)}^{(*)}$ form factors is smaller. Furthermore, the form factors $F_1(q^2)$, $V(q^2)$, and $A_0(q^2)$ involving M_{1^-} and M_{0^-} poles are affected by roughly $(22-25)\%$ for $B_c \to B^{(*)}$ transitions, while $B_c \to B_s^{(*)}$ transitions are less affected, i.e., by $(5-7)\%$. Thus, these form factors show very small variations in the $0 \le q^2 \le q^2_{\rm max}$. Similarly, $F_0(q^2)$, $A_1(q^2)$, and $A_2(q^2)$ are affected by M_{0^+} and M_{1^+} poles, which lie farther away from $q^2_{\rm max}$, show the least variation with q^2, and therefore show near flat behavior. Additionally, the numerical values of the form factors for $B_c \to B_{(s)}^{(*)}$ transitions at both $q^2 = 0$ and $q^2_{\rm max}$ vary less than 5% between the T2A and T2B. Therefore, we expect that the variation in the form factors over a small q^2 range in bottom-conserving transitions can be reliably estimated by a simple VMD-type pole behavior. However, the parameterizations described by Eqs. (37) and (39) are necessary for the accuracy of the numerical evaluation of the form factors. Moreover, such extension beyond the available q^2 range is important for the understanding of semileptonic decays. This is due to the distinct feature of the semileptonic decays in which resonances are not only observed within the kinematic range of meson decay, but also extend beyond the available q^2 region [85,86].

(vi) For $B_c \to B_{(s)}^*$ transitions, the slope parameters a and b are numerically closer to unity in magnitude and are positive, except for the form factors $A_2^{B_c B^*}$ in type-II correspondence for Eq. (37). Interestingly, the magnitude of the parameter a is very small for $A_2^{B_c B_s^*}$ and is negative

Table 8 Branching ratios of bottom-conserving $B_c \to PV$ decays for CKM-favored, CKM-suppressed, and CKM-doubly-suppressed modes. For the definitions of T2A, T2B, and T1, refer to the caption of Table 4

Decay	Type-II scheme				Type-I scheme	
	T2A		T2B		T1	
	$N_c = \infty$	$N_c = 3$	$N_c = \infty$	$N_c = 3$	$N_c = \infty$	$N_c = 3$
CKM-favored ($\Delta b = 0,\ \Delta C = -1,\ \Delta S = -1$)						
$B_c^+ \to \pi^+ B_s^{*0}$	$(4.86^{+0.01+0.73}_{-0.14-1.08}) \times 10^{-2}$	$(3.64^{+0.01+0.55}_{-0.11-0.81}) \times 10^{-2}$	$(5.21^{+0.03+0.55}_{-0.17-0.66}) \times 10^{-2}$	$(3.90^{+0.02+0.41}_{-0.13-0.50}) \times 10^{-2}$	$(4.48^{+0.00+4.03}_{-0.36-2.95}) \times 10^{-3}$	$(3.35^{+0.00+3.02}_{-0.27-2.21}) \times 10^{-3}$
$B_c^+ \to \overline{K}^0 B^{*+}$	$(7.74^{+0.44+1.81}_{-0.63-2.71}) \times 10^{-3}$	$(2.41^{+0.14+0.56}_{-0.20-0.84}) \times 10^{-4}$	$(9.46^{+0.54+1.22}_{-0.79-1.47}) \times 10^{-3}$	$(2.95^{+0.17+0.38}_{-0.25-0.46}) \times 10^{-4}$	$(1.38^{+0.06+2.43}_{-0.04-1.17}) \times 10^{-5}$	$(4.29^{+0.18+7.58}_{-0.12-3.64}) \times 10^{-7}$
$B_c^+ \to B^+ \overline{K}^{*0}$	$(3.09^{+0.69+0.43}_{-0.57-0.90}) \times 10^{-3}$	$(9.61^{+2.14+1.35}_{-1.76-2.79}) \times 10^{-5}$	$(4.19^{+0.84+0.00}_{-0.74-0.07}) \times 10^{-3}$	$(1.30^{+0.26+0.00}_{-0.23-0.02}) \times 10^{-4}$	$(8.20^{+0.99+6.52}_{-0.93-4.87}) \times 10^{-4}$	$(2.55^{+0.31+2.03}_{-0.29-1.52}) \times 10^{-5}$
$B_c^+ \to B_s^0 \rho^+$	$(3.46^{+0.53+0.25}_{-0.54-0.63}) \times 10^{-2}$	$(2.59^{+0.39+0.19}_{-0.40-0.47}) \times 10^{-2}$	$(4.12^{+0.58+0.00}_{-0.62-0.06}) \times 10^{-2}$	$(3.08^{+0.44+0.00}_{-0.47-0.05}) \times 10^{-2}$	$(1.67^{+0.15+0.68}_{-0.18-0.76}) \times 10^{-2}$	$(1.25^{+0.11+0.51}_{-0.14-0.57}) \times 10^{-2}$
CKM-suppressed ($\Delta b = 0,\ \Delta C = -1,\ \Delta S = 0$)						
$B_c^+ \to K^+ B_s^{*0}$	$(2.45^{+0.04+0.37}_{-0.10-0.64}) \times 10^{-3}$	$(1.83^{+0.03+0.28}_{-0.07-0.48}) \times 10^{-3}$	$(2.83^{+0.05+0.21}_{-0.13-0.28}) \times 10^{-3}$	$(2.11^{+0.04+0.16}_{-0.09-0.21}) \times 10^{-3}$	$(8.43^{+0.00+10.72}_{-0.57-6.03}) \times 10^{-5}$	$(6.31^{+0.00+8.02}_{-0.43-4.51}) \times 10^{-5}$
$B_c^+ \to \pi^+ B^{*0}$	$(2.27^{+0.08+0.50}_{-0.16-0.67}) \times 10^{-3}$	$(1.70^{+0.06+0.38}_{-0.12-0.50}) \times 10^{-3}$	$(2.54^{+0.10+0.41}_{-0.18-0.46}) \times 10^{-3}$	$(1.90^{+0.08+0.31}_{-0.14-0.35}) \times 10^{-3}$	$(1.51^{+0.01+2.40}_{-0.01-1.27}) \times 10^{-5}$	$(1.13^{+0.01+1.79}_{-0.00-0.95}) \times 10^{-5}$
$B_c^+ \to \pi^0 B^{*+}$	$(1.86^{+0.07+0.41}_{-0.13-0.55}) \times 10^{-4}$	$(5.79^{+0.21+1.29}_{-0.41-1.71}) \times 10^{-6}$	$(2.08^{+0.08+0.34}_{-0.15-0.38}) \times 10^{-4}$	$(6.48^{+0.26+1.06}_{-0.46-1.18}) \times 10^{-6}$	$(1.25^{+0.01+1.98}_{-0.00-1.05}) \times 10^{-6}$	$(3.89^{+0.02+6.17}_{-0.01-3.27}) \times 10^{-8}$
$B_c^+ \to \eta B^{*+}$	$(6.99^{+0.43+1.66}_{-0.59-2.54}) \times 10^{-4}$	$(2.18^{+0.13+0.52}_{-0.18-0.79}) \times 10^{-5}$	$(8.64^{+0.51+1.08}_{-0.74-1.31}) \times 10^{-4}$	$(2.69^{+0.16+0.34}_{-0.23-0.41}) \times 10^{-5}$	$(9.77^{+0.44+17.51}_{-0.29-8.31}) \times 10^{-7}$	$(3.04^{+0.14+5.45}_{-0.09-2.59}) \times 10^{-8}$
$B_c^+ \to B^+ \rho^0$	$(2.28^{+0.48+0.26}_{-0.41-0.56}) \times 10^{-4}$	$(7.10^{+1.49+0.81}_{-1.26-1.74}) \times 10^{-6}$	$(2.98^{+0.58+0.00}_{-0.52-0.06}) \times 10^{-4}$	$(9.28^{+1.82+0.00}_{-1.62-0.19}) \times 10^{-6}$	$(8.25^{+1.09+5.12}_{-1.02-4.49}) \times 10^{-5}$	$(2.57^{+0.34+1.59}_{-0.32-1.40}) \times 10^{-6}$
$B_c^+ \to B^+ \omega$	$(2.19^{+0.46+0.26}_{-0.39-0.55}) \times 10^{-4}$	$(6.82^{+1.44+0.80}_{-1.22-1.70}) \times 10^{-6}$	$(2.87^{+0.56+0.00}_{-0.50-0.06}) \times 10^{-4}$	$(8.95^{+1.76+0.00}_{-1.56-0.17}) \times 10^{-6}$	$(7.69^{+1.01+4.90}_{-0.94-4.22}) \times 10^{-5}$	$(2.39^{+0.31+1.52}_{-0.29-1.32}) \times 10^{-6}$
$B_c^+ \to B^0 \rho^+$	$(2.77^{+0.58+0.32}_{-0.49-0.68}) \times 10^{-3}$	$(2.08^{+0.44+0.24}_{-0.37-0.51}) \times 10^{-3}$	$(3.63^{+0.71+0.00}_{-0.63-0.07}) \times 10^{-3}$	$(2.71^{+0.53+0.00}_{-0.47-0.05}) \times 10^{-3}$	$(1.01^{+0.13+0.62}_{-0.12-0.55}) \times 10^{-3}$	$(7.52^{+0.99+4.66}_{-0.93-4.09}) \times 10^{-4}$
$B_c^+ \to B_s^0 K^{*+}$	$(5.62^{+0.93+0.47}_{-0.91-1.21}) \times 10^{-5}$	$(4.20^{+0.70+0.35}_{-0.68-0.90}) \times 10^{-5}$	$(6.80^{+0.99+0.00}_{-1.05-0.14}) \times 10^{-5}$	$(5.09^{+0.74+0.00}_{-0.78-0.11}) \times 10^{-5}$	$(2.13^{+0.17+1.15}_{-0.22-1.11}) \times 10^{-5}$	$(1.60^{+0.13+0.86}_{-0.16-0.83}) \times 10^{-5}$
CKM-doubly-suppressed ($\Delta b = 0,\ \Delta C = -1,\ \Delta S = 1$)						
$B_c^+ \to K^+ B^{*0}$	$(1.29^{+0.07+0.30}_{-0.11-0.45}) \times 10^{-4}$	$(9.69^{+0.54+2.27}_{-0.79-3.38}) \times 10^{-5}$	$(1.58^{+0.09+0.20}_{-0.13-0.25}) \times 10^{-4}$	$(1.18^{+0.07+0.15}_{-0.10-0.18}) \times 10^{-4}$	$(2.35^{+0.10+4.15}_{-0.06-1.99}) \times 10^{-7}$	$(1.76^{+0.07+3.10}_{-0.05-1.49}) \times 10^{-7}$
$B_c^+ \to K^0 B^{*+}$	$(2.11^{+0.12+0.49}_{-0.17-0.74}) \times 10^{-5}$	$(6.57^{+0.37+1.54}_{-0.54-2.30}) \times 10^{-7}$	$(2.58^{+0.15+0.33}_{-0.22-0.40}) \times 10^{-5}$	$(8.03^{+0.45+1.04}_{-0.67-1.25}) \times 10^{-7}$	$(3.75^{+0.15+6.64}_{-0.10-3.19}) \times 10^{-8}$	$(1.17^{+0.05+2.07}_{-0.03-0.99}) \times 10^{-9}$
$B_c^+ \to B^+ K^{*0}$	$(8.42^{+1.87+1.18}_{-1.54-2.44}) \times 10^{-6}$	$(2.62^{+0.58+0.37}_{-0.48-0.76}) \times 10^{-7}$	$(1.14^{+0.23+0.00}_{-0.20-0.02}) \times 10^{-5}$	$(3.56^{+0.71+0.00}_{-0.63-0.06}) \times 10^{-7}$	$(2.24^{+0.27+1.78}_{-0.25-1.33}) \times 10^{-6}$	$(6.96^{+0.84+5.53}_{-0.79-4.14}) \times 10^{-8}$
$B_c^+ \to B^0 K^{*+}$	$(5.10^{+1.13+0.71}_{-0.94-1.48}) \times 10^{-5}$	$(3.82^{+0.85+0.54}_{-0.70-1.11}) \times 10^{-5}$	$(6.93^{+1.39+0.00}_{-1.23-0.11}) \times 10^{-5}$	$(5.18^{+1.04+0.00}_{-0.92-0.08}) \times 10^{-5}$	$(1.36^{+0.16+1.08}_{-0.15-0.81}) \times 10^{-5}$	$(1.02^{+0.12+0.81}_{-0.12-0.60}) \times 10^{-5}$

Table 9 Branching ratios of bottom-changing $B_c \to PV$ decays for CKM-favored modes. For the definitions of T2A, T2B, and T1, refer to the caption of Table 4

Decay	Type-II scheme				Type-I scheme	
	T2A		T2B		T1	
	$N_c = \infty$	$N_c = 3$	$N_c = \infty$	$N_c = 3$	$N_c = \infty$	$N_c = 3$
$\Delta b = -1,\ \Delta C = -1,\ \Delta S = 0$						
$B_c^+ \to \pi^+ J/\psi$	$(1.65^{+0.31+0.10}_{-0.29-0.15}) \times 10^{-3}$	$(1.40^{+0.27+0.09}_{-0.24-0.12}) \times 10^{-3}$	$(1.66^{+0.32+0.10}_{-0.29-0.15}) \times 10^{-3}$	$(1.41^{+0.27+0.09}_{-0.25-0.12}) \times 10^{-3}$	$(1.23^{+0.09+0.04}_{-0.08-0.08}) \times 10^{-3}$	$(1.05^{+0.07+0.04}_{-0.07-0.07}) \times 10^{-3}$
$B_c^+ \to \overline{D}^0 D^{*+}$	$(4.10^{+0.83+2.94}_{-0.78-2.31}) \times 10^{-5}$	$(7.79^{+1.57+5.59}_{-1.47-4.40}) \times 10^{-6}$	$(3.54^{+0.66+2.67}_{-0.63-1.96}) \times 10^{-5}$	$(6.73^{+1.26+5.07}_{-1.20-3.73}) \times 10^{-6}$	$(2.44^{+0.58+4.81}_{-1.79-1.91}) \times 10^{-6}$	$(4.64^{+1.11+9.13}_{-3.39-3.63}) \times 10^{-7}$
$B_c^+ \to D^+ \overline{D}^{*0}$	$(3.94^{+2.05+1.29}_{-1.28-1.21}) \times 10^{-5}$	$(7.48^{+3.90+2.45}_{-2.44-2.30}) \times 10^{-6}$	$(3.27^{+1.64+1.11}_{-1.03-0.97}) \times 10^{-5}$	$(6.22^{+3.12+2.11}_{-1.96-1.83}) \times 10^{-6}$	$(3.13^{+1.92+1.37}_{-1.15-1.22}) \times 10^{-5}$	$(5.95^{+3.65+2.61}_{-2.18-2.31}) \times 10^{-6}$
$B_c^+ \to \eta_c \rho^+$	$(3.91^{+0.13+0.11}_{-0.12-0.24}) \times 10^{-3}$	$(3.33^{+0.11+0.10}_{-0.10-0.20}) \times 10^{-3}$	$(3.96^{+0.12+0.11}_{-0.12-0.23}) \times 10^{-3}$	$(3.37^{+0.10+0.09}_{-0.10-0.20}) \times 10^{-3}$	$(3.90^{+0.13+0.12}_{-0.12-0.24}) \times 10^{-3}$	$(3.32^{+0.11+0.10}_{-0.11-0.20}) \times 10^{-3}$
$\Delta b = -1,\ \Delta C = 0,\ \Delta S = 1$						
$B_c^+ \to \pi^0 D_s^{*+}$	$(4.40^{+0.37+3.42}_{-0.70-2.45}) \times 10^{-9}$	$(8.37^{+0.71+6.50}_{-1.34-4.65}) \times 10^{-10}$	$(4.83^{+0.39+3.57}_{-0.74-2.59}) \times 10^{-9}$	$(9.19^{+0.74+6.77}_{-1.40-4.92}) \times 10^{-10}$	$(2.47^{+0.56+1.92}_{-0.75-1.37}) \times 10^{-9}$	$(4.69^{+1.07+3.66}_{-1.43-2.61}) \times 10^{-10}$
$B_c^+ \to \eta D_s^{*+}$	$(5.16^{+0.43+3.96}_{-0.82-2.85}) \times 10^{-9}$	$(9.81^{+0.82+7.53}_{-1.56-5.42}) \times 10^{-10}$	$(5.75^{+0.44+4.15}_{-0.86-3.05}) \times 10^{-9}$	$(1.09^{+0.08+0.79}_{-0.16-0.58}) \times 10^{-9}$	$(2.70^{+0.39+2.22}_{-0.78-1.56}) \times 10^{-9}$	$(5.12^{+0.74+4.22}_{-1.48-2.96}) \times 10^{-10}$
$B_c^+ \to K^+ D^{*0}$	$(1.70^{+0.35+1.38}_{-0.32-0.98}) \times 10^{-7}$	$(1.45^{+0.30+1.18}_{-0.27-0.83}) \times 10^{-7}$	$(1.75^{+0.36+1.40}_{-0.33-1.00}) \times 10^{-7}$	$(1.49^{+0.30+1.20}_{-0.28-0.85}) \times 10^{-7}$	$(7.36^{+0.00+6.76}_{-1.68-4.53}) \times 10^{-8}$	$(6.26^{+0.00+5.76}_{-1.43-3.86}) \times 10^{-8}$
$B_c^+ \to \eta' D_s^{*+}$	$(1.73^{+0.14+1.29}_{-0.27-0.95}) \times 10^{-9}$	$(3.30^{+0.26+2.46}_{-0.52-1.80}) \times 10^{-10}$	$(1.89^{+0.14+1.34}_{-0.28-0.99}) \times 10^{-9}$	$(3.60^{+0.26+2.54}_{-0.53-1.89}) \times 10^{-10}$	$(7.55^{+0.00+7.05}_{-1.91-4.68}) \times 10^{-10}$	$(1.44^{+0.00+1.34}_{-0.36-0.89}) \times 10^{-10}$
$B_c^+ \to D^0 K^{*+}$	$(2.31^{+1.20+0.85}_{-0.74-0.73}) \times 10^{-7}$	$(1.97^{+1.02+0.73}_{-0.63-0.62}) \times 10^{-7}$	$(2.34^{+1.20+0.85}_{-0.75-0.72}) \times 10^{-7}$	$(1.99^{+1.02+0.72}_{-0.64-0.62}) \times 10^{-7}$	$(2.26^{+1.20+0.86}_{-0.73-0.73}) \times 10^{-7}$	$(1.92^{+1.02+0.73}_{-0.62-0.62}) \times 10^{-7}$
$B_c^+ \to D_s^+ \rho^0$	$(1.34^{+0.46+0.21}_{-0.39-0.20}) \times 10^{-8}$	$(2.55^{+0.87+0.41}_{-0.75-0.38}) \times 10^{-9}$	$(1.37^{+0.46+0.21}_{-0.40-0.20}) \times 10^{-8}$	$(2.59^{+0.88+0.41}_{-0.75-0.38}) \times 10^{-9}$	$(1.33^{+0.46+0.22}_{-0.39-0.20}) \times 10^{-8}$	$(2.52^{+0.87+0.41}_{-0.74-0.38}) \times 10^{-9}$
$B_c^+ \to D_s^+ \omega$	$(9.28^{+3.17+1.47}_{-2.72-1.37}) \times 10^{-10}$	$(1.76^{+0.60+0.28}_{-0.52-0.26}) \times 10^{-10}$	$(9.44^{+3.21+1.47}_{-2.75-1.38}) \times 10^{-10}$	$(1.79^{+0.61+0.28}_{-0.52-0.26}) \times 10^{-10}$	$(9.18^{+3.18+1.49}_{-2.71-1.40}) \times 10^{-10}$	$(1.75^{+0.60+0.28}_{-0.51-0.27}) \times 10^{-10}$
$B_c^+ \to D_s^+ \phi$	$(1.50^{+0.51+0.23}_{-0.44-0.22}) \times 10^{-8}$	$(2.85^{+0.97+0.44}_{-0.83-0.41}) \times 10^{-9}$	$(1.50^{+0.51+0.23}_{-0.43-0.21}) \times 10^{-8}$	$(2.84^{+0.96+0.43}_{-0.82-0.41}) \times 10^{-9}$	$(1.47^{+0.51+0.24}_{-0.43-0.22}) \times 10^{-8}$	$(2.79^{+0.97+0.45}_{-0.83-0.42}) \times 10^{-9}$
$B_c^+ \to D_s^+ J/\psi$	$(2.44^{+0.99+0.00}_{-0.81-0.07}) \times 10^{-3}$	$(4.69^{+0.62+0.17}_{-0.58-0.33}) \times 10^{-3}$	$(2.40^{+0.83+0.06}_{-0.70-0.14}) \times 10^{-3}$	$(3.97^{+0.59+0.21}_{-0.55-0.31}) \times 10^{-3}$	$(1.93^{+0.45+0.00}_{-0.51-0.06}) \times 10^{-3}$	$(3.12^{+0.09+0.25}_{-0.15-0.40}) \times 10^{-3}$
$B_c^+ \to \eta_c D_s^{*+}$	$(1.69^{+0.05+0.29}_{-0.00-0.26}) \times 10^{-3}$	$(3.01^{+0.12+0.19}_{-0.15-0.32}) \times 10^{-3}$	$(1.56^{+0.03+0.14}_{-0.00-0.18}) \times 10^{-3}$	$(2.54^{+0.08+0.18}_{-0.10-0.25}) \times 10^{-3}$	$(2.63^{+0.16+0.00}_{-0.11-0.07}) \times 10^{-3}$	$(2.41^{+0.08+0.09}_{-0.09-0.15}) \times 10^{-3}$

Table 10 Branching ratios of bottom-changing $B_c \to PV$ decays for CKM-suppressed modes. For the definitions of T2A, T2B, and T1, refer to the caption of Table 4

Decay	Type-II scheme				Type-I scheme	
	T2A		T2B		T1	
	$N_c = \infty$	$N_c = 3$	$N_c = \infty$	$N_c = 3$	$N_c = \infty$	$N_c = 3$
$\Delta b = -1,\ \Delta C = -1,\ \Delta S = 1$						
$B_c^+ \to K^+ J/\psi$	$(1.23^{+0.23+0.07}_{-0.21-0.11}) \times 10^{-4}$	$(1.05^{+0.20+0.06}_{-0.18-0.09}) \times 10^{-4}$	$(1.25^{+0.24+0.07}_{-0.22-0.11}) \times 10^{-4}$	$(1.06^{+0.20+0.06}_{-0.19-0.09}) \times 10^{-4}$	$(9.19^{+0.65+0.32}_{-0.64-0.63}) \times 10^{-5}$	$(7.82^{+0.56+0.27}_{-0.54-0.54}) \times 10^{-5}$
$B_c^+ \to \overline{D}^0 D_s^{*+}$	$(2.92^{+0.21+1.97}_{-0.46-1.57}) \times 10^{-6}$	$(5.55^{+0.41+3.74}_{-0.87-2.98}) \times 10^{-7}$	$(2.74^{+0.18+1.85}_{-0.39-1.40}) \times 10^{-6}$	$(5.21^{+0.34+3.52}_{-0.73-2.67}) \times 10^{-7}$	$(4.36^{+0.00+6.69}_{-1.70-3.23}) \times 10^{-7}$	$(8.29^{+0.00+12.70}_{-3.24-6.13}) \times 10^{-8}$
$B_c^+ \to D_s^+ \overline{D}^{*0}$	$(4.08^{+1.36+0.51}_{-1.19-0.51}) \times 10^{-6}$	$(7.76^{+2.58+0.96}_{-2.26-0.96}) \times 10^{-7}$	$(3.43^{+1.14+0.48}_{-0.98-0.46}) \times 10^{-6}$	$(6.53^{+2.16+0.91}_{-1.86-0.87}) \times 10^{-7}$	$(3.54^{+1.36+0.62}_{-1.13-0.63}) \times 10^{-6}$	$(6.72^{+2.59+1.17}_{-2.14-1.20}) \times 10^{-7}$
$B_c^+ \to \eta_c K^{*+}$	$(1.94^{+0.06+0.05}_{-0.06-0.11}) \times 10^{-4}$	$(1.65^{+0.05+0.05}_{-0.05-0.10}) \times 10^{-4}$	$(1.95^{+0.06+0.05}_{-0.06-0.11}) \times 10^{-4}$	$(1.66^{+0.05+0.05}_{-0.05-0.10}) \times 10^{-4}$	$(1.93^{+0.06+0.06}_{-0.06-0.12}) \times 10^{-4}$	$(1.64^{+0.05+0.05}_{-0.05-0.10}) \times 10^{-4}$
$\Delta b = -1,\ \Delta C = 0,\ \Delta S = 0$						
$B_c^+ \to \pi^0 D^{*+}$	$(5.98^{+1.25+4.91}_{-1.13-3.45}) \times 10^{-8}$	$(1.14^{+0.24+0.93}_{-0.22-0.66}) \times 10^{-8}$	$(6.05^{+1.26+4.94}_{-1.14-3.48}) \times 10^{-8}$	$(1.15^{+0.24+0.94}_{-0.22-0.66}) \times 10^{-8}$	$(2.90^{+0.00+2.46}_{-0.76-1.71}) \times 10^{-8}$	$(5.51^{+0.00+4.67}_{-1.45-3.25}) \times 10^{-9}$
$B_c^+ \to \pi^+ D^{*0}$	$(2.22^{+0.47+1.82}_{-0.42-1.28}) \times 10^{-6}$	$(1.89^{+0.40+1.55}_{-0.36-1.09}) \times 10^{-6}$	$(2.25^{+0.47+1.84}_{-0.43-1.29}) \times 10^{-6}$	$(1.91^{+0.40+1.56}_{-0.36-1.11}) \times 10^{-6}$	$(1.08^{+0.00+0.91}_{-0.28-0.63}) \times 10^{-6}$	$(9.17^{+0.00+7.78}_{-2.41-5.40}) \times 10^{-7}$
$B_c^+ \to \eta D^{*+}$	$(7.03^{+1.46+5.70}_{-1.33-4.04}) \times 10^{-8}$	$(1.33^{+0.28+1.08}_{-0.25-0.77}) \times 10^{-8}$	$(7.21^{+1.46+5.78}_{-1.35-4.12}) \times 10^{-8}$	$(1.37^{+0.28+1.10}_{-0.26-0.78}) \times 10^{-8}$	$(2.95^{+0.00+2.76}_{-0.65-1.83}) \times 10^{-8}$	$(5.60^{+0.00+5.25}_{-1.23-3.48}) \times 10^{-9}$
$B_c^+ \to \eta' D^{*+}$	$(2.37^{+0.49+1.87}_{-0.44-1.35}) \times 10^{-8}$	$(4.51^{+0.92+3.56}_{-0.84-2.57}) \times 10^{-9}$	$(2.39^{+0.47+1.88}_{-0.44-1.35}) \times 10^{-8}$	$(4.54^{+0.90+3.57}_{-0.84-2.57}) \times 10^{-9}$	$(7.03^{+0.00+8.07}_{-3.18-4.77}) \times 10^{-9}$	$(1.34^{+0.00+1.53}_{-0.60-0.91}) \times 10^{-9}$
$B_c^+ \to D^+ \rho^0$	$(1.22^{+0.64+0.46}_{-0.39-0.39}) \times 10^{-7}$	$(2.32^{+1.21+0.87}_{-0.74-0.74}) \times 10^{-8}$	$(1.25^{+0.64+0.46}_{-0.40-0.39}) \times 10^{-7}$	$(2.37^{+1.22+0.87}_{-0.76-0.74}) \times 10^{-8}$	$(1.20^{+0.64+0.46}_{-0.39-0.39}) \times 10^{-7}$	$(2.28^{+1.21+0.87}_{-0.74-0.74}) \times 10^{-8}$
$B_c^+ \to D^+ \omega$	$(8.45^{+4.41+3.15}_{-2.71-2.68}) \times 10^{-9}$	$(1.61^{+0.84+0.60}_{-0.51-0.51}) \times 10^{-9}$	$(8.62^{+4.45+3.16}_{-2.76-2.68}) \times 10^{-9}$	$(1.64^{+0.85+0.60}_{-0.52-0.51}) \times 10^{-9}$	$(8.31^{+4.39+3.17}_{-2.69-2.69}) \times 10^{-9}$	$(1.58^{+0.84+0.60}_{-0.51-0.51}) \times 10^{-9}$
$B_c^+ \to D^+ \phi$	$(1.37^{+0.71+0.50}_{-0.44-0.43}) \times 10^{-7}$	$(2.61^{+1.36+0.95}_{-0.84-0.82}) \times 10^{-8}$	$(1.38^{+0.71+0.50}_{-0.44-0.42}) \times 10^{-7}$	$(2.61^{+1.34+0.94}_{-0.83-0.81}) \times 10^{-8}$	$(1.33^{+0.71+0.51}_{-0.43-0.43}) \times 10^{-7}$	$(2.53^{+1.35+0.96}_{-0.83-0.82}) \times 10^{-8}$
$B_c^+ \to D^0 \rho^+$	$(4.54^{+2.37+1.69}_{-1.46-1.44}) \times 10^{-6}$	$(3.87^{+2.02+1.44}_{-1.24-1.22}) \times 10^{-6}$	$(4.64^{+2.39+1.70}_{-1.48-1.44}) \times 10^{-6}$	$(3.95^{+2.04+1.45}_{-1.26-1.23}) \times 10^{-6}$	$(4.47^{+2.36+1.70}_{-1.45-1.44}) \times 10^{-6}$	$(3.80^{+2.01+1.45}_{-1.23-1.23}) \times 10^{-6}$
$B_c^+ \to D^+ J/\psi$	$(9.51^{+3.79+0.45}_{-3.43-0.54}) \times 10^{-5}$	$(1.63^{+0.21+0.10}_{-0.18-0.16}) \times 10^{-4}$	$(9.32^{+3.11+0.00}_{-2.83-0.21}) \times 10^{-5}$	$(1.42^{+0.21+0.09}_{-0.19-0.13}) \times 10^{-4}$	$(8.10^{+1.60+0.07}_{-2.03-0.61}) \times 10^{-5}$	$(1.08^{+0.04+0.10}_{-0.04-0.15}) \times 10^{-4}$
$B_c^+ \to \eta_c D^{*+}$	$(1.12^{+0.03+0.16}_{-0.03-0.14}) \times 10^{-4}$	$(1.73^{+0.09+0.10}_{-0.09-0.18}) \times 10^{-4}$	$(1.05^{+0.00+0.07}_{-0.00-0.10}) \times 10^{-4}$	$(1.49^{+0.06+0.10}_{-0.06-0.14}) \times 10^{-4}$	$(1.63^{+0.09+0.00}_{-0.07-0.07}) \times 10^{-4}$	$(1.43^{+0.05+0.04}_{-0.05-0.08}) \times 10^{-4}$

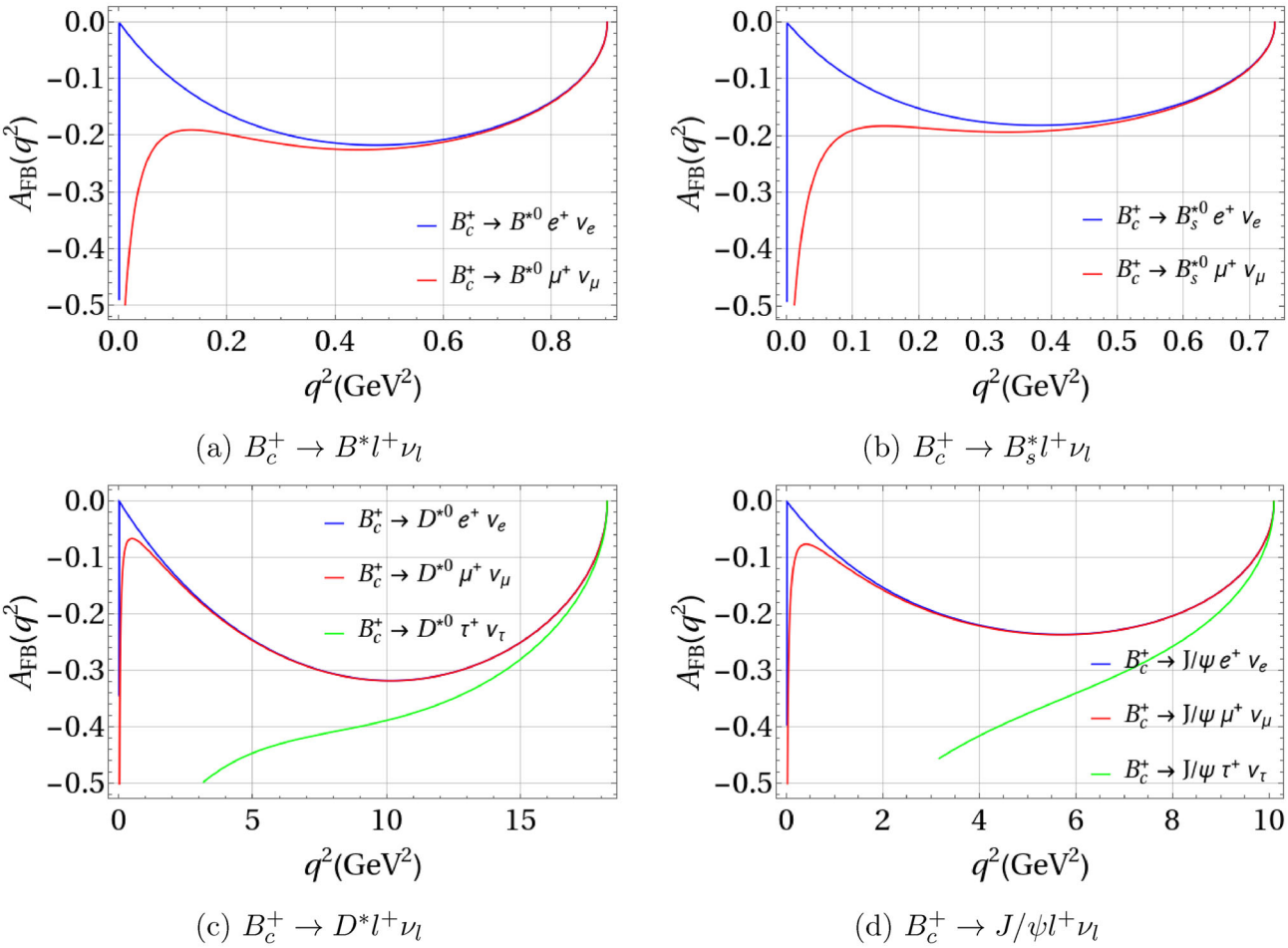

Fig. 11 q^2 variation in forward-backward asymmetries of $B_c^+ \to V l^+ \nu_l$ decays in T2A CLFQM using Eq. (50)

for $A_2^{B_c B^*}$, which explains the flat behavior, as shown in Fig. 3. We found that the numerical values of all the form factors for the type-I scheme (using Eq. (38) and parent pole mass) are less than 1, except for $V(0)$, and the same can be observed for T2A and T2B. Although the numerical values of $V(0)$ between T1 and T2A (T2B) differ by an average of roughly 15%, the slope parameters are substantially different. Interestingly, the slope parameter a is negative and greater than 1 for all the form factors except $A_1^{B_c B_{(s)}^*}$. The parameter b has very large values in the range of roughly $130 - 1150$ (largest for $A_0(q^2)$ in type-I) with a positive sign. It may be noted that both slope parameters (a and b) are exceptionally large for the form factor $A_0^{B_c B_{(s)}^*}$. Similar observations can be made for the remaining form factors, where the slope parameters a and b are typically large for the type-I scheme. Like the $B_c \to P$ bottom-conserving transitions, we observe smaller numerical values for the $B_c \to B_{(s)}^*$ form factors along with a decreasing trend in the type-I scheme compared to type-II correspondence (inclusive of both T2A and T2B predictions). In addition, we observe that the form factors $A_0(q^2)$ and $A_1(q^2)$ affected by the zero-mode contributions show a substantial decrease in the numerical values with respect to the type-I scheme. Furthermore, the $A_1(0)$ form factors change by $\sim 23\%$ for both T2A and T2B in addition to the a and b parameters. We want to emphasize that the numerical values of the T2A and T2B $B_c \to B_{(s)}^*$ form factors exhibit a significant variation in the magnitude of $A_0(0)$ form factors, i.e., $\sim 90\%(70\%)$, compared to type-I scheme. The impact of the spectator quark mass on the numerical values of $B_c \to B_{(s)}^*$ transition form factors over the available q^2 is negligible, which was also recently observed by LQCD calculations [20].

(vii) Furthermore, we analyze the z-series parameterization of the form factors at maximum recoil point (a_0'), as given in Eq. (39). The numerical results obtained from z-series parameterization are surprisingly consistent with those obtained from the q^2 dependence used in Eq. (37). In addition, the free parameters a_1' and a_2' take very large values, as shown in Table 4. However, the sign for the

Table 11 Branching ratios of bottom-changing $B_c \to PV$ decays for CKM-doubly-suppressed modes. For the definitions of T2A, T2B, and T1, refer to the caption of Table 4

Decay	Type-II scheme				Type-I scheme	
	T2A		T2B		T1	
	$N_c = \infty$	$N_c = 3$	$N_c = \infty$	$N_c = 3$	$N_c = \infty$	$N_c = 3$
$\Delta b = -1,\ \Delta C = 1,\ \Delta S = 1$						
$B_c^+ \to D^0 D_s^{*+}$	$(3.06^{+2.22+0.60}_{-1.20-0.63}) \times 10^{-6}$	$(6.55^{+3.06+2.38}_{-2.02-2.22}) \times 10^{-6}$	$(2.32^{+1.66+0.46}_{-0.90-0.43}) \times 10^{-6}$	$(5.39^{+2.38+2.03}_{-1.59-1.74}) \times 10^{-6}$	$(3.47^{+2.86+1.13}_{-1.43-1.19}) \times 10^{-6}$	$(4.34^{+2.45+2.21}_{-1.57-1.85}) \times 10^{-6}$
$B_c^+ \to D_s^+ D^{*0}$	$(5.69^{+0.91+5.34}_{-0.88-3.88}) \times 10^{-6}$	$(1.10^{+0.24+0.70}_{-0.22-0.58}) \times 10^{-5}$	$(4.79^{+0.66+4.74}_{-0.67-3.18}) \times 10^{-6}$	$(9.27^{+1.86+6.27}_{-1.76-4.76}) \times 10^{-6}$	$(5.46^{+297.99+139.86}_{-0.00-0.00}) \times 10^{-9}$	$(9.44^{+0.50+12.42}_{-4.32-5.89}) \times 10^{-7}$
$\Delta b = -1,\ \Delta C = 1,\ \Delta S = 0$						
$B_c^+ \to D^+ D^{*0}$	$(2.06^{+0.24+1.73}_{-0.30-1.29}) \times 10^{-7}$	$(3.60^{+0.83+2.43}_{-0.73-1.95}) \times 10^{-7}$	$(1.80^{+0.18+1.58}_{-0.25-1.11}) \times 10^{-7}$	$(3.09^{+0.66+2.20}_{-0.59-1.64}) \times 10^{-7}$	$(5.52^{+54.35+100.42}_{-0.00-0.00}) \times 10^{-10}$	$(3.36^{+0.16+4.98}_{-1.57-2.32}) \times 10^{-8}$
$B_c^+ \to D^0 D^{*+}$	$(1.93^{+1.21+0.42}_{-0.71-0.42}) \times 10^{-7}$	$(3.48^{+1.70+1.27}_{-1.09-1.17}) \times 10^{-7}$	$(1.58^{+0.96+0.35}_{-0.56-0.32}) \times 10^{-7}$	$(2.90^{+1.36+1.10}_{-0.88-0.94}) \times 10^{-7}$	$(2.30^{+1.72+0.81}_{-0.92-0.82}) \times 10^{-7}$	$(2.38^{+1.33+1.13}_{-0.84-0.96}) \times 10^{-7}$

a_1' parameter is consistently negative, and the a_2' parameter is positive, except for $A_2^{B_c B^*}(q^2)$. Further, the magnitude of the a_2' parameter is much larger than the a_1' parameter because the coefficients take large values for smaller $\pm|z|_{\max}$ (i.e., $\approx \pm 0.0008$ for B_c to $B_{(s)}^{(*)}$ transition). In addition, the uncertainties corresponding to the quark masses and β values in a_2' are larger than those of the a_1' parameter. As already pointed out, the q^2 behavior of power series expansion, as shown by T2B in Figs. 2 and 3, is consistent with the q^2 behavior corresponding to Eq. (37). However, it shows a relatively large variation toward the maximum q^2, particularly for $V(q^2)$ form factors. Therefore, we reemphasize that both q^2 formulations for T2A (T2B) appear to be consistent with each other within very small numerical variations.

3.1.2 *Bottom-changing transition form factors*

(i) The bottom-changing transitions typically exhibit a wider range of q^2 than bottom-conserving transitions. In the case of $B_c \to D^{(*)}$ transition form factors, it is expected that the q^2 range will be considerably broader with respect to $B_c \to \eta_c(J/\psi)$ form factors, spanning from $0 \le q^2 \lesssim 20\,\text{GeV}^2$. This extended range offers an opportunity to examine how the form factors are influenced by the dependence on q^2 and to highlight the importance of the resonance pole contribution below the threshold. We plot the bottom-changing B_c to P and V transition form factors to observe their variation with respect to q^2, as shown in Figs. 4 and 5, respectively. The form factors remain the same at $q^2 = 0$ for all the bottom-changing transitions in both T2A and T2B formulations. For bottom-changing transitions, the slope parameters of both $B_c \to P$ and $B_c \to V$ form factors are positive and in the range of $a, b \subset (0,\ 2)$ and $a, b \subset (0,\ 3)$, respectively, as given in Table 5.

(ii) Similar to the bottom-conserving case, to understand the dynamics of the $B_c \to D^{(*)}$ transitions, we plot the wave function overlap between the initial $\psi_{B_c}(x_1)$ and final $\psi_{D^{(*)}}(x_1)$ wave functions at $q^2 = 0$ using Eq. (5), as shown in Fig. 7a. Due to the limited overlap near $q^2 = 0$, the numerical values of the form factors are expected to be smaller than those for $B_c \to B_{(s)}^{(*)}$ and $B_c \to \eta_c(J/\psi)$ transitions. Since the fraction of momentum carried by the spectator c quark is of the order of the decaying b quark, u quark takes minimal momentum. Consequently, $\psi_{D^{(*)}}(x_1)$ exhibits its maximum near $x_1 \sim 1/4$ with a larger width, while the peak for $\psi_{B_c}(x_1)$ lies at $x_1 \sim 3/4$. The available q^2 for B_c to $D^{(*)}$ transitions is significantly large ($0 \le q^2 \lesssim 20$ GeV^2); hence, these $b \to u$ transitions involve B^{**} poles fluctuating in the weak current $b\bar{u}$. Moreover, the

Table 12 Branching ratios of bottom-conserving $B_c \to PV$ decays as predicted in other models

Decay	RIQM [38]	RCQM [35]	RQM [33]	QCDF [42]
$B_c^+ \to \pi^+ B_s^{*0}$	8.61×10^{-2}	2.1×10^{-2}	1.6×10^{-2}	–
$B_c^+ \to \overline{K}^0 B^{*+}$	2.26×10^{-2}	8.8×10^{-4}	1.1×10^{-3}	–
$B_c^+ \to B^+ \overline{K}^{*0}$	1.83×10^{-2}	1.1×10^{-3}	9.0×10^{-4}	3.72×10^{-3}
$B_c^+ \to B_s^0 \rho^+$	9.97×10^{-2}	2.3×10^{-2}	1.4×10^{-2}	4.44×10^{-2}
$B_c^+ \to K^+ B_s^{*0}$	4.99×10^{-3}	1.3×10^{-3}	1.1×10^{-3}	–
$B_c^+ \to \pi^+ B^{*0}$	5.55×10^{-3}	5.7×10^{-4}	2.6×10^{-4}	–
$B_c^+ \to \pi^0 B^{*+}$	4.70×10^{-4}	2.0×10^{-5}	1.0×10^{-5}	–
$B_c^+ \to B^+ \rho^0$	1.06×10^{-3}	7.1×10^{-5}	5.0×10^{-5}	2.86×10^{-4}
$B_c^+ \to B^+ \omega$	–	–	–	2.05×10^{-4}
$B_c^+ \to B^0 \rho^+$	1.30×10^{-2}	2.0×10^{-3}	1.3×10^{-3}	5.32×10^{-3}
$B_c^+ \to B_s^0 K^{*+}$	4.00×10^{-4}	1.1×10^{-4}	3.0×10^{-5}	1.25×10^{-4}
$B_c^+ \to K^+ B^{*0}$	3.90×10^{-4}	3.6×10^{-5}	4.0×10^{-5}	–
$B_c^+ \to B^+ K^{*0}$	–	–	–	1.07×10^{-5}
$B_c^+ \to B^0 K^{*+}$	3.20×10^{-5}	4.8×10^{-5}	4.0×10^{-5}	1.06×10^{-4}

Table 13 Branching ratios of bottom-changing $B_c^+ \to D_{(s)}^{(*)+} \overline{D}^{(*)0}$ and $D_{(s)}^{(*)+} D^{(*)0}$ decays as predicted in other models

Decay	RIQM [38]	pQCD [40]	RCQM [35]	PDG [12]
$B_c^+ \to D^0 D_s^{*+}$	4.18×10^{-7}	2.5×10^{-6}	9.3×10^{-6}	$< 9.0 \times 10^{-4}$
$B_c^+ \to D_s^+ D^{*0}$	2.25×10^{-7}	1.9×10^{-6}	1.3×10^{-6}	$< 6.6 \times 10^{-4}$
$B_c^+ \to D^+ D^{*0}$	8.00×10^{-9}	7.0×10^{-8}	5.2×10^{-8}	$< 3.7 \times 10^{-4}$
$B_c^+ \to D^0 D^{*+}$	1.80×10^{-8}	9.0×10^{-8}	4.4×10^{-7}	$< 2.0 \times 10^{-4}$
$B_c^+ \to \overline{D}^0 D_s^{*+}$	3.15×10^{-7}	7.0×10^{-8}	6.5×10^{-7}	$< 5.3 \times 10^{-4}$
$B_c^+ \to D_s^+ \overline{D}^{*0}$	4.91×10^{-7}	2.6×10^{-7}	2.4×10^{-6}	$< 4.6 \times 10^{-4}$
$B_c^+ \to \overline{D}^0 D^{*+}$	1.60×10^{-6}	1.2×10^{-6}	8.8×10^{-6}	$< 3.8 \times 10^{-4}$
$B_c^+ \to D^+ \overline{D}^{*0}$	2.61×10^{-5}	3.4×10^{-6}	3.8×10^{-5}	$< 6.5 \times 10^{-4}$

Table 14 Branching ratios of bottom-changing $B_c \to PV$ decays involving one charmonium ($\eta_c(J/\psi)$) state as predicted in other models

Decay	CLFQM (Type-I) [28]	RIQM [39]	pQCD [41]	RCQM [35]
$B_c^+ \to D_s^+ J/\psi$	6.09×10^{-3}	1.15×10^{-3}	8.05×10^{-3}	3.4×10^{-3}
$B_c^+ \to D^+ J/\psi$	2.00×10^{-4}	3.69×10^{-5}	2.80×10^{-4}	1.5×10^{-4}
$B_c^+ \to K^+ J/\psi$	1.60×10^{-4}	3.00×10^{-5}	1.90×10^{-4}	1.3×10^{-4}
$B_c^+ \to \pi^+ J/\psi$	1.97×10^{-3}	3.80×10^{-4}	2.33×10^{-3}	1.7×10^{-3}
$B_c^+ \to \eta_c D_s^{*+}$	6.97×10^{-3}	2.16×10^{-3}	1.65×10^{-2}	3.7×10^{-3}
$B_c^+ \to \eta_c D^{*+}$	3.10×10^{-4}	7.60×10^{-5}	5.80×10^{-4}	1.9×10^{-4}
$B_c^+ \to \eta_c K^{*+}$	3.40×10^{-4}	6.30×10^{-5}	5.70×10^{-4}	2.5×10^{-4}
$B_c^+ \to \eta_c \rho^+$	6.01×10^{-3}	1.20×10^{-3}	9.83×10^{-3}	4.5×10^{-3}

Table 15 $f(q^2)$ and $a_-(q^2)$ form factors of bottom-conserving $B_c \to V$ transitions for $\lambda = 0$ and $\lambda = \pm$ polarization states in type-II and type-I schemes at different q^2 in the space-like region

Form factor	Type-II scheme					Type-I scheme				
	$q^2_\perp = 0.01$	$q^2_\perp = 0.1$	$q^2_\perp = 1.0$	$q^2_\perp = 5.0$	$q^2_\perp = 10.0$	$q^2_\perp = 0.01$	$q^2_\perp = 0.1$	$q^2_\perp = 1.0$	$q^2_\perp = 5.0$	$q^2_\perp = 10.0$
$B_c \to B^*$										
$[f(q^2)]^{\lambda=0}$	−6.54	−6.36	−4.84	−1.62	−0.50	−5.23	−5.11	−3.99	−1.41	−0.44
$[f(q^2)]^{\lambda=\pm}$	−6.54	−6.36	−4.84	−1.62	−0.50	−5.32	−5.16	−3.86	−1.21	−0.35
$[a_-(q^2)]^{\lambda=0}$	−0.85	−0.81	−0.52	−0.10	−0.02	7.51	−0.58	−0.87	−0.19	−0.04
$[a_-(q^2)]^{\lambda=\pm}$	−0.85	−0.81	−0.52	−0.10	−0.02	−1.21	−1.16	−0.73	−0.15	−0.03
$B_c \to B_s^*$										
$[f(q^2)]^{\lambda=0}$	−8.07	−7.84	−6.00	−2.12	−0.70	−6.50	−6.34	−4.96	−1.83	−0.62
$[f(q^2)]^{\lambda=\pm}$	−8.07	−7.84	−6.00	−2.12	−0.70	−6.59	−6.40	−4.83	−1.61	−0.51
$[a_-(q^2)]^{\lambda=0}$	−0.86	−0.82	−0.55	−0.12	−0.03	8.32	−0.49	−0.89	−0.22	−0.05
$[a_-(q^2)]^{\lambda=\pm}$	−0.86	−0.82	−0.55	−0.12	−0.03	−1.21	−1.16	−0.76	−0.17	−0.04

Table 16 $f(q^2)$ and $a_-(q^2)$ form factors of bottom-changing $B_c \to V$ transitions for $\lambda = 0$ and $\lambda = \pm$ polarization states in type-II and type-I schemes at different q^2 in the space-like region

Form factor	Type-II scheme					Type-I scheme				
	$q^2_\perp = 0.01$	$q^2_\perp = 0.1$	$q^2_\perp = 5.0$	$q^2_\perp = 10.0$	$q^2_\perp = 20.0$	$q^2_\perp = 0.01$	$q^2_\perp = 0.1$	$q^2_\perp = 5.0$	$q^2_\perp = 10.0$	$q^2_\perp = 20.0$
$B_c \to D^*$										
$[f(q^2)]^{\lambda=0}$	−1.26	−1.26	−0.90	−0.65	−0.36	−1.16	−1.15	−0.83	−0.61	−0.34
$[f(q^2)]^{\lambda=\pm}$	−1.26	−1.26	−0.90	−0.65	−0.36	−1.09	−1.08	−0.77	−0.56	−0.31
$[a_-(q^2)]^{\lambda=0}$	−0.02	−0.02	−0.01	−0.01	−0.004	−6.89	−0.73	−0.04	−0.02	−0.01
$[a_-(q^2)]^{\lambda=\pm}$	−0.02	−0.02	−0.01	−0.01	−0.004	−0.05	−0.05	−0.03	−0.02	−0.01
$B_c \to D_s^*$										
$[f(q^2)]^{\lambda=0}$	−1.65	−1.64	−1.19	−0.87	−0.49	−1.51	−1.50	−1.10	−0.81	−0.47
$[f(q^2)]^{\lambda=\pm}$	−1.65	−1.64	−1.19	−0.87	−0.49	−1.44	−1.43	−1.03	−0.76	−0.43
$[a_-(q^2)]^{\lambda=0}$	−0.03	−0.03	−0.02	−0.01	−0.01	−7.06	−0.76	−0.05	−0.03	−0.01
$[a_-(q^2)]^{\lambda=\pm}$	−0.03	−0.03	−0.02	−0.01	−0.01	−0.06	−0.06	−0.04	−0.02	−0.01
$B_c \to J/\psi$										
$[f(q^2)]^{\lambda=0}$	−5.61	−5.59	−4.53	−3.69	−2.53	−5.14	−5.12	−4.16	−3.41	−2.36
$[f(q^2)]^{\lambda=\pm}$	−5.61	−5.59	−4.53	−3.69	−2.53	−5.09	−5.07	−4.11	−3.35	−2.29
$[a_-(q^2)]^{\lambda=0}$	−0.08	−0.08	−0.06	−0.05	−0.03	−4.49	−0.58	−0.11	−0.08	−0.05
$[a_-(q^2)]^{\lambda=\pm}$	−0.08	−0.08	−0.06	−0.05	−0.03	−0.14	−0.14	−0.10	−0.08	−0.04

$q^2_{\rm max}$ is around 65% of the $M^2_{B^{**}} \lesssim 34\ {\rm GeV}^2$, which is not far from the $q^2_{\rm max}$, in contrast to $B_c \to B^{(*)}_{(s)}$ transitions. Thus, we expect reasonable contributions from the resonance poles in the available q^2 range, as shown in Figs. 4 and 5. As a result, the form factors will have larger numerical values at $q^2_{\rm max}$, as can be seen from Table 5. As previously noted, in addition to the wave function overlap factor (described in Sect. 3.1.1(iv)), the magnitude of the form factors is further influenced by contributions from vertex functions and current operators as depicted in Eq. (27). Thus, similar to the $B_c \to B^{(*)}_{(s)}$ form factors, we also plot the total integrand for bottom-changing transition form factors with respect to the momentum fraction x_1, as shown in Figs. 8 and 9. Note that the total integrand of bottom-changing transition form factors shows a substantial decrease in magnitude compared to bottom-conserving transition form factors. Additionally, we observe constructive interference for all the bottom-changing transition form factors.

(iii) As stated previously, we wish to emphasize that our numerical values of form factors $F_0^{B_c D_{(s)}}(q^2)$ and $F_1^{B_c D_{(s)}}(q^2)$ are in excellent agreement with the LQCD predictions [21]. The form factor results from LQCD both at $q^2 = 0$ and $q^2_{\rm max}$ are as follows [21]: $F^{B_c D}_{0[1]}(0) =$

Table 17 Branching ratios of $B_c^+ \to Pl^+\nu_l$ decays. For the definitions of T2A, T2B, and T1, refer to the caption of Table 4

Decay	Type-II scheme		Type-I scheme
	T2A	T2B	T1
$B_c^+ \to B^0 e^+ \nu_e$	$(9.12^{+1.76+0.82}_{-1.55-1.72}) \times 10^{-4}$	$(1.27^{+0.25+0.00}_{-0.23-0.02}) \times 10^{-3}$	$(5.00^{+0.74+1.84}_{-0.68-2.04}) \times 10^{-4}$
$B_c^+ \to B^0 \mu^+ \nu_\mu$	$(8.79^{+1.71+0.76}_{-1.50-1.63}) \times 10^{-4}$	$(1.21^{+0.24+0.00}_{-0.21-0.02}) \times 10^{-3}$	$(4.79^{+0.69+1.73}_{-0.64-1.91}) \times 10^{-4}$
$B_c^+ \to B_s^0 e^+ \nu_e$	$(1.56^{+0.20+0.10}_{-0.23-0.22}) \times 10^{-2}$	$(2.03^{+0.29+0.00}_{-0.31-0.04}) \times 10^{-2}$	$(1.06^{+0.10+0.24}_{-0.12-0.33}) \times 10^{-3}$
$B_c^+ \to B_s^0 \mu^+ \nu_\mu$	$(1.48^{+0.20+0.09}_{-0.22-0.20}) \times 10^{-2}$	$(1.90^{+0.28+0.00}_{-0.30-0.04}) \times 10^{-2}$	$(1.01^{+0.10+0.22}_{-0.12-0.30}) \times 10^{-3}$
$B_c^+ \to D^0 e^+ \nu_e$	$(2.89^{+1.95+1.17}_{-1.12-1.15}) \times 10^{-5}$	$(1.77^{+0.91+0.64}_{-0.57-0.55}) \times 10^{-5}$	$(1.36^{+1.02+0.80}_{-0.55-0.60}) \times 10^{-5}$
$B_c^+ \to D^0 \mu^+ \nu_\mu$	$(2.89^{+1.94+1.17}_{-1.12-1.15}) \times 10^{-5}$	$(1.77^{+0.91+0.64}_{-0.56-0.55}) \times 10^{-5}$	$(1.36^{+1.01+0.80}_{-0.54-0.60}) \times 10^{-5}$
$B_c^+ \to D^0 \tau^+ \nu_\tau$	$(2.18^{+1.47+0.77}_{-0.86-0.83}) \times 10^{-5}$	$(1.13^{+0.58+0.41}_{-0.36-0.35}) \times 10^{-5}$	$(7.83^{+6.93+5.36}_{-3.52-3.93}) \times 10^{-6}$
$B_c^+ \to \eta_c e^+ \nu_e$	$(7.76^{+0.26+0.09}_{-0.24-0.35}) \times 10^{-3}$	$(6.60^{+0.20+0.18}_{-0.20-0.39}) \times 10^{-3}$	$(7.48^{+0.32+0.17}_{-0.29-0.43}) \times 10^{-3}$
$B_c^+ \to \eta_c \mu^+ \nu_\mu$	$(7.73^{+0.26+0.09}_{-0.24-0.35}) \times 10^{-3}$	$(6.57^{+0.20+0.18}_{-0.20-0.38}) \times 10^{-3}$	$(7.46^{+0.32+0.17}_{-0.29-0.43}) \times 10^{-3}$
$B_c^+ \to \eta_c \tau^+ \nu_\tau$	$(2.29^{+0.05+0.02}_{-0.05-0.10}) \times 10^{-3}$	$(1.78^{+0.05+0.05}_{-0.05-0.11}) \times 10^{-3}$	$(2.18^{+0.07+0.05}_{-0.06-0.13}) \times 10^{-3}$

0.186 ± 0.023 [0.186 ± 0.023], $F_{0[1]}^{B_c D}(q^2_{\rm max}) = 0.668 \pm 0.020$ [1.50 ± 0.18]; $F_{0[1]}^{B_c D_s}(0) = 0.217 \pm 0.018$ [0.217 ± 0.018], $F_{0[1]}^{B_c D_s}(q^2_{\rm max}) = 0.736 \pm 0.011$ [1.45 ± 0.12]. The numerical values of $B_c \to D$ form factors differ by $\sim 9\%$ at $q^2 = 0$ compared to the LQCD results. However, the agreement substantially improves at $q^2_{\rm max}$ for $F_0^{B_c D}(q^2_{\rm max})$ and $F_1^{B_c D}(q^2_{\rm max})$ for T2A and T2B, respectively. Furthermore, for the $B_c \to D_s$ form factors, our results are in good agreement with the LQCD results, where the results match within $\sim 15\%$. It is interesting to note that the q^2 variation in T2B form factors in Fig. 4 shows behavior similar to that observed in LQCD [21]. The numerical values of the form factors in T2B vary more sharply near the maximum q^2 than those in T2A. It is significant that the pole at $M^2_{B^{**}_{(s)}}$ lies away from $q^2_{\rm max}$, i.e., $\sim (50-70)\%$ of $M^2_{B^{**}_{(s)}}$ for $B_c \to D^{(*)}_{(s)}$ transitions. Furthermore, the form factors $F_0(q^2)$ and $F_1(q^2)$ receive pole contributions from M_{0^+} and M_{1^-}, respectively, which result in visibly different behavior corresponding to the squared mass of resonances. We observe similar q^2 behavior for the $B_c \to D^*_{(s)}$ form factors. In addition, the form factors $V(q^2)$ and $A_0(q^2)$ which receive pole contributions from the M_{1^-} and M_{0^-} poles show expected behavior. In addition, the form factors $A_1(q^2)$ and $A_2(q^2)$ that receive contributions from M_{1^+} poles vary less sharply, as expected. Furthermore, we notice that the effect of the variation in the quark masses and β parameters leads to larger uncertainties in the $B_c \to D_{(s)}$ form factors, as much as $\sim 40\%$, which has not been previously analyzed and reported in the literature. In contrast, the uncertainties in $B_c \to \eta_c$ form factors are as small as $\sim 3\%$. These observations highlight the importance of the quantitative perspective of this analysis.

(iv) One of the most peculiar aspects of bottom-changing transition form factors, especially for $B_c \to V$, is that they have larger values of a and b parameters due to the smaller magnitude of form factors as compared to bottom-conserving ones. It is worth mentioning that even though the values of all the bottom-changing transition form factors at $q^2 = 0$ are numerically similar between type-I and type-II schemes (except $A_0(q^2)$ and $A_1(q^2)$), their respective slope parameters as well as values at $q^2_{\rm max}$ differ significantly with larger magnitudes, observed exclusively for parameter b. This shows that the form factors with q^2 dependence given by Eq. (38) vary more sharply. It should be emphasized that similar to the bottom-conserving transition form factors in the type-I scheme, we observe significant numerical variation in the magnitudes of the form factors $A_0(0)$ and $A_1(0)$, i.e., $\sim 30\%$ and $\sim 10\%$, respectively, compared to both T2A and T2B for $B_c \to D^*_{(s)}$ transitions. Therefore, the effect of self-consistency cannot be determined simply from the numerical values of the affected form factors at $q^2 = 0$. In particular, in the z-series parameterization (T2B), the values of the form factors at the maximum recoil point (a'_0) are comparable to those of the T2A form factors at $q^2 = 0$; however, they differ significantly at $q^2_{\rm max}$. For the $B_c \to D^*$ transition, the numerical values of $A_0(0)$ differ by $\sim 30\%$ between T1 and T2B. On the other hand, the free parameters a'_1 and a'_2 have large values and follow a consistent pattern across all the $B_c \to V$ bottom-changing transitions. Among these, B_c to $D^{(*)}_{(s)}$ transitions have smaller values of a'_1 and a'_2 as compared to transitions involving charmonia, due to the larger value of $\pm|z|_{\rm max} = \pm 0.039$ for $D^{(*)}_{(s)}$ mesons.

(v) In the case of $B_c \to D^*_{(s)}$ bottom-changing transitions, the form factors show increased sensitivity to uncertainties in constituent quark masses and β values, resulting in more substantial collective uncertainties. For instance, we observe a maximum uncertainty of approximately 86% for the $A_2^{B_c D^*}(0)$ form factor. As stated earlier, the quantitative analysis of $B_c \to D^*_{(s)}$ transition form factors highlights the critical role of uncertainties propagating through the form factors via the input parameters. We believe that these uncertainties are crucial for the accurate assessment of both semileptonic and nonleptonic decay processes. In addition, the slope parameters associated with these transitions demonstrate increased uncertainties. It should be noted that the uncertainties corresponding to the quark mass are smaller than those of β values for the form factors $A_0(0)$ and $A_1(0)$, while the remaining form factors show comparable variations. As previously noted, we observe the maximum collective uncertainties of approximately 60% in the case of $V(0)$ and $A_2(0)$ for both T2A and T2B scenarios, exhibiting similar behavior, i.e., demonstrating roughly comparable sensitivity to β parameters and quark masses. In general, a comparison of the numerical values of the form factors between type-I and type-II correspondence schemes reveals that the effect of self-consistency and covariance leads to significant changes in the numerical values of $A_0(q^2)$ and $A_1(q^2)$. The type-I scheme exhibits similar sensitivity to quark masses and β values in the $B_c \to D^*_{(s)}$ transition form factors. In addition, as observed in bottom-conserving transitions, the $A_0(q^2)$ form factor shows a decreasing trend, contrasting with the behavior of the $A_1(q^2)$ form factor as q^2 is varied within the type-I scheme. Such deviations between the two schemes are expected to be decisive for the study of weak semileptonic and nonleptonic decays. We also observe that the effects of self-consistency on bottom-changing transition form factors are smaller than those of bottom-conserving transition form factors.

(vi) Among the bottom-changing transitions, we observe that B_c decaying to charmonium states have larger numerical values of the form factors. This is because, in $B_c \to c\bar{c}$ meson transitions, the fractional momentum of the charm quark in the final state is of the order of the spectator c quark. Therefore, $\psi_{\eta_c(J/\psi)}(x_1)$ have a peak near $x \sim 1/2$ which shows a larger overlap with $\psi_{B_c}(x_1)$ at $x \sim 3/4$ as compared to the overlap between $\psi_{B_c}(x_1)$ and $\psi_{D^{(*)}_{(s)}}(x_1)$ (see Fig. 7c); in fact, the overlap is even larger than for the bottom-conserving transitions. As explained earlier, the form factor is not determined solely by the wave function overlap area. It is influenced by the vertex functions and mass factors (given by Eq. (17)) introduced in the integrand given by Eq. (27). This yields an intermediate integrand amplitude for the $B_c \to \eta_c(J/\psi)$ form factors that lie between those of the $B_c \to B^{(*)}_{(s)}$ and $B_c \to D^{(*)}_{(s)}$ form factors, even though the former possess a larger overlap factor. Thus, the overlap plots for the total integrand are shown in Figs. 8 and 9. A similar trend can be observed for T2B and T1 results using the q^2 dependence given by Eqs. (39) and (38), respectively. It may be noted that for $B_c \to \eta_c(J/\psi)$, the resonance pole $M^2_{B_c^{**}}$ lies much farther as compared to the $B_c \to D^*_{(s)}$ transitions, which is $\sim (21-26)\%$ of $M^2_{B_c^{**}}$. Furthermore, we observed that, similar to other bottom-changing transition form factors, $B_c \to \eta_c(J/\psi)$ form factors show increasing behavior toward the maximum q^2, though less sharply, as shown in Figs. 4 and 5. The T2A and T2B q^2 formulations show roughly similar behavior. In addition, it is interesting to note that the effects of self-consistency on bottom-changing $B_c \to J/\psi$ transition form factors are minimal as compared to both bottom-conserving and other bottom-changing transition form factors. Interestingly, we note that $B_c \to J/\psi$ form factors are least affected by the quark mass and β uncertainties (for both type-I and type-II schemes), i.e., the maximum uncertainty of $\sim 14\%$ for the $A_0(0)$ form factor, while the rest of the form factors have even smaller uncertainties.

We have employed type-I and type-II correspondence schemes for $B_c \to P$ and $B_c \to V$ transition form factors for both bottom-conserving and bottom-changing transitions. Moreover, we confirm that on the application of type-II correspondence (T2A and T2B), the B_c to V transition form factors are self-consistent, i.e., zero-mode contributions vanish numerically. We now proceed to calculate the branching ratios of semileptonic $B_c \to P l \nu_l$ and $B_c \to V l \nu_l$ decays involving $B_c \to P$ and V transition form factors, respectively.

3.2 Semileptonic decays

In this subsection, we study the branching ratios of the semileptonic B_c meson decays obtained by using the transition form factors given in Tables 4 and 5. We list our predictions of the branching ratios of $B_c^+ \to V l^+ \nu_l$ in type-II correspondence (T2A) as shown in Table 6. In addition, we list the relative decay widths and the average values of other observables for the B_c transitions including the FB asymmetry ($\langle A_{\rm FB}\rangle$), convexity parameter ($\langle C_F^l\rangle$), longitudinal (transverse) ($\langle P^l_{L(T)}\rangle$) polarization of the charged lepton, and asymmetry parameter (α^*) for T2A in Table 6. Furthermore, we contrast the semileptonic branching ratios using T2B and T1 (type-I scheme) form factors, as tabulated in columns

2 and 3 of Table 7, respectively. In addition, we compute the uncertainties in the branching ratios propagating through form factor uncertainties. The uncertainties corresponding to the quark masses and β values are treated independently. Moreover, we compare these results with other theoretical predictions from Refs. [27,29,32,35], as given in Table 7. Additionally, we plot the q^2 variation of the differential decay rates and $A_{\rm FB}(q^2)$ of $B_c^+ \to V l^+ \nu_l$ decays in Figs. 10 and 11, respectively.

	T2A	T2B	LQCD [20]
$\frac{\Gamma(B_c^+ \to B_s^0 e^+ \nu_e)\lvert V_{cd}\rvert^2}{\Gamma(B_c^+ \to B^0 e^+ \nu_e)\lvert V_{cs}\rvert^2}$	$0.88^{+0.20+0.21}_{-0.20-0.10}$	$0.82^{+0.19+0.02}_{-0.20-0.00}$	0.759 ± 0.044;
$\frac{\Gamma(B_c^+ \to B_s^0 \mu^+ \nu_\mu)\lvert V_{cd}\rvert^2}{\Gamma(B_c^+ \to B^0 \mu^+ \nu_\mu)\lvert V_{cs}\rvert^2}$	$0.87^{+0.20+0.20}_{-0.20-0.09}$	$0.81^{+0.19+0.02}_{-0.20-0.00}$	0.759 ± 0.044.

3.2.1 Bottom-conserving decays

The bottom-conserving CKM-enhanced ($\Delta b = 0, \Delta C = -1, \Delta S = -1$) and CKM-suppressed ($\Delta b = 0, \Delta C = -1, \Delta S = 0$) semileptonic decay modes of B_c mesons undergo kinematic suppression due to the large mass of the $B^*_{(s)}$ meson in the final states. These semileptonic decay processes provide an excellent opportunity to observe the effects of form factors on the branching ratios and, therefore, to test the theoretical models. In addition to form factors, kinematic and CKM factors play an important role in determining their magnitude. We analyzed $B_c^+ \to B^{*0}_{(s)} l^+ \nu_l$ decays using the self-consistent CLFQM. We observed the following.

(i) We observe that the branching ratios of bottom-conserving decays are of $\mathcal{O}(10^{-2})$ to $\mathcal{O}(10^{-3})$ despite the kinematic suppression. Among these decays, the CKM-enhanced modes have dominant branching ratios, i.e., $\mathcal{B}(B_c^+ \to B_s^{*0} e^+ \nu_e) = (3.53^{+0.15+0.49}_{-0.24-0.81}) \times 10^{-2}$ and $\mathcal{B}(B_c^+ \to B_s^{*0} \mu^+ \nu_\mu) = (3.30^{+0.14+0.46}_{-0.22-0.77}) \times 10^{-2}$, as listed in Table 6 for T2A. This is because the kinematic suppression is dominated by the CKM factor (V_{cs}). On the other hand, the branching ratios of $B_c \to B^* l \nu_l$ decays involving $c \to d$ transition (governed by V_{cd}) are smaller by an order of magnitude. In general, the branching ratios of $P \to V$ semileptonic decays are expected to be larger than $P \to P$ decays, which can also be observed from our results. We found that our results are in good agreement with recent LQCD predictions within the uncertainties [20]. Although we focused on $P \to V$ semileptonic decays of the B_c meson, we also list $B_c^+ \to P l^+ \nu_l$ decays in CLFQM for T2A, T2B, and T1, as shown in columns 2, 3, and 4 of Table 17, respectively, in Appendix B. The LQCD results of bottom-conserving branching ratios are as follows [20]: $\mathcal{B}(B_c^+ \to B^0 l^+ \nu_l) = (8.47 \pm 0.31 \pm 0.43 \pm 0.24) \times 10^{-4}$ and $\mathcal{B}(B_c^+ \to B_s^0 l^+ \nu_l) = (1.348 \pm 0.046 \pm 0.033 \pm 0.043) \times 10^{-2}$. In an effort to ensure the reliability of the CLF approach, we compare the decay width ratios of our results with LQCD expectations:

Our results are in good agreement with LQCD ratios for T2B (q^2 formulation); however, they are marginally larger for T2A (q^2 formulation).[9] Moreover, the semileptonic branching ratios of bottom-conserving modes for T2A are smaller by $\sim (22-28)\%$ as compared to T2B results. It may be noted that the uncertainties in our branching ratios for T2A (T2B), stemming individually from both quark masses and β parameters, are generally modest, with maximum deviations of the $\mathcal{O}(20\%)$, as shown in Table 17. Furthermore, the T1 predictions for semileptonic branching ratios of $B_c^+ \to B^0_{(s)} l^+ \nu_l$ are $\sim 45\%(93\%)$ smaller than those of T2A and roughly $\sim 60\%(95\%)$ smaller than those of T2B. The form factors, $F_0(q^2)$ and $F_1(q^2)$, are not subject to self-consistency issues within CLFQM. Consequently, the numerical discrepancies observed in the type-II correspondence scheme for decays involving $F_0(q^2)$ and $F_1(q^2)$ form factors can be attributed to variations arising from different q^2 formulations. Similarly, for $B_c \to B^*_{(s)} l \nu_l$ decays, we predict the following:

	T2A	T2B
$\frac{\Gamma(B_c^+ \to B_s^{*0} e^+ \nu_e)\lvert V_{cd}\rvert^2}{\Gamma(B_c^+ \to B^{*0} e^+ \nu_e)\lvert V_{cs}\rvert^2}$	$0.87^{+0.12+0.35}_{-0.09-0.20}$	$0.83^{+0.09+0.19}_{-0.06-0.17}$.
$\frac{\Gamma(B_c^+ \to B_s^{*0} \mu^+ \nu_\mu)\lvert V_{cd}\rvert^2}{\Gamma(B_c^+ \to B^{*0} \mu^+ \nu_\mu)\lvert V_{cs}\rvert^2}$	$0.86^{+0.11+0.35}_{-0.09-0.20}$	$0.82^{+0.09+0.18}_{-0.06-0.16}$.

(ii) Due to larger uncertainties in the form factors corresponding to β parameters than constituent quark masses, the semileptonic branching ratios show greater sensitivity to variation in β parameters, leading to enhanced uncertainties. The uncertainties in β (quark mass) result

[9] Note that the uncertainties in the ratios of the branching fractions are bound to increase because of their additive nature. As mentioned before, we have ignored the uncertainties of the CKM factors in our analysis.

in a maximum change in branching ratios on the order of $\sim 33\%$ ($\sim 12\%$) for $B_c^+ \to B^{*0} l^+ \nu_l$ decays. On the other hand, the uncertainties for $B_c^+ \to B_s^{*0} l^+ \nu_l$ are smaller, with a maximum deviation of approximately 18% inclusive of the uncertainties from both quark mass and β values. Notably, for $B_c^+ \to B_{(s)}^{*0} l^+ \nu_l$ decays, uncertainties range from approximately 18% to 45% collectively. Such an expanded range of uncertainties would provide a reasonable scope for experimental investigations.

(iii) The $B_c \to V l \nu_l$ branching ratios are mainly influenced by the form factors $V(q^2)$, $A_1(q^2)$, and $A_2(q^2)$. However, it is worth mentioning that the contribution of the form factor $A_0(q^2)$ to these branching ratios can be considered insignificant (see Eq. (41)). It is well known that in the semileptonic $P \to V$ weak decays, the contribution from the form factor $A_2(q^2)$ can be ignored due to the negligible coefficient in the decay rates [29,123]. Furthermore, the branching ratios of the semileptonic decays depend upon the magnitude and signs of the form factors. We want to emphasize that the numerical values of the form factors, especially $A_0(q^2)$ and $A_1(q^2)$, have changed significantly in type-II correspondence (T2A and T2B formulations). Therefore, to quantify the effect of self-consistency on the branching ratios of the semileptonic decay modes, we compared our results with those of type-I correspondence (T1). We found that the numerical results for T2A are enhanced by $\sim (50-60)\%$ as compared to the branching ratios in T1. Similar observations can be made for the comparison between T2B and T1 results, because the results between T2B and T2A differ by less than $\sim 10\%$ for bottom-conserving modes. As expected, the differences between the results for type-I and type-II correspondences (inclusive of T2B) are sufficiently large and hence cannot be ignored. It may be emphasized that the uncertainties in the type-I scheme results, arising from variations in form factors, are considerably larger than those in the type-II scheme results, in some cases differing by an order of magnitude. In addition, we also compared our results with other works [27,29,32,35], as listed in columns 4–7 of Table 7. We found that our results for bottom-conserving semileptonic decays are of the same order as compared to predictions from other theoretical models, except for $B_c^+ \to B^{*0} l^+ \nu_l$ by Li et al. [27], which employs the CLFQM framework within the type-I scheme.

(iv) The mass difference between the electrons and muons has minimal impact ($\sim 6\%$) on the branching ratios and other physical observables of bottom-conserving semileptonic $B_c \to B_{(s)}^*$ decays. Additionally, the comparative variation in bottom-conserving semileptonic differential decay rates for e and μ lepton modes with respect to q^2 is plotted in Figs. 10a, b. It should be noted that in semileptonic decay processes, the physical observables depend on the mass of the final lepton, with $q^2_{\rm min} = m_l^2$ (assuming the mass of a neutrino is negligible). The differential decay rate plots show distinct peaks corresponding to the lepton mass for the available q^2 range, with the same endpoints at $q^2_{\rm max}$ as expected. We also have calculated relative longitudinal and transverse decay widths, and their ratios for bottom-conserving $B_c^+ \to V l^+ \nu_l$ decays, as shown in columns 4, 5, and 6 of Table 6, respectively. It is noteworthy to mention that the longitudinal component of the decay widths dominates the transverse component. The magnitude of this difference is relatively modest, with the longitudinal component exceeding the transverse by approximately $(4-6)\%$. The longitudinal decay widths of $B_c \to B_{(s)}^* l \nu_l$ decays decrease marginally with increasing lepton mass.

(v) As noted, we also calculated the longitudinal and transverse decay widths for $B_c \to B_{(s)}^* l \nu_l$ decays. We observe that longitudinal decay widths marginally dominate over the transverse. We also calculated the expectation values of FB asymmetry, $\langle A_{FB} \rangle$, using Eq. (50), as shown in column 7 of Table 6. As discussed previously, the A_{FB} is considered as a more discriminating probe for uncovering physics beyond the SM as compared to branching ratios [124]. The FB asymmetry, being sensitive to the difference in helicity amplitudes, is susceptible to sign changes induced by helicity flip factors, particularly for the heavier lepton.[10] In addition to the sensitivity to NP contributions, A_{FB} provides the test SM predictions of lepton universality, and constraints on possible nonstandard interactions. It is noteworthy that all of the $A_{FB}(B_c^+ \to V l^+ \nu_l)$ values are negative. The negative values of A_{FB} in bottom-conserving semileptonic decays reflect the dominance of the parity-violating helicity structure-function, $\mathcal{H}_P$, particularly with a larger contribution from H_- amplitude. The $\mathcal{H}_{SL}$ contributions (associated with helicity flip factor) are negligible for electron decay modes, and their values increase with increasing lepton mass. We observe that the magnitude of $\mathcal{H}_{SL}$ in $A_{FB}(B_c^+ \to B_{(s)}^{*0} \mu^+ \nu_\mu)$ increases by $(16-19)\%$, leading to a more negative value. In addition to the minimal discrepancy between T2A and T2B in form factors and semileptonic branching ratios, a similar trend can be observed for A_{FB} and other observables. Note that the calculations for observables beyond branching ratios have not been reported in the existing literature in the CLFQM approach. Consequently, we exclusively present the physical observables

[10] In Eq. (50), the helicity flip factor is generally associated with $\mathcal{H}_{SL}$, which can change significantly with lepton mass.

obtained from the T2A formulation. Furthermore, we plot the q^2 variation in the FB asymmetry of $B_c^+ \to B_{(s)}^{*0} l^+ \nu_l$ decays in Fig. 11a, b. Notably, A_{FB} shows a distinct rise near $q^2_{\rm min}$, particularly in the electron decay mode. The high-precision calculation shows that $A_{FB} \to 0$ as $q^2 \to 0$. Such behavior can also be observed in other works [31,125,126].

(vi) Furthermore, we calculated the mean values of $\langle C_F^l \rangle$, $\langle P_L^l \rangle$, and $\langle P_T^l \rangle$, as shown in columns 8, 9, and 10 of Table 6, respectively. It is noteworthy that the bottom-conserving semileptonic decay modes have a negative lepton-side convexity parameter, C_F^l, which is due to the predominance of the longitudinal helicity component, $\mathcal{H}_L$. Additionally, the transverse polarization parameter, P_T^l, is very small for e decay modes, i.e., $\mathcal{O}(10^{-3})$. Furthermore, we also computed the asymmetry parameter, α^*, by using Eq. (54), as illustrated in column 11 of Table 6. The asymmetry parameter α^* is consistently negative for all B_c to V semileptonic decays, indicating the dominance of the longitudinal helicity components, $\mathcal{H}_L$ and $\mathcal{H}_S$. Notably, parameters such as C_F^l, P_L^l, and α^* show a decrease in magnitude with increases in lepton mass.

3.2.2 Bottom-changing decays

In this subsection, we focus on the bottom-changing CKM-enhanced ($\Delta b = -1, \Delta C = -1, \Delta S = 0$) and CKM-suppressed ($\Delta b = -1, \Delta C = 0, \Delta S = 0$) semileptonic decay modes of B_c mesons, which involve the charm mesons in the final states. One notable aspect of bottom-changing semileptonic decays is that they include $\tau^+ \nu_\tau$ alongside $e^+ \nu_e$ and $\mu^+ \nu_\mu$ lepton pairs in the final state. We have analyzed and listed our major findings on $B_c \to D^*(J/\psi) l \nu_l$ decays as follows:

(i) The branching ratios of bottom-changing $B_c^+ \to V l^+ \nu_l$ decays range from $\mathcal{O}(10^{-2})$ to $\mathcal{O}(10^{-5})$, as given in Table 6 for T2A. Among these decays, $B_c^+ \to J/\psi e^+ \nu_e$ and $B_c^+ \to J/\psi \mu^+ \nu_\mu$ are most dominant with branching ratios $(2.35^{+0.36+0.04}_{-0.33-0.12}) \times 10^{-2}$ and $(2.34^{+0.36+0.04}_{-0.33-0.12}) \times 10^{-2}$, respectively, since $B_c^+ \to J/\psi l^+ \nu_l$ decays are both CKM- and kinematically enhanced. On the other hand, the CKM-suppressed $B_c^+ \to D^{*0} l^+ \nu_l$ decays, involving $b \to u$ transition, have smaller branching ratios, i.e., $\mathcal{O}(10^{-5})$. Similar to bottom-conserving decays, the semileptonic $B_c \to V$ branching ratios of bottom-changing decays generally show greater sensitivity to variations in the β parameter than to uncertainties in the constituent quark masses, with the exception of $B_c^+ \to J/\psi l^+ \nu_l$. The branching ratios of $B_c^+ \to D^{*0} l^+ \nu_l$ demonstrate a maximum variation of approximately 78%(39%), while $B_c^+ \to J/\psi l^+ \nu_l$ shows variations on the order of 5%(15%) corresponding to uncertainties in β (quark masses). As previously noted, the $B_c \to V l \nu_l$ branching ratios are predominantly determined by $V(q^2)$ and $A_1(q^2)$, while $A_2(q^2)$ and $A_0(q^2)$ have minimal impact. Therefore, the larger uncertainties in these branching ratios can be attributed primarily to the collective influence of form factors $V(q^2)$ and $A_1(q^2)$. Furthermore, the uncertainties in $B_c^+ \to D^{*0} l^+ \nu_l$ decays resulting from quark mass variations exhibit a more symmetric distribution than those observed in bottom-conserving decays.

(ii) Similar to bottom-conserving $B_c \to P$ semileptonic decays, the branching ratios of bottom-changing $B_c^+ \to D^0 l^+ \nu_l$ decays (Table 3) are consistent with the recent LQCD results [21]. The LQCD results of bottom-changing branching ratios are as follows [21]: $\mathcal{B}(B_c^+ \to D^0 e^+ \nu_e) = (3.37 \pm 0.48 \pm 0.08 \pm 0.42) \times 10^{-5}$ and $\mathcal{B}(B_c^+ \to D^0 \tau^+ \nu_\tau) = (2.29 \pm 0.23 \pm 0.06 \pm 0.29) \times 10^{-5}$. Interestingly, unlike bottom-conserving $B_c^+ \to P l^+ \nu_l$ decays, the semileptonic branching ratios of bottom-changing $B_c^+ \to D^0 l^+ \nu_l$ decays for the T2B formulation are smaller by $\sim$ (39−48)% when compared to T2A predictions. It should be noted that the $B_c \to D$ branching ratios exhibit maximum uncertainty of $\sim$ 67% (50%) in T2A (T2B) results due to variations in quark masses affecting the form factors. Additionally, uncertainties arising from variations in the β parameter contribute to a maximum deviation of $\sim$ 40% (36%). These variations in the branching ratio arise from differences in $F_0(q^2)$ and $F_1(q^2)$ corresponding to the q^2 formulation, despite being self-consistent. Furthermore, T1 predictions for the semileptonic branching ratios of $B_c^+ \to D^0 l^+ \nu_l$ are significantly smaller than those of T2A and T2B, exhibiting a decrease of approximately (52−64)% and (23−31)%, respectively.

(iii) In bottom-changing semileptonic B_c transitions, the phase space is usually larger than in bottom-conserving transitions. Specifically, the semileptonic branching ratios for T2A (listed in Table 6) involving $B_c \to D^*$ and $B_c \to J/\psi$ have $\sim$ 44% and 75% difference between the e (or μ) and τ semileptonic decays, respectively. It is worth noting that the mass difference between the electron and muon does not significantly affect $b \to u(c)$ semileptonic decays. As observed before, the branching ratios decrease with increasing lepton mass, i.e., the branching ratios of $B_c \to J/\psi e(\mu) \nu_{e(\mu)}$ are larger by roughly a factor of 4 than those of $\mathcal{B}(B_c \to J/\psi \tau \nu_\tau)$. Similarly, for $B_c \to D^* e(\mu) \nu_{e(\mu)}$ decays, the branching ratios of corresponding decay modes are approximately twice as large as those for $\mathcal{B}(B_c \to D^* \tau \nu_\tau)$. In the case of $B_c \to D^* e(\mu) \nu_{e(\mu)}$ decays, the relative longitudi-

nal and transverse decay widths are equal. Conversely, for $B_c \to J/\psi e(\mu)\nu_{e(\mu)}$ decays, the relative longitudinal decay widths exhibit a larger magnitude than the transverse decay widths. Notably, in all bottom-changing semileptonic decays involving a τ lepton in the final state, the relative transverse decay widths exceed the longitudinal decay widths. The LQCD prediction for the branching ratio $B_c^+ \to J/\psi\mu^+\nu_\mu$ is $(1.50 \pm 0.11 \pm 0.10 \pm 0.03)\%$ [19]. It is interesting to note that their result exhibits significant deviation from the branching ratio predictions of a majority of theoretical models [35,103,127–130], including our T2A (T2B) predictions, which span a range of (2.07−6.70)%. The exceptions to this trend are the results reported in Refs. [29,32], as listed in Table 7. The discrepancies observed among these results can be attributed to variations in input parameters—primarily quark and pole masses—as well as the diverse q^2 parameterizations employed in form factor calculations. In addition, we calculate the LFU ratios between τ and $e(\mu)$ leptons for both T2A and T2B results as follows:

	T2A	T2B	LQCD [18]	
$\mathcal{R}_{D^*} = \frac{\mathcal{B}(B_c^+ \to D^{*0}\tau^+\nu_\tau)}{\mathcal{B}(B_c^+ \to D^{*0}e(\mu)^+\nu_{e(\mu)})}$	$= 0.56^{+0.30+0.60}_{-0.30-0.00}$	$0.60^{+0.20+0.50}_{-0.16-0.00}$	$-$	;
$\mathcal{R}_{J/\psi} = \frac{\mathcal{B}(B_c^+ \to J/\psi\tau^+\nu_\tau)}{\mathcal{B}(B_c^+ \to J/\psi e(\mu)^+\nu_{e(\mu)})}$	$= 0.25^{+0.05+0.02}_{-0.05-0.00}$	$0.25^{+0.05+0.02}_{-0.06-0.00}$	0.2582 ± 0.0038.	

Note that the experimental measurement for the LFU ratios involving $b \to c\tau\nu_\tau$ for J/ψ in the final state is $\mathcal{R}_{J/\psi} = 0.71 \pm 0.18 \pm 0.17$ [17], which is much larger than the theoretical estimates. We want to emphasize that the current SM predictions for these ratios, including ours, fall within a range of 0.25–0.28 [24,31,32,131,132]. It is worth mentioning that the difference between multiple approaches is very small, which also agrees with the LQCD observation [18]. Furthermore, the experimental observation is substantially larger than the theoretical expectations, even though the cumulative uncertainties in the experimental value are on the order of 50%. Thus, further experimental observations would result in a clear picture to establish the scope of NP beyond the SM in these decays. Similarly, for bottom-conserving $B_c \to B^*_{(s)}$ semileptonic decays, we found the following:

	T2A	T2B	
$\mathcal{R}_{B^*} = \frac{\mathcal{B}(B_c^+ \to B^{*0}\mu^+\nu_\mu)}{\mathcal{B}(B_c^+ \to B^{*0}e^+\nu_e)}$	$= 0.95^{+0.16+0.40}_{-0.13-0.25}$	$0.95^{+0.13+0.24}_{-0.10-0.22}$	;
$\mathcal{R}_{B_s^*} = \frac{\mathcal{B}(B_c^+ \to B_s^{*0}\mu^+\nu_\mu)}{\mathcal{B}(B_c^+ \to B_s^{*0}e^+\nu_e)}$	$= 0.93^{+0.09+0.31}_{-0.06-0.18}$	$0.94^{+0.07+0.17}_{-0.04-0.15}$	,

which is in good agreement with Ref. [32].

(iv) As previously noted, the self-consistency effects are expected to be significant in semileptonic $B_c \to D^*$ decays. The branching ratios of $B_c^+ \to D^{*0}l^+\nu_l$ decays in the T2A and T2B schemes deviate from the T1 scheme by approximately (57−69)% and (67−78)%, respectively. However, self-consistency has a minimal effect on the branching ratios of semileptonic decays of the B_c to J/ψ states, with variation of $\sim$ 20% across T1 results when compared to T2A (T2B) results. The uncertainty in the branching fractions for the semileptonic $B_c \to D^*$ decays is substantial in the type-I scheme, reaching $\sim$ 200% for the $B_c \to D^*\tau\nu_\tau$ decay mode. In contrast, the uncertainties associated with the $B_c \to J/\psi l\nu_l$ decays are significantly smaller. It may be noted that for $B_c^+ \to D^{*0}l^+\nu_l$ decays for T2B, the branching ratios are larger than those of T2A by $\sim$ (24−29)%, and this behavior is opposite to the observation made for $B_c^+ \to Pl^+\nu_l$ decays. However, the $B_c^+ \to J/\psi l^+\nu_l$ decays differ by less than $\sim$ 1% on comparison between T2A and T2B. Additionally, to compare our results with other works, we have included the branching ratios from the literature [27,29,32,35], as presented in Table 7. Interestingly, a similar order of discrepancy can be observed in type-I correspondence scheme results from other works [27,29] as compared to that of type-II correspondence predictions from our work. For $B_c^+ \to J/\psi l^+\nu_l$, numerical results for the branching ratios are consistent with other literature; in fact, all the models yield branching ratios of the same order, as mentioned earlier. In general, we observed substantial differences in the numerical values of branching ratios for bottom-changing semileptonic decays from different models, ranging up to $\sim$ 60%. In particular, the discrepancy between $\mathcal{B}(B_c^+ \to D^{*0}e(\mu)^+\nu_{e(\mu)})$ results in the type-I scheme from other works [27,29] and the type-II scheme (T2A) in our work also range from approximately 20% to 57%. We have also plotted the q^2 variation in the differential decay rates of $B_c^+ \to D^{*0}l^+\nu_l$ and $B_c^+ \to J/\psi l^+\nu_l$ in Figs. 10c and 10d, respectively.

(v) In contrast to bottom-conserving decays, we observe larger transverse decay widths for the τ lepton in the

final state (see Table 6) for bottom-changing semileptonic decays. Furthermore, we calculated the A_{FB} for these decays, as listed in column 7 of Table 6. The A_{FB} values for bottom-changing decays are consistently negative due to the dominant contributions from $\mathcal{H}_{SL}$, with a larger magnitude for the H_0 helicity amplitude. The exception is evident in the decays involving an electron in the final state, where $\mathcal{H}_P$ is predominantly large because of the larger magnitude of H_- helicity amplitude. However, the contributions from $\mathcal{H}_P$ decrease with increasing lepton mass. Further, as the mass of the lepton increases, the $A_{FB}(B_c \to D^*\tau\nu_\tau)$ increases by approximately 20% as compared to $A_{FB}(B_c \to D^* e\nu_e)$; however, $A_{FB}(B_c \to J/\psi\tau\nu_\tau)$ increase up to 30% from $A_{FB}(B_c \to J/\psi e\nu_e)$. This indicates the dominant $\mathcal{H}_{SL}$ contributions for the τ lepton in the final state.

(vi) We observed behavior similar to that of A_{FB} for observables such as C_F^l and P_L^l with respect to the lepton mass. In this case, the numerical values of channels involving e and μ are almost identical, while the decays involving τ show some significant change. Furthermore, the α^* value leads to an observable difference in the case of $B_c \to J/\psi\tau\nu_\tau$ decay, which varies by 34% with respect to $B_c \to J/\psi e(\mu)\nu_{e(\mu)}$ decays. This distinction arises from the influence of the lepton's mass on the decay process. It should be noted that for $B_c \to J/\psi l\nu_l$, the uncertainty corresponding to the β values is negligible for physical observables like A_{FB}, C_F^l, and α^*, as shown in Table 6.

3.3 Nonleptonic decays

In this subsection, we discuss our predictions for the branching ratios of nonleptonic $B_c \to PV$ decays. As noted earlier, the nonleptonic decays of the B_c meson consist of CKM-enhanced ($\Delta b = 0, \Delta C = -1, \Delta S = -1$; $\Delta b = -1, \Delta C = -1, \Delta S = 0$; and $\Delta b = -1, \Delta C = 0, \Delta S = 1$), CKM-suppressed ($\Delta b = 0, \Delta C = -1, \Delta S = 0$; $\Delta b = -1, \Delta C = -1, \Delta S = 1$; and $\Delta b = -1, \Delta C = 0, \Delta S = 0$), and CKM-doubly-suppressed ($\Delta b = 0, \Delta C = -1, \Delta S = 1$; $\Delta b = -1, \Delta C = 1, \Delta S = 1$; and $\Delta b = -1, \Delta C = 1, \Delta S = 0$) bottom-conserving and bottom-changing decay modes. We calculated the decay amplitude using the decay constants listed in Table 2. Among the form factors listed in Tables 4 and 5 for $B_c \to P$ and $B_c \to V$ transitions, only the form factors $F_1(q^2)$ and $A_0(q^2)$ are relevant for the numerical evaluation of the branching ratios of $B_c \to PV$ decays. Since the $A_0(q^2)$ form factor is affected by self-consistency issues related to the $B_j^{(i)}$ functions, the study of nonleptonic $B_c \to PV$ decays provides an excellent opportunity to investigate such effects between type-I and type-II correspondences. We determine the branching ratios for nonleptonic B_c decays involving a color-favored diagram (class I), color-suppressed diagram (class II), and their interference (class III) for both large N_c limit and $N_c = 3$, as given by Eqs. (60) and (61) in Sect. 2.3. We list all the possible bottom-conserving $B_c \to PV$ decays in Table 8. Tables 9, 10, and 11 show our predictions for bottom-changing decays. As was done with semileptonic decays, we also calculate the uncertainties in branching ratios originating from the uncertainties in the form factors. Furthermore, we compare our results with other theoretical models, namely RIQM [38,39], RCQM [35], RQM [33], QCDF [42], pQCD [40,41], and CLFQM (type-I) [28], as given in Tables 12, 13, and 14. We list our key findings as follows.

(i) For bottom-conserving decay modes, the branching ratios of the B_c meson decays into $B^{(*)}$, and $B_s^{(*)}$ mesons in the final state range from $\mathcal{O}(10^{-2})$ to $\mathcal{O}(10^{-6})$ for the T2A formulation and up to $\mathcal{O}(10^{-5})$ for T2B, as shown in Table 8. It is well known for the case of CKM-favored decays that the CKM enhancement dominates the kinematic suppression, resulting in branching ratios of $\mathcal{O}(10^{-2}) \sim \mathcal{O}(10^{-3})$ for $N_c = \infty$. Due to the significant dominance of color-favored decays in both T2A and T2B, with a difference in branching ratios of less than 18%, our numerical discussions will primarily center on T2A. Among them, the most dominant CKM and color-favored (class I) decays are $B_c^+ \to \pi^+ B_s^{*0}$ and $B_c^+ \to B_s^0 \rho^+$, which have branching ratios of $(4.86^{+0.01+0.73}_{-0.14-1.08}) \times 10^{-2}$ and $(3.46^{+0.53+0.25}_{-0.54-0.63}) \times 10^{-2}$, respectively. It is worth noting that for the $B_c \to B_{(s)}^{(*)}$ transition, the mass of the spectator b quark is significantly larger than that of the decaying c quark, and the whole momentum is carried by the b quark. Therefore, the transition form factors at $q^2 = 0$ in such case differ up to $\sim$ 28% from those at maximum momentum transfer between the initial and final states. This increase in the form factor at $q^2_{\rm max}$ leads to an enhancement of up to $\sim$ 40% in the branching ratio of $B_c^+ \to \pi^+ B_s^{*0}/\overline{K}^0 B^{*+}$ decays (involving $A_0(q^2)$ form factors) for both T2A and T2B formulations. However, the decays involving the form factor $F_1(q^2)$ are affected by less than 14% at $q^2_{\rm max}$. Furthermore, we observe that the CKM-favored nonleptonic bottom-conserving decays for T2A exhibit uncertainties typically ranging from approximately 15% to 50%, correlating with the uncertainties in their respective form factors. These uncertainties are notably enhanced in color-suppressed channels characterized by lower branching ratios. Moreover, the branching ratios of these decays generally demonstrate increased sensitivity to variations in the β values, with a few exceptions to this trend.

(ii) It is important to note that the $A_0(q^2)$ transition form factors are affected by the self-consistency problems, and their contribution to semileptonic decays involving vector mesons in the final state is generally suppressed. However, nonleptonic $B_c \to PV$ decays that explicitly involve $A_0(q^2)$ form factors would give a quantitative measure of self-consistency effects between type-II and type-I correspondence schemes. Therefore, we compare our predictions in T2A and T2B with the results in T1, as listed in columns 2, 4, and 6 of Table 8. It may be noted that the results in the tables follow the order in which decays involving $A_0(q^2)$ are listed first, decays involving $F_1(q^2)$ are listed next, and class III decays involving both (if allowed) are given last for each CKM mode. We found that the results of the type-I scheme for CKM-favored bottom-conserving modes are significantly smaller for $B_c^+ \to \pi^+ B_s^{*0}/\overline{K}^0 B^{*+}$ decays. The branching ratio of color-favored $B_c^+ \to \pi^+ B_s^{*0}$ decay in the type-I scheme is $\sim$ 90% smaller than that of the type-II scheme (for both T2A and T2B). However, the branching ratio of color-suppressed $B_c^+ \to \overline{K}^0 B^{*+}$ decay changes by $\mathcal{O}(10^{-2})$ in the type-II scheme as compared to T1 predictions. This is due to the more pronounced self-consistency effects in $A_0^{B_c B_{(s)}^*}$ transition form factors. In addition, as previously noted, the uncertainties in the branching ratios arising from variations in the form factors are substantially larger (ranging from 70% to 180%) for the type-I scheme compared to the type-II scheme involving $A_0(q^2)$ form factors, as evident from Table 8. Moreover, to accurately assess the magnitude of self-consistency effects, we compare the numerical results of type-I and type-II schemes utilizing an identical q^2 formulation for both,[11] i.e., for Eq. (38), we found that $\mathcal{B}(B_c^+ \to \pi^+ B_s^{*0})$ decay decreases by $\sim$ 88%, while $\mathcal{B}(B_c^+ \to \overline{K}^0 B^{*+})$ decay decreases by $\mathcal{O}(10^{-2})$. Consequently, these substantial discrepancies between the type-I and type-II scheme predictions indicate that the effects of self-consistency on such decays are significant and cannot be ignored. In addition, we observe that the difference between the T2A and T2B formulations yields larger variations in the branching ratios for decays involving the $F_1(q^2)$ form factor than those involving the $A_0(q^2)$ form factor. However, the maximum differences between T2A and T2B is 19% and 27% for decays involving $A_0(q^2)$ and $F_1(q^2)$ form factors, respectively, where the T2B formulation predicts larger branching ratios. We reiterate that the form factor $F_1(q^2)$ does not exhibit any self-consistency issues. Therefore, the observed changes in the numerical results of the type-II correspondence scheme for the decays involving only the $F_1(q^2)$ form factor can be attributed to variations arising from the q^2 formulations.

(iii) In the bottom-conserving CKM-suppressed ($\Delta b = 0, \Delta C = -1, \Delta S = 0$) modes, the branching ratios for the dominant decays are $\mathcal{B}(B_c^+ \to B^0 \rho^+) = (2.77^{+0.58+0.32}_{-0.49-0.68}) \times 10^{-3}$, $\mathcal{B}(B_c^+ \to K^+ B_s^{*0}) = (2.45^{+0.04+0.37}_{-0.10-0.64}) \times 10^{-3}$, and $\mathcal{B}(B_c^+ \to \pi^+ B^{*0}) = (2.27^{+0.08+0.50}_{-0.16-0.67}) \times 10^{-3}$. All these decays involve color-favored (class I) processes. The next order branching ratios are of $\mathcal{O}(10^{-4})$, which correspond to the color-suppressed process, as shown in Table 8. It is interesting to note that the branching ratios of CKM-doubly-suppressed decays are of $\mathcal{O}(10^{-4}) \sim \mathcal{O}(10^{-6})$ with dominant branching ratio, $\mathcal{B}(B_c^+ \to K^+ B^{*0}) = (1.29^{+0.07+0.30}_{-0.11-0.45}) \times 10^{-4}$, for color-favored decay. As observed in CKM-enhanced decays, apart from the variation due to different q^2 formulations, the branching ratios of the decays (in the type-II scheme) involving $A_0(q^2)$ form factors change substantially as compared to those of the type-I scheme. We wish to emphasize that the branching ratios of the decays involving $A_0(q^2)$ form factors and color-favored processes in CKM-suppressed and CKM-doubly-suppressed modes are more seriously affected by self-consistency. The branching ratios of these decays change by roughly $\mathcal{O}(10^{-2}) \sim \mathcal{O}(10^{-3})$ for the type-I scheme as compared to the type-II scheme (for both T2A and T2B formulations). Likewise, for CKM-enhanced decays within the type-II correspondence, the T2B branching ratios are larger ($\sim 10-26\%$) than the T2A predictions for both CKM-suppressed and CKM-doubly-suppressed modes. In addition, the T1 predictions involving $A_0(q^2)$ form factors are subject to substantial uncertainties, reaching a maximum of $\sim$ 180% (for both CKM-suppressed and CKM-doubly-suppressed modes). It is intriguing to note that despite the nearly symmetric uncertainties in the form factors, the uncertainties in the nonleptonic branching ratios are more asymmetric. The substantial discrepancies between type-I and type-II scheme predictions within the CLFQM framework for nonleptonic bottom-conserving weak decays highlight the inherent inconsistencies in the type-I scheme. These deviations cast doubt on the reliability of results obtained through the type-I scheme. Furthermore, the uncertainties in the T2B formulation are generally smaller than those of the T2A formulation, with a few exceptions.

[11] Note that the numerical results of the type-II correspondence scheme for Eq. (38) (with parent pole mass), i.e., $A_0^{B_c B^*}(0) = 0.50$, $a = -9.92$, $b = 356.83$ and $A_0^{B_c B_s^*}(0) = 0.62$, $a = -4.25$, $b = 285.25$, are used.

(iv) In addition to the large N_c limit, we also predict branching ratios at $N_c = 3$, as shown in columns 3, 5, and 7 of Table 8 for T2A, T2B, and T1, respectively. As mentioned earlier, we have considered tree-dominated B_c decays and have neglected the small nonfactorizable and penguin contributions within our formalism. As previously noted, the number of color degrees of freedom (N_c) is usually treated as a phenomenological parameter in weak meson decays to account for nonfactorizable contributions. In the present case, we have used the $N_c = 3$ based on the model-independent analysis of B decays, which suggests that a_2 has a smaller magnitude [101]. We obtain $a_1 = 1.09$ and $a_2 = -0.09$ (from Eq. (61)) at $N_c = 3$ for bottom-conserving B_c decays. Since the bottom-conserving weak decays do not involve any class III decays, we expect an overall decrease in the branching ratios of these decays corresponding to smaller values of a_1 and a_2 at $N_c = 3$. We observe that the numerical values of color-suppressed decays at $N_c = 3$ are more seriously affected owing to the substantial reduction in the magnitude of the coefficient a_2. Given that we performed calculations for both $N_c = 3$ and at the large N_c limit, we disregarded the uncertainties in the parameters a_1 and a_2. Consequently, these predictions can be interpreted as representing a reasonable range of numerical results within the current formalism.

(v) In the case of bottom-changing B_c decays to $D^{(*)}$, $D_s^{(*)}$, and $\eta_c(J/\psi)$ mesons in the final state, we enlist the branching ratio predictions for T2A, T2B, and T1 in Tables 9, 10, and 11. Analogous to bottom-conserving decays, the branching ratios of T2A and T2B exhibit differences of less than 5% in most cases, with a few exceptions in CKM-suppressed decay modes. Thus, for numerical discussions, we will primarily consider T2A predictions. The most dominant CKM-enhanced decay modes, $B_c^+ \to \eta_c \rho^+$, $B_c^+ \to D_s^+ J/\psi$, $B_c^+ \to \eta_c D_s^{*+}$, and $B_c^+ \to \pi^+ J/\psi$, have branching ratios $(3.91^{+0.13+0.11}_{-0.12-0.24}) \times 10^{-3}$, $(2.44^{+0.99+0.00}_{-0.81-0.07}) \times 10^{-3}$, $(1.69^{+0.05+0.29}_{-0.00-0.26}) \times 10^{-3}$, and $(1.65^{+0.31+0.10}_{-0.29-0.15}) \times 10^{-3}$, respectively, at the large N_c limit for the T2A formulation. Among these, $B_c^+ \to \eta_c \rho^+$ and $B_c^+ \to \pi^+ J/\psi$ decays are color-favored (class I) decays, while $B_c^+ \to D_s^+ J/\psi$ and $B_c^+ \to \eta_c D_s^{*+}$ are class III decays. We wish to emphasize that the $B_c^+ \to D_s^+ J/\psi$ and $B_c^+ \to \eta_c D_s^{*+}$ decays receive contributions from both color-favored and color-suppressed diagrams and interfere destructively at the large N_c limit. However, for $N_c = 3$, color-favored and color-suppressed contributions for both of these decays interfere constructively, yielding larger branching ratios due to the positive values of a_1 and a_2 (as shown in Eq. (61)). In the CKM-enhanced ($\Delta C = -1, \Delta S = 0$) mode, the branching ratios of $B_c^+ \to \overline{D}^0 D^{*+}$ and $B_c^+ \to D^+ \overline{D}^{*0}$ decays for both T2A and T2B are of $\mathcal{O}(10^{-5})$, which falls within the experimental upper limits [12]. In contrast, for ($\Delta C = 0, \Delta S = 1$) mode, the next order branching ratios for the CKM-favored decays, e.g., $B_c^+ \to \pi^0 D_s^{*+}$, $B_c^+ \to K^+ D^{*0}$, $B_c^+ \to D^0 K^{*+}$, $B_c^+ \to D_s^+ \rho^0$, etc., remain highly suppressed. The branching ratios of these decays range from $\mathcal{O}(10^{-7})$ to $\mathcal{O}(10^{-10})$ as they occur through suppressed $b \to u$ weak transitions. We observe that the uncertainties in the branching ratios for T2A of CKM-favored ($\Delta C = -1, \Delta S = 0$) and color-suppressed decays are larger (up to $\sim 90\%$). Conversely, the uncertainties for color-favored decays involving $B_c \to \eta_c(J/\psi)$ transitions are below roughly 25%. Interestingly, the class III decays in ($\Delta C = 0, \Delta S = 1$) mode have intermediate uncertainties of approximately 40% or less. Furthermore, the dominant branching ratios of bottom-changing decays are smaller than those of bottom-conserving decays. As expected, due to the smaller values of a_1 and a_2 at $N_c = 3$, the branching ratios of all the decays show a decreasing trend, except for class III decays.[12]

(vi) In the CKM-suppressed ($\Delta C = -1, \Delta S = 1$) decay mode, the dominant $B_c^+ \to \eta_c K^{*+}$ and $B_c^+ \to K^+ J/\psi$ decays have branching ratios of $\mathcal{O}(10^{-4})$, and the branching ratios for the rest of the decays are of $\mathcal{O}(10^{-6})$. For ($\Delta C = 0, \Delta S = 0$) mode, the branching ratios are of $\mathcal{O}(10^{-4}) \sim \mathcal{O}(10^{-9})$, where the dominant modes $B_c^+ \to \eta_c D^{*+}$ and $B_c^+ \to D^+ J/\psi$ belong to class III decays. These decays arise from destructive interference between color-favored and color-suppressed processes, and have branching ratios of $\mathcal{O}(10^{-4})$ and $\mathcal{O}(10^{-5})$, respectively. At $N_c = 3$, coefficients a_1 and a_2 become positive, enhancing their branching ratios compared to the values at $N_c = \infty$. Furthermore, B_c meson decaying to $D^0 \rho^+$ and $\pi^+ D^{*0}$ in the final states are the only decays that involve the color-favored diagram and have branching ratios of $\mathcal{O}(10^{-6})$. In addition, $\mathcal{B}(B_c^+ \to D_s^+ \overline{D}^{*0}) = (4.08^{+1.36+0.51}_{-1.19-0.51}) \times 10^{-6}$ and $\mathcal{B}(B_c^+ \to \overline{D}^0 D_s^{*+}) = (2.92^{+0.21+1.97}_{-0.46-1.57}) \times 10^{-6}$ at the large N_c limit, which are within the experimental upper limit [12] (see Table 13). As previously observed, decays involving $B_c \to \eta_c(J/\psi)$ transition form factors show varying degrees of uncertainty. For the CKM-favored and

[12] Note that the reduction in the values of a_1 and a_2 at $N_c = 3$ leads to a proportional decrease in uncertainties across all decay modes, including class III decays. This comprehensive uncertainty reduction occurs despite the additive nature of uncertainties, as both color-favored and color-suppressed contributions experience a decrease in magnitude.

CKM-suppressed class III modes, these uncertainties range from approximately 15% to 45%, whereas class I decays demonstrate a more moderate variation of $\sim (5-25)\%$, as given in Tables 9 and 10.

(vii) Since we have focused on the discrepancies arising because of the self-consistency problem in form factors and consequently on the decays of the B_c meson, we compared our results for the type-II scheme with those for the type-I bottom-changing decays. We observed significant variations in branching ratios for CKM and color-favored bottom-changing decays involving $A_0(q^2)$ form factors between T1 and T2A(T2B), ranging from 25% to 58%. However, dominant class III decays, involving $F_1(q^2)$ and $A_0(q^2)$ form factors, exhibited branching ratio changes of approximately $(20-56)\%$ between T1 and T2A. In the type-I scheme, we observe that the branching ratios for bottom-changing CKM-suppressed class I decays, influenced by the $A_0(q^2)$ form factor (subject to self-consistency issues), decrease by approximately an order of magnitude, with associated uncertainties exceeding 150%. Moreover, as previously noted for bottom-conserving decays, the uncertainties in bottom-changing CKM-favored decays affected by self-consistency issues are markedly more pronounced in the type-I scheme, reaching over 200%. It may be noted that in the abovementioned changes corresponding to self-consistency, we have only considered the branching ratios up to $\mathcal{O}(10^{-6})$. We infer that, similarly to bottom-conserving decays, bottom-changing decays are significantly impacted by self-consistency issues, particularly for color-favored decays. The substantial discrepancies between type-I and type-II scheme predictions underscore that the effects of self-consistency on such decays are significant and warrant careful consideration.

(viii) It is worth noting that all of the bottom-changing CKM-doubly-suppressed B_c decays belong to the class III category. The color-favored and color-suppressed amplitudes interfere destructively to give the branching ratios $\mathcal{O}(10^{-6}) \sim \mathcal{O}(10^{-7})$ for these decays. As intended, the branching ratios of these modes are enhanced at $N_c = 3$. However, the effects of self-consistency on the branching ratios of these decays are roughly $(20-90)\%$. In particular, for $B_c^+ \to D_s^+ D^{*0}$ and $B_c^+ \to D^+ D^{*0}$ decays, the effect of self-consistency on branching ratios is roughly 90%. For example, in $B_c^+ \to D_s^+ D^{*0}$ decay, this stems from the color-favored $B_c^+ \to D^{*0}$ transition, characterized by the affected $A_0^{B_c D^*}(q^2)$ form factor, which contributes predominantly to the branching ratio. Conversely, the color-suppressed $B_c^+ \to D_s^+$ transition, involving the $F_1^{B_c D_s}(q^2)$ form factor, contributes marginally[13]. Therefore, the $A_0^{B_c D^*}(q^2)$ form factor exhibits a significant impact of self-consistency on the branching ratios of these decay processes. In addition, the uncertainties in the T2A branching ratios, corresponding to variations in quark mass and β values, range from approximately 10% to 70% and 20% to 90%, respectively. On the other hand, in the type-I scheme, the uncertainties become exceptionally large, making the results questionable. Furthermore, all the bottom-changing CKM-doubly-suppressed $B_c \to PV$ decays such as $B_c^+ \to D^0 D_{(s)}^{*+}$ and $B_c^+ \to D_{(s)}^+ D^{*0}$ are within the observed experimental upper limit [12]. In the case of bottom-changing decays, both CKM-favored and CKM-suppressed, the difference in branching ratios between T2A and T2B predictions typically remains below $\sim$ 10%. Notable exceptions include $\mathcal{B}(B_c^+ \to \overline{D}^0 D^{*+})$, $\mathcal{B}(B_c^+ \to D^+ \overline{D}^{*0})$, and $\mathcal{B}(B_c^+ \to D_s^+ \overline{D}^0)$, where differences of up to $\sim$ 20% are observed. For CKM-doubly-suppressed decays, the differences are more substantial, ranging from approximately 14% to 32%. Consistent with previous observations, T2B branching ratios are in general larger than those of T2A. However, for all the B_c decays to two charmed mesons in the final state (including class III decays), the branching ratios are lower than those predicted by T2A.

(ix) It should be noted that the recent experimental observations provide the ratios of branching fractions of nonleptonic B_c decays involving a J/ψ meson in the final state. Therefore, we compared our results with the experimental values reported by LHCb and ATLAS [13–16]. The ratios of the branching fractions determined theoretically are expressed as follows:

[13] In the branching ratio of $B_c^+ \to D_s^+ D^{*0}$ decay, the dominant contribution of 81% arises from the term involving the $A_0^{B_c D^*}$ form factor. The term involving the $F_1^{B_c D_s}$ form factor contributes 12%, while their interference term destructively contributes 7% to the branching ratio.

	T2A	T2B	Experimental values
$\frac{\mathcal{B}(B_c^+ \to J/\psi D_s^+)}{\mathcal{B}(B_c^+ \to J/\psi \pi^+)}$	$3.35^{+0.71+0.37}_{-0.78-0.25}$ $(1.48^{+0.56+0.14}_{-0.66-0.09})$	$2.82^{+0.63+0.33}_{-0.68-0.23}$ $(1.45^{+0.49+0.16}_{-0.57-0.09})$	$2.76 \pm 0.33 \pm 0.33$ [14];
$\frac{\mathcal{B}(B_c^+ \to J/\psi K^+)}{\mathcal{B}(B_c^+ \to J/\psi \pi^+)}$	$0.08^{+0.02+0.01}_{-0.02-0.01}$ $(0.07^{+0.02+0.01}_{-0.02-0.01})$	$0.08^{+0.02+0.01}_{-0.02-0.01}$ $(0.08^{+0.02+0.01}_{-0.02-0.01})$	$0.079 \pm 0.007 \pm 0.003$ [15],

where the values in the parentheses are obtained for the large N_c limit. We wish to point out that our results for $N_c = 3$ match well with the experimental values within the uncertainties. Similarly, we compare the ratio of the branching fractions for the nonleptonic $B_c^+ \to J/\psi\pi^+$ decay to the semileptonic $B_c^+ \to J/\psi\mu^+\nu_\mu$ decay with the experiment, as given below.

	T2A	T2B	Experimental value
$\frac{\mathcal{B}(B_c^+ \to J/\psi \pi^+)}{\mathcal{B}(B_c^+ \to J/\psi \mu^+ \nu_\mu)}$	$0.06^{+0.01+0.01}_{-0.02-0.00}$ $(0.07^{+0.02+0.01}_{-0.02-0.00})$	$0.06^{+0.01+0.01}_{-0.01-0.00}$ $(0.07^{+0.02+0.01}_{-0.02-0.00})$	$0.0469 \pm 0.0028 \pm 0.0046$ [133].

We note that our results, though larger in magnitude, are very close to the experimental observation, including the errors.

Finally, we compare our numerical results for the branching ratios with those of other theoretical models, including RIQM [38,39], RCQM [35], RQM [33], QCDF [42], pQCD [40,41], and CLFQM (type-I) [28], as shown in Tables 12, 13, and 14. All branching ratio predictions from different models are of the same order, with a few exceptions. Among them, our numerical results for the bottom-conserving branching ratios of B_c decays involving a B meson in the final state match well with the QCDF [42] results. We observe that our T2A predictions for the most dominant bottom-changing CKM-favored B_c decays, i.e., involving $\eta_c\rho^+$, $D_s^+ J/\psi$, $\eta_c D_s^{*+}$, and $\pi^+ J/\psi$ in the final state, match very well with the predictions of RCQM [35], except the $B_c^+ \to \eta_c D_s^{*+}$ decay. Notably, for these decays, the predictions from other theoretical models are larger than our results. We also compared our T1 results with CLFQM (type-I) [28] and observed that their values are of the same order but larger than ours by roughly (30−70)%, due to the different input parameters and the exponential q^2 formulation used in their work.

4 Summary and conclusions

In this work, we provide a comprehensive analysis of weak transition form factors, semileptonic decays, and nonleptonic decays of the B_c meson involving P and V mesons in CLFQM. We employed type-II correspondence in the CLF approach to resolve the self-consistency issues due to the presence of residual ω-dependencies associated with the $B_j^{(i)}$ functions, which remain independent of zero-mode contributions. It may be noted that the issues of inconsistency and violation of covariance in type-I correspondence, which affect the $A_0(q^2)$ and $A_1(q^2)$ form factors, can be simultaneously resolved by $M'^{(\prime)} \to M_0'^{(\prime)}$ considered in type-II correspondence [63]. However, the quantitative measure of these effects in type-II correspondence has never been studied in semileptonic and nonleptonic decays of the B_c meson. In this analysis, the effects of self-consistency originating from transition form factors on weak decays are quantitatively established. Furthermore, the impacts of self-consistency and covariance on bottom-conserving and bottom-changing semileptonic and nonleptonic decays within the CLFQM framework are comprehensively investigated. Two primary objectives are pursued: (i) the impact of self-consistency on weak semileptonic and nonleptonic decays is examined using modified form factors within a CLFQM approach, and (ii) self-consistency in bottom-conserving transition form factors, previously unexplored, is established and its effects on bottom-conserving weak decays are quantified. Furthermore, ambiguities related to the q^2 parameterization are addressed in the analysis to provide a more robust understanding of these decay processes. The self-consistency affects the numerical results of the form factors $A_0(q^2)$ and $A_1(q^2)$, which in turn appear in the semileptonic and nonleptonic decays of the B_c meson. It is well known that the coefficient of the $A_0(q^2)$ form factor is suppressed in the semileptonic decay rates; therefore, semileptonic decays only provide a comprehensive picture that corresponds to the effects originating from the $A_1(q^2)$ form factor. Thus, to observe the effect of the $A_0(q^2)$ form factor, we calculated the

$B_c \to PV$ decays which involve $F_1(q^2)$ and $A_0(q^2)$ form factors. Therefore, we calculated the transition form factors in CLFQM formalism in Tables 4 and 5. In the current work, we thoroughly examined the appropriate q^2 formulations, in particular for bottom-conserving transitions involving $B_c \to V(P)$ form factors. Therefore, we analyzed two different q^2 formulations in type-II correspondence referred to as T2A and T2B, using Eqs. (37) and (39), respectively. We also compared our results with type-I correspondence for the q^2 formulation in Eq. (38) to quantitatively assess the effects of self-consistency. In addition, we incorporated the uncertainties in form factors originating from quark masses and β parameters in our analysis. Consequently, we observed their implications for semileptonic and nonleptonic weak decays of the B_c meson. In addition, we calculated the experimentally significant physical observables, namely, the FB asymmetry, lepton-side convexity parameter, longitudinal (transverse) polarization of the charged lepton, and asymmetry parameter. We list our major conclusions as follows.

- We reconfirmed that the form factors $A_0(q^2)$ and $A_1(q^2)$ in the CLFQM type-I correspondence scheme acquire zero-mode contributions through $B_j^{(i)}$ functions, which results in different numerical values for the longitudinal and transverse polarization states. These issues are resolved within type-II correspondence, which ensures self-consistency and covariance of matrix elements. It may be emphasized that the zero-mode contributions in type-II correspondence vanish numerically, though existing formally in the analytical relations of the form factors. For bottom-conserving transitions, the numerical results of the T2A (T2B) form factors, $A_0(0)$ and $A_1(0)$, show a significant change of $(70-90)\%$ and $\sim 23\%$, respectively, as compared to those of the type-I scheme. Similarly, for bottom-changing transitions, we observed that the numerical values of the form factor $A_0(0)(A_1(0))$ in type-II correspondence, for both Eqs. (37) and (39), vary by roughly $\sim 30\%$ (10%) as compared to type-I for $B_c \to D_{(s)}^*$ transitions. We also observed that these form factors are sensitive to q^2 formulations, resulting in significantly different slope parameters (coefficients). Therefore, we conclude that the improvement in the numerical results of type-II correspondence cannot be determined simply from the variation in form factors at $q^2 = 0$; the modification in the numerical values of slope parameters also plays a significant role in the quantitative evaluation of these effects. Furthermore, the influence of type-II correspondence on $B_c \to J/\psi$ transition form factors is minimal compared to both bottom-conserving and other bottom-changing transition form factors.
- We also found that the $M'^{(\prime\prime)} \to M_0'^{(\prime\prime)}$ transformation, in general, affects the numerical values of all the transition form factors irrespective of the spin-parity of the final-state meson. Therefore, the numerical values of the form factors which do not suffer from self-consistency issues were also modified. We found that the numerical results for the T2A (T2B) form factors $F^{B_c B_{(s)}}(q^2)$ are in very good agreement with the LQCD observations at both $q^2 = 0$ and $q^2_{\rm max}$. On the other hand, the numerical values of the form factors $F^{B_c D_s}(q^2)$ $(F^{B_c D}(q^2))$ are in good agreement with the LQCD predictions within $\sim 15\%(\sim 9\%)$.
- We found that $\mathcal{B}(B_c \to B_s^{(*)} l \nu_l)$ and $\mathcal{B}(B_c \to J/\psi(\eta_c) l \nu_l)$ are the most dominant among the $B_c \to V(P) l \nu_l$ semileptonic decays. Our results for $\mathcal{B}(B_c^+ \to B_{(s)}^0 l^+ \nu_l)$ are in good agreement with the recent LQCD predictions. In addition, the decay width ratios of bottom-conserving semileptonic decays involving the pseudoscalar meson (B_s^0 and B^0) in the final state for T2B match well with LQCD expectations. Furthermore, the decays involving the τ lepton have the lowest branching ratios among all the decays because of the significantly larger mass of the τ lepton. We quantified the effect of self-consistency on the branching ratios of the semileptonic decay modes by comparing our results with those of type-I correspondence. We found that the numerical results for the type-II scheme are larger by $(50-60)\%$, $(57-78)\%$, and around 20% as compared to the branching ratios in the type-I scheme involving $B_c \to B_{(s)}^*$, $B_c \to D^*$, and $B_c \to J/\psi$ semileptonic decays, respectively. Furthermore, we found that our LFU ratio involving $b \to c\tau\nu_\tau$ for J/ψ in the final state matches well with LQCD and other theoretical models; however, it is smaller than the experimental measurement.
- For the nonleptonic B_c decays, branching ratios are affected by the self-consistency issues for decays involving $A_0(q^2)$ transition form factors. These decays presented an excellent opportunity to observe these effects in a quantitative manner. Interestingly, we found that the branching ratios of CKM- and color-favored bottom-conserving $B_c \to PV$ decays are affected by approximately $\sim 90\%$, while those of bottom-changing decays are impacted by $\sim (25-57)\%$. However, the color-favored CKM-suppressed and CKM-doubly-suppressed modes are more seriously affected, where some of the branching ratios are changed by $\sim 100\%$. Therefore, we conclude that the self-consistency effects are predominant in $B_c \to PV$ decays. Furthermore, we observed that the impact of uncertainties associated with quark mass and β parameters is more pronounced in bottom-changing transitions (except for $B_c \to J/\psi$) and decays. Notably, the substantial uncertainties in the slope parameters of q^2 formulations do not significantly affect the branching ratio values in semileptonic and nonleptonic decays.

- Finally, we conclude that both bottom-conserving and bottom-changing decays are significantly affected by self-consistency issues arising through the form factors. These impacts can influence the branching ratios by up to two orders of magnitude, with certain decay channels exhibiting particularly large uncertainties in the type-I scheme. Consequently, the substantial variation in predictions, coupled with uncertainties of greater magnitude, casts doubt on the validity of the results obtained through the type-I scheme. Furthermore, the observed discrepancies between type-I and type-II scheme predictions highlight the crucial role of self-consistency considerations. These findings emphasize the critical importance of thoroughly evaluating self-consistency effects in future studies on such decays.

Thus, the agreement between our predictions in the type-II correspondence scheme and the LQCD results confirms the reliability of our numerical results for B_c meson decays. We wish to note that we have ignored nonfactorizable processes, for example, W-exchange, W-annihilation, and penguin processes, in our analysis of nonleptonic B_c weak decays. However, the study of nonfactorizable contributions and CP-asymmetries can be conducted more reliably in a model-independent manner that requires a huge amount of experimental data. We hope that the experimental observation of these B_c weak decays can help to shed some light on the underlying physics of the B_c meson.

Acknowledgements The authors are pleased to express their thanks to H. Y. Cheng, C. K. Chua, H. M. Choi, C. R. Ji, and Gautam Bhattacharyya for their helpful comments and discussions. The author (RD) gratefully acknowledges the financial support by the Department of Science and Technology (SERB:CRG/2018/002796), New Delhi.

Data Availability Statement This manuscript has no associated data. [Author's' comment: All the data associated is given in the manuscript.]

Code Availability Statement This manuscript has no associated code/software. [Author's comment: xxx].

Funded by SCOAP[3].

Appendix A: Resolution of inconsistency

Using Eq. (27), the expressions for $f(q^2)$ and $a_-(q^2)$ form factors of $B_c \to V$ transitions are given as follows:

$$f(q^2) = N_c \int \frac{\mathrm{d}x_1 \mathrm{d}^2\boldsymbol{k}'_\perp}{(2\pi)^3} \frac{\chi'_{B_c}\chi''_V}{2x_2} \widetilde{f}(x_1, \boldsymbol{k}'_\perp, q^2), \tag{A1}$$

$$a_-(q^2) = N_c \int \frac{\mathrm{d}x_1 \mathrm{d}^2\boldsymbol{k}'_\perp}{(2\pi)^3} \frac{\chi'_{B_c}\chi''_V}{2x_2} \widetilde{a}_-(x_1, \boldsymbol{k}'_\perp, q^2), \tag{A2}$$

where $\widetilde{f}(x_1, \boldsymbol{k}'_\perp, q^2)$ and $\widetilde{a}_-(x_1, \boldsymbol{k}'_\perp, q^2)$ are defined in Eqs. (32) and (34), respectively. As discussed in Sect. 2.1, the expressions in Eqs. (32) and (34) correspond to $\lambda = 0$ for the type-I correspondence scheme. The corresponding expressions for the type-II scheme can be obtained by replacing $M'^{(\prime\prime)}$ with $M_0'^{(\prime\prime)}$ [62]. For the cases of $\lambda = \pm$, the terms associated with $B_j^{(i)}$ functions should be excluded.

We calculated the space-like $f(q^2)$ and $a_-(q^2)$ bottom-conserving and bottom-changing transition form factors at various $q^2_\perp$ values[14] for $\lambda = 0$ and $\lambda = \pm$, as listed in Tables 15 and 16, for both the type-I and type-II correspondence schemes.

Appendix B: Branching ratios of $B_c^+ \to Pl^+\nu_l$ decays

We list the numerical values of $B_c^+ \to Pl^+\nu_l$ semileptonic decays using the form factors given in Tables 4 and 5, and the numerical inputs are discussed in Sect. 3.

References

1. S.S. Gershtein, V.V. Kiselev, A.K. Likhoded, A.V. Tkabladze, Phys. Usp. **38**, 1–37 (1995). https://doi.org/10.1070/PU1995v038n01ABEH000063. arXiv:hep-ph/9504319
2. I.P. Gouz, V.V. Kiselev, A.K. Likhoded, V.I. Romanovsky, O.P. Yushchenko, Phys. Atom. Nucl. **67**, 1559–1570 (2004). https://doi.org/10.1134/1.1788046. arXiv:hep-ph/0211432
3. G. Chen, C.H. Chang, X.G. Wu, Phys. Rev. D **97**(11), 114022 (2018). https://doi.org/10.1103/PhysRevD.97.114022. arXiv:1803.11447 [hep-ph]
4. R. Aaij et al. (LHCb), JHEP **07**, 123 (2020). https://doi.org/10.1007/JHEP07(2020)123. arXiv:2004.08163 [hep-ex]
5. R. Aaij et al. (LHCb), Phys. Lett. B **742**, 29–37 (2015). https://doi.org/10.1016/j.physletb.2015.01.010. arXiv:1411.6899 [hep-ex]
6. R. Aaij et al. (LHCb), Phys. Rev. Lett. **122**(23), 232001 (2019). https://doi.org/10.1103/PhysRevLett.122.232001. arXiv:1904.00081 [hep-ex]
7. A.M. Sirunyan et al. (CMS), Phys. Rev. Lett. **122**(13), 132001 (2019). https://doi.org/10.1103/PhysRevLett.122.132001. arXiv:1902.00571 [hep-ex]

[14] We employed the five distinct q^2 points given in Tables 15 and 16 to fit the physical form factors and their slope parameters for bottom-conserving and bottom-changing transitions, respectively.

8. G. Aad et al. (ATLAS), Phys. Rev. Lett. **113**(21), 212004 (2014). https://doi.org/10.1103/PhysRevLett.113.212004. arXiv:1407.1032 [hep-ex]
9. R. Aaij et al. (LHCb), Phys. Rev. Lett. **111**(18), 181801 (2013). https://doi.org/10.1103/PhysRevLett.111.181801. arXiv:1308.4544 [hep-ex]
10. R. Aaij et al. (LHCb), JHEP **12**, 117 (2021). https://doi.org/10.1007/JHEP12(2021)117. arXiv:2109.00488 [hep-ex]
11. R. Aaij et al. (LHCb), Nucl. Phys. B **930**, 563–582 (2018). https://doi.org/10.1016/j.nuclphysb.2018.03.015. arXiv:1712.04702 [hep-ex]
12. R.L. Workman et al. (Particle Data Group), PTEP **2022**, 083C01 (2022). https://doi.org/10.1093/ptep/ptac097
13. Y.S. Amhis et al. (HFLAV), Phys. Rev. D **107**(5), 052008 (2023). https://doi.org/10.1103/PhysRevD.107.052008. arXiv:2206.07501 [hep-ex]
14. G. Aad et al. (ATLAS), JHEP **08**, 087 (2022). https://doi.org/10.1007/JHEP08(2022)087. arXiv:2203.01808 [hep-ex]
15. R. Aaij et al. (LHCb), JHEP **09**, 153 (2016). https://doi.org/10.1007/JHEP09(2016)153. arXiv:1607.06823 [hep-ex]
16. G. Aad et al. (ATLAS), Eur. Phys. J. C **76**(1), 4 (2016). https://doi.org/10.1140/epjc/s10052-015-3743-8. arXiv:1507.07099 [hep-ex]
17. R. Aaij et al. (LHCb), Phys. Rev. Lett. **120**(12), 121801 (2018). https://doi.org/10.1103/PhysRevLett.120.121801. arXiv:1711.05623 [hep-ex]
18. J. Harrison et al. (LATTICE-HPQCD), Phys. Rev. Lett. **125**(22), 222003 (2020). https://doi.org/10.1103/PhysRevLett.125.222003. arXiv:2007.06956 [hep-lat]
19. J. Harrison et al. (HPQCD), Phys. Rev. D **102**(9), 094518 (2020). https://doi.org/10.1103/PhysRevD.102.094518. arXiv:2007.06957 [hep-lat]
20. L.J. Cooper et al. (HPQCD), Phys. Rev. D **102**(1), 014513 (2020). https://doi.org/10.1103/PhysRevD.102.014513. arXiv:2003.00914 [hep-lat]. [Erratum: Phys. Rev. D **103**(9), 099901 (2021)]
21. L.J. Cooper et al. (HPQCD), Phys. Rev. D **105**(1), 014503 (2022). https://doi.org/10.1103/PhysRevD.105.014503. arXiv:2108.11242 [hep-lat]
22. V.V. Kiselev, A.E. Kovalsky, A.K. Likhoded, Nucl. Phys. B **585**, 353–382 (2000). https://doi.org/10.1016/S0550-3213(00)00386-2. arXiv:hep-ph/0002127
23. V.V. Kiselev, O.N. Pakhomova, V.A. Saleev, J. Phys. G **28**, 595–606 (2002). https://doi.org/10.1088/0954-3899/28/4/301. arXiv:hep-ph/0110180
24. V.V. Kiselev, arXiv:hep-ph/0211021
25. A. Abd El-Hady, M.A.K. Lodhi, J.P. Vary, Phys. Rev. D **59**, 094001 (1999). https://doi.org/10.1103/PhysRevD.59.094001. arXiv:hep-ph/9807225
26. A. Abd El-Hady, J.H. Munoz, J.P. Vary, Phys. Rev. D **62**, 014019 (2000). https://doi.org/10.1103/PhysRevD.62.014019. arXiv:hep-ph/9909406
27. X. J. Li, Y. S. Li, F. L. Wang, X. Liu, Eur. Phys. J. C **83**(11), 1080 (2023). https://doi.org/10.1140/epjc/s10052-023-12237-9. arXiv: 2308.07206 [hep-ph]
28. Z.Q. Zhang, Z.J. Sun, Y.C. Zhao, Y.Y. Yang, Z.Y. Zhang, Eur. Phys. J. C **83**(6), 477 (2023). https://doi.org/10.1140/epjc/s10052-023-11576-x. arXiv:2301.11107 [hep-ph]
29. W. Wang, Y.L. Shen, C.D. Lu, Phys. Rev. D **79**, 054012 (2009). https://doi.org/10.1103/PhysRevD.79.054012. arXiv:0811.3748 [hep-ph]
30. W. Wang, Y.L. Shen, C.D. Lu, Eur. Phys. J. C **51**, 841–847 (2007). https://doi.org/10.1140/epjc/s10052-007-0334-3. arXiv:0704.2493 [hep-ph]
31. Z.J. Sun, S.Y. Wang, Z.Q. Zhang, Y.Y. Yang, Z.Y. Zhang, Eur. Phys. J. C **83**(10), 945 (2023). https://doi.org/10.1140/epjc/s10052-023-12034-4. arXiv:2308.03114 [hep-ph]
32. R.N. Faustov, V.O. Galkin, X.W. Kang, Phys. Rev. D **106**(1), 013004 (2022). https://doi.org/10.1103/PhysRevD.106.013004. arXiv:2206.10277 [hep-ph]
33. D. Ebert, R.N. Faustov, V.O. Galkin, Eur. Phys. J. C **32**, 29–43 (2003). https://doi.org/10.1140/epjc/s2003-01347-5. arXiv:hep-ph/0308149
34. D. Ebert, R.N. Faustov, V.O. Galkin, Phys. Rev. D **68**, 094020 (2003). https://doi.org/10.1103/PhysRevD.68.094020. arXiv:hep-ph/0306306
35. M.A. Ivanov, J.G. Korner, P. Santorelli, Phys. Rev. D **73**, 054024 (2006). https://doi.org/10.1103/PhysRevD.73.054024. arXiv:hep-ph/0602050
36. M.A. Ivanov, J.G. Korner, O.N. Pakhomova, Phys. Lett. B **555**, 189–196 (2003). https://doi.org/10.1016/S0370-2693(03)00052-2. arXiv:hep-ph/0212291
37. M.A. Ivanov, J.G. Körner, P. Santorelli. https://doi.org/10.1007/978-88-470-0530-3_43. arXiv:hep-ph/0609122
38. S. Naimuddin, S. Kar, M. Priyadarsini, N. Barik, P.C. Dash, Phys. Rev. D **86**, 094028 (2012). https://doi.org/10.1103/PhysRevD.86.094028
39. L. Nayak, P.C. Dash, S. Kar, N. Barik, Phys. Rev. D **105**(5), 053007 (2022). https://doi.org/10.1103/PhysRevD.105.053007. arXiv:2202.01167 [hep-ph]
40. Z. Rui, Z. Zhitian, C.D. Lu, Phys. Rev. D **86**, 074019 (2012). https://doi.org/10.1103/PhysRevD.86.074019. arXiv:1203.2303 [hep-ph]
41. Z. Rui, Z.T. Zou, Phys. Rev. D **90**(11), 114030 (2014). https://doi.org/10.1103/PhysRevD.90.114030. arXiv:1407.5550 [hep-ph]
42. J. Sun, N. Wang, Q. Chang, Y. Yang, Adv. High Energy Phys. **2015**, 104378 (2015). https://doi.org/10.1155/2015/104378. arXiv:1504.01286 [hep-ph]
43. H.J. Melosh, Phys. Rev. D **9**, 1095 (1974). https://doi.org/10.1103/PhysRevD.9.1095
44. H.Y. Cheng, C.K. Chua, C.W. Hwang, Phys. Rev. D **69**, 074025 (2004). https://doi.org/10.1103/PhysRevD.69.074025. arXiv:hep-ph/0310359
45. H.M. Choi, C.R. Ji, Phys. Rev. D **89**(3), 033011 (2014). https://doi.org/10.1103/PhysRevD.89.033011. arXiv:1308.4455 [hep-ph]
46. R.C. Verma, J. Phys. G **39**, 025005 (2012). https://doi.org/10.1088/0954-3899/39/2/025005. arXiv:1103.2973 [hep-ph]
47. H.Y. Cheng, C.Y. Cheung, C.W. Hwang, W.M. Zhang, Phys. Rev. D **57**, 5598–5610 (1998). https://doi.org/10.1103/PhysRevD.57.5598. arXiv:hep-ph/9709412
48. W. Jaus, Phys. Rev. D **41**, 3394 (1990). https://doi.org/10.1103/PhysRevD.41.3394
49. W. Jaus, Phys. Rev. D **44**, 2851–2859 (1991). https://doi.org/10.1103/PhysRevD.44.2851
50. C.R. Ji, P.L. Chung, S.R. Cotanch, Phys. Rev. D **45**, 4214–4220 (1992). https://doi.org/10.1103/PhysRevD.45.4214
51. H.Y. Cheng, C.Y. Cheung, C.W. Hwang, Phys. Rev. D **55**, 1559–1577 (1997). https://doi.org/10.1103/PhysRevD.55.1559. arXiv:hep-ph/9607332
52. W. Jaus, Phys. Rev. D **60**, 054026 (1999). https://doi.org/10.1103/PhysRevD.60.054026
53. E.E. Salpeter, H.A. Bethe, Phys. Rev. **84**, 1232–1242 (1951). https://doi.org/10.1103/PhysRev.84.1232
54. E.E. Salpeter, Phys. Rev. **87**, 328–342 (1952). https://doi.org/10.1103/PhysRev.87.328
55. H.M. Choi, C.R. Ji, Phys. Rev. D **58**, 071901 (1998). https://doi.org/10.1103/PhysRevD.58.071901. arXiv:hep-ph/9805438
56. W. Jaus, Phys. Rev. D **67**, 094010 (2003). https://doi.org/10.1103/PhysRevD.67.094010. arXiv:hep-ph/0212098

57. B.L.G. Bakker, H.M. Choi, C.R. Ji, Phys. Rev. D **63**, 074014 (2001). https://doi.org/10.1103/PhysRevD.63.074014. arXiv:hep-ph/0008147
58. B.L.G. Bakker, H.M. Choi, C.R. Ji, Phys. Rev. D **65**, 116001 (2002). https://doi.org/10.1103/PhysRevD.65.116001. arXiv:hep-ph/0202217
59. B.L.G. Bakker, H.M. Choi, C.R. Ji, Phys. Rev. D **67**, 113007 (2003). https://doi.org/10.1103/PhysRevD.67.113007. arXiv:hep-ph/0303002
60. H.M. Choi, C.R. Ji, Phys. Rev. D **72**, 013004 (2005). https://doi.org/10.1103/PhysRevD.72.013004. arXiv:hep-ph/0504219
61. Q. Chang, X.L. Wang, L.T. Wang, Chin. Phys. C **44**(8), 083105 (2020). https://doi.org/10.1088/1674-1137/44/8/083105. arXiv:2003.10833 [hep-ph]
62. Q. Chang, X.N. Li, L.T. Wang, Eur. Phys. J. C **79**(5), 422 (2019). https://doi.org/10.1140/epjc/s10052-019-6949-3. arXiv:1905.05098 [hep-ph]
63. Q. Chang, X.N. Li, X.Q. Li, F. Su, Y.D. Yang, Phys. Rev. D **98**(11), 114018 (2018). https://doi.org/10.1103/PhysRevD.98.114018. arXiv:1810.00296 [hep-ph]
64. A. Hazra, S.T. Mary, N. Sharma, R. Dhir, Eur. Phys. J. C **84**(9), 944 (2024). https://doi.org/10.1140/epjc/s10052-024-13249-9
65. H.M. Choi, Phys. Rev. D **103**(7), 073004 (2021). https://doi.org/10.1103/PhysRevD.103.073004. arXiv:2102.02015 [hep-ph]
66. P. Sun, X.B. Tong, F. Yuan, Phys. Lett. B **822**, 136655 (2021). https://doi.org/10.1016/j.physletb.2021.136655. arXiv:2103.12047 [hep-ph]
67. N. Brambilla, A. Pineda, J. Soto, A. Vairo, Rev. Mod. Phys. **77**, 1423 (2005). https://doi.org/10.1103/RevModPhys.77.1423. arXiv:hep-ph/0410047
68. S.J. Brodsky, T. Huang, G.P. Lepage, Conf. Proc. C **810816**, 143–199 (1981). SLAC-PUB-16520
69. S.J. Brodsky, T. Huang, G.P. Lepage, SLAC-PUB-2857, published in the Proceedings of the Summer Institute on Particle Physics, Stanford, California (1981)
70. S.J. Brodsky, T. Huang, G.P. Lepage, SLAC-PUB-2540, published in the Proceedings of the XXth International Conference on High Energy Physics, Madison, Wisconsin (1980)
71. S.J. Brodsky, H.C. Pauli, S.S. Pinsky, Phys. Rep. **301**, 299–486 (1998). https://doi.org/10.1016/S0370-1573(97)00089-6. arXiv:hep-ph/9705477
72. M. Wirbel, B. Stech, M. Bauer, Z. Phys. C **29**, 637 (1985). https://doi.org/10.1007/BF01560299
73. P.P. Srivastava, S.J. Brodsky, Phys. Rev. D **61**, 025013 (2000). https://doi.org/10.1103/PhysRevD.61.025013. arXiv:hep-ph/9906423
74. S.J. Brodsky, SLAC-PUB-10871, arXiv:hep-ph/0412101 (58th Scottish Universities Summer School in physics (SUSSP58), St. Andrews, United Kingdom (2004))
75. S.J. Brodsky, SLAC-PUB-7645, arXiv:hep-ph/9710288 (10th summer school and symposium on nuclear physics: QCD, light-cone physics and hadron phenomenology, Seoul, Korea (1997))
76. S.J. Brodsky, Few Body Syst. **59**(5), 83 (2018). https://doi.org/10.1007/s00601-018-1409-4. arXiv:1802.08552 [hep-ph]
77. N.E. Ligterink, B.L.G. Bakker, Phys. Rev. D **52**, 5954–5979 (1995). https://doi.org/10.1103/PhysRevD.52.5954. arXiv:hep-ph/9412315
78. W. Jaus, Phys. Rev. D **53**, 1349 (1996). https://doi.org/10.1103/PhysRevD.53.1349. [Erratum: Phys. Rev. D **54**, 5904 (1996)]
79. S. Tang, S. Jia, P. Maris, J.P. Vary, Phys. Rev. D **104**(1), 016002 (2021). https://doi.org/10.1103/PhysRevD.104.016002. arXiv:2011.05454 [hep-ph]
80. M. Li, Y. Li, P. Maris, J.P. Vary, Phys. Rev. D **100**(3), 036006 (2019). https://doi.org/10.1103/PhysRevD.100.036006. arXiv:1906.07306 [nucl-th]
81. O. Heger, M. Gómez-Rocha, W. Schweiger, Phys. Rev. D **104**(11), 116005 (2021). https://doi.org/10.1103/PhysRevD.104.116005. arXiv:2109.07849 [hep-ph]
82. J.D. Richman, P.R. Burchat, Rev. Mod. Phys. **67**, 893–976 (1995). https://doi.org/10.1103/RevModPhys.67.893. arXiv:hep-ph/9508250
83. D. Becirevic, A.B. Kaidalov, Phys. Lett. B **478**, 417–423 (2000). https://doi.org/10.1016/S0370-2693(00)00290-2. arXiv:hep-ph/9904490
84. D. Melikhov, Phys. Rev. D **53**, 2460–2479 (1996). https://doi.org/10.1103/PhysRevD.53.2460. arXiv:hep-ph/9509268
85. D. Melikhov, B. Stech, Phys. Rev. D **62**, 014006 (2000). https://doi.org/10.1103/PhysRevD.62.014006. arXiv:hep-ph/0001113
86. R.J. Hill, Phys. Rev. D **73**, 014012 (2006). https://doi.org/10.1103/PhysRevD.73.014012. arXiv:hep-ph/0505129
87. R.J. Hill, eConf **C060409**, 027 (2006). arXiv:hep-ph/0606023
88. D. Melikhov, Eur. Phys. J. direct **4**(1), 2 (2002). https://doi.org/10.1007/s1010502c0002. arXiv:hep-ph/0110087
89. D. Becirevic, A. Le Yaouanc, A. Oyanguren, P. Roudeau, F. Sanfilippo, arXiv:1407.1019 [hep-ph]
90. M. Bauer, M. Wirbel, Z. Phys. C **42**, 671 (1989). https://doi.org/10.1007/BF01557675
91. J. Wiss, eConf **C060409**, 025 (2006). arXiv:hep-ex/0605030
92. R. Poling, eConf **C060409**, 005 (2006). arXiv:hep-ex/0606016
93. N. Gubernari, A. Khodjamirian, R. Mandal, T. Mannel, JHEP **05**, 029 (2022). https://doi.org/10.1007/JHEP05(2022)029. arXiv:2203.08493 [hep-ph]
94. C. Bourrely, I. Caprini, L. Lellouch, Phys. Rev. D **79**, 013008 (2009). https://doi.org/10.1103/PhysRevD.82.099902. arXiv:0807.2722 [hep-ph]. [Erratum: Phys. Rev. D **82**, 099902 (2010)]
95. J.G. Korner, G.A. Schuler, Z. Phys. C **46**, 93 (1990). https://doi.org/10.1007/BF02440838
96. M.A. Ivanov, J.G. Korner, P. Santorelli, Phys. Rev. D **71**, 094006 (2005). https://doi.org/10.1103/PhysRevD.75.019901. arXiv:hep-ph/0501051. [Erratum: Phys. Rev. D **75**, 019901 (2007)]
97. A. Ali, P. Ball, L.T. Handoko, G. Hiller, Phys. Rev. D **61**, 074024 (2000). https://doi.org/10.1103/PhysRevD.61.074024. arXiv:hep-ph/9910221
98. G. Burdman, Phys. Rev. D **57**, 4254–4257 (1998). https://doi.org/10.1103/PhysRevD.57.4254. arXiv:hep-ph/9710550
99. D. Becirevic, S. Fajfer, I. Nisandzic, A. Tayduganov, Nucl. Phys. B **946**, 114707 (2019). https://doi.org/10.1016/j.nuclphysb.2019.114707. arXiv:1602.03030 [hep-ph]
100. R. Dhir, C.S. Kim, Phys. Rev. D **88**(3), 034024 (2013). https://doi.org/10.1103/PhysRevD.88.034024. arXiv:1307.0216 [hep-ph]
101. T.E. Browder, K. Honscheid, Prog. Part. Nucl. Phys. **35**, 81–220 (1995). https://doi.org/10.1016/0146-6410(95)00042-H. arXiv:hep-ph/9503414
102. M. Wirbel, Prog. Part. Nucl. Phys. **21**, 33–98 (1988). https://doi.org/10.1016/0146-6410(88)90031-2
103. P. Colangelo, F. De Fazio, Phys. Rev. D **61**, 034012 (2000). https://doi.org/10.1103/PhysRevD.61.034012. arXiv:hep-ph/9909423
104. R. Dhir, R.C. Verma, Phys. Rev. D **79**, 034004 (2009). https://doi.org/10.1103/PhysRevD.79.034004. arXiv:0810.4284 [hep-ph]
105. T.E. Browder, K. Honscheid, S. Playfer, https://doi.org/10.1142/9789814503846_0004. arXiv:hep-ph/9404314
106. F. Jugeau, A. Le Yaouanc, L. Oliver, J.C. Raynal, Phys. Rev. D **72**, 094010 (2005). https://doi.org/10.1103/PhysRevD.72.094010. arXiv:hep-ph/0504206
107. R. Dhir, C.S. Kim, Phys. Rev. D **87**(3), 034004 (2013). https://doi.org/10.1103/PhysRevD.87.034004. arXiv:1210.7890 [hep-ph]
108. H.Y. Cheng, C.W. Chiang, Phys. Rev. D **81**, 074021 (2010). https://doi.org/10.1103/PhysRevD.81.074021. arXiv:1001.0987 [hep-ph]

109. H.Y. Cheng, C.W. Chiang, A.L. Kuo, Phys. Rev. D **91**(1), 014011 (2015). https://doi.org/10.1103/PhysRevD.91.014011. arXiv:1409.5026 [hep-ph]
110. Y. Aoki et al. [Flavour Lattice Averaging Group (FLAG)], Eur. Phys. J. C **82**(10), 869 (2022). https://doi.org/10.1140/epjc/s10052-022-10536-1. arXiv:2111.09849 [hep-lat]
111. A. Bharucha, D.M. Straub, R. Zwicky, JHEP **08**, 098 (2016). https://doi.org/10.1007/JHEP08(2016)098. arXiv:1503.05534 [hep-ph]
112. M. Ablikim et al. (BESIII), Phys. Rev. Lett. **131**(14), 141802 (2023). https://doi.org/10.1103/PhysRevLett.131.141802. arXiv:2304.12159 [hep-ex]
113. R.J. Dowdall, C.T.H. Davies, G.P. Lepage, C. McNeile, Phys. Rev. D **88**, 074504 (2013). https://doi.org/10.1103/PhysRevD.88.074504. arXiv:1303.1670 [hep-lat]
114. B. Chakraborty et al. (HPQCD), Phys. Rev. D **96**(7), 074502 (2017). https://doi.org/10.1103/PhysRevD.96.074502. arXiv:1703.05552 [hep-lat]
115. V. Lubicz et al. (ETM), Phys. Rev. D **96**(3), 034524 (2017). https://doi.org/10.1103/PhysRevD.96.034524. arXiv:1707.04529 [hep-lat]
116. S. Narison, Nucl. Part. Phys. Proc. **309–311**, 135–147 (2020). https://doi.org/10.1016/j.nuclphysbps.2019.11.024. arXiv:2001.06346 [hep-ph]
117. S. Narison, Phys. Lett. B **802**, 135221 (2020). https://doi.org/10.1016/j.physletb.2020.135221. arXiv:1906.03614 [hep-ph]
118. Y.J. Shi, W. Wang, Z.X. Zhao, Eur. Phys. J. C **76**(10), 555 (2016). https://doi.org/10.1140/epjc/s10052-016-4405-1. arXiv:1607.00622 [hep-ph]
119. B. Colquhoun et al. (HPQCD), Phys. Rev. D **91**(11), 114509 (2015). https://doi.org/10.1103/PhysRevD.91.114509. arXiv:1503.05762 [hep-lat]
120. H.M. Choi, C.R. Ji, Phys. Rev. D **80**, 054016 (2009). https://doi.org/10.1103/PhysRevD.80.054016. arXiv:0903.0455 [hep-ph]
121. C.W. Hwang, Phys. Rev. D **81**, 114024 (2010). https://doi.org/10.1103/PhysRevD.81.114024. arXiv:1003.0972 [hep-ph]
122. C.Y. Cheung, C.W. Hwang, W.M. Zhang, Z. Phys. C **75**, 657–664 (1997). https://doi.org/10.1007/s002880050511. arXiv:hep-ph/9602309
123. M. Neubert, V. Rieckert, B. Stech, Q.P. Xu, Adv. Ser. Direct. High Energy Phys. **10**, 286–333 (1992). https://doi.org/10.1142/9789814503587_0005
124. Y. Sato et al. (Belle), Phys. Rev. D **93**(3), 032008 (2016). https://doi.org/10.1103/PhysRevD.93.059901. arXiv:1402.7134 [hep-ex]
125. J.N. Pandya, P. Santorelli, N.R. Soni, https://doi.org/10.1140/epjs/s11734-023-01006-0. arXiv:2307.14245 [hep-ph]
126. P. Colangelo, F. De Fazio, F. Loparco, Phys. Rev. D **103**(7), 075019 (2021). https://doi.org/10.1103/PhysRevD.103.075019. arXiv:2102.05365 [hep-ph]
127. S. Patnaik, L. Nayak, P.C. Dash, S. Kar, N. Barik, Eur. Phys. J. Plus **135**(11), 936 (2020). https://doi.org/10.1140/epjp/s13360-020-00898-4. arXiv:1910.13206 [hep-ph]
128. T. Huang, F. Zuo, Eur. Phys. J. C **51**, 833–839 (2007). https://doi.org/10.1140/epjc/s10052-007-0333-4. arXiv:hep-ph/0702147
129. C.F. Qiao, R.L. Zhu, Phys. Rev. D **87**(1), 014009 (2013). https://doi.org/10.1103/PhysRevD.87.014009. arXiv:1208.5916 [hep-ph]
130. Z. Rui, H. Li, G.X. Wang, Y. Xiao, Eur. Phys. J. C **76**(10), 564 (2016). https://doi.org/10.1140/epjc/s10052-016-4424-y. arXiv:1602.08918 [hep-ph]
131. E. Hernandez, J. Nieves, J.M. Verde-Velasco, Phys. Rev. D **74**, 074008 (2006). https://doi.org/10.1103/PhysRevD.74.074008. arXiv:hep-ph/0607150
132. A.Y. Anisimov, I.M. Narodetsky, C. Semay, B. Silvestre-Brac, Phys. Lett. B **452**, 129–136 (1999). https://doi.org/10.1016/S0370-2693(99)00273-7. arXiv:hep-ph/9812514
133. R. Aaij et al. (LHCb), Phys. Rev. D **90**(3), 032009 (2014). https://doi.org/10.1103/PhysRevD.90.032009. arXiv:1407.2126 [hep-ex]